RICE YIELD ESTIMATION USING REMOTE SENSING AND CROP SIMULATION MODEL IN NALGONDA DISTRICT, TELANGANA

G. SNIGDHA

B.Sc. (Ag.)

MASTER OF SCIENCE IN AGRICULTURE

AGRONOMY (WATER MANAGEMENT)

2022

RICE YIELD ESTIMATION USING REMOTE SENSING AND CROP SIMULATION MODEL IN NALGONDA DISTRICT, TELANGANA

BY

G. SNIGDHA

B.Sc. (Ag.)

THESIS SUBMITTED TO THE

PROFESSOR JAYASHANKAR TELANGANA STATE AGRICULTURAL UNIVERSITY

IN PARTIAL FULFILMENT OF THE REQUIREMENTS FOR THE AWARD OF THE DEGREE OF

MASTER OF SCIENCE IN AGRICULTURE
AGRONOMY (WATER MANAGEMENT)

CHAIRPERSON: Dr. GUMMA MURALI KRISHNA

WATER TECHNOLOGY CENTRE

PROFESSOR JAYASHANKAR TELANGANA STATE AGRICULTURAL UNIVERSITY

RAJENDRANAGAR, HYDERABAD-500 030

2022

CERTIFICATE

G. SNIGDHA has satisfactorily prosecuted the course of research and that thesis entitled **"RICE YIELD ESTIMATION USING REMOTE SENSING AND CROP SIMULATION MODEL IN NALGONDA DISTRICT, TELANGANA"** submitted is the result of original research work and is of a sufficiently high standard to warrant its presentation to the examination. I also certify that neither the thesis nor its part thereof has been previously submitted by him for a degree of any university.

(**Dr. GUMMA MURALI KRISHNA)**

Date: **Chairperson**

CERTIFICATE

This is to certify that the thesis entitled **"RICE YIELD ESTIMATION USING REMOTE SENSING AND CROP SIMULATION MODEL IN NALGONDA DISTRICT, TELANGANA"** submitted in partial fulfilment of the requirements for the degree of 'Master of Science in Agriculture of the Professor Jayashankar Telangana State Agricultural University, Hyderabad is a record of the bonafide original research work carried out by **Ms. G. SNIGDHA** under our guidance and supervision. No part of the thesis has been submitted by the student for any other degree or diploma. The published part and all assistance received during the course of the investigations have been duly acknowledged by the author of the thesis.

Date: **(Dr. GUMMA MURALI KRISHNA)**

                                                                    Chairperson of the Advisor committee

Thesis approved by the Student's Advisory Committee

Chairperson	**Dr. Gumma Murali Krishna**	
	Cluster head and Principal scientist	
	Geospatial sciences and Big data,	
	ICRISAT, Patancheru, 502324.	_____
Member	**Dr. T. L. Neelima**	
	Senior scientist (Agronomy)	
	Water Technology Centre,	
	College of Agriculture, PJTSAU,	_____
	Rajendranagar, Hyderabad-500030	
Member	**Dr. K. Avil Kumar**	
	Director	
	Water Technology Centre,	
	College of Agriculture, PJTSAU	
	Rajendranagar, Hyderabad-500030	_____

.

Date of final viva voce:

_____

DECLARATION

I, **G. SNIGDHA**, hereby declare that the thesis entitled **"RICE YIELD ESTIMATION USING REMOTE SENSING AND CROP SIMULATION MODEL IN NALGONDA DISTRICT, TELANGANA"** submitted to **Professor Jayashankar Telangana State Agricultural University** for the degree of **Master of Science in Agriculture** is the result of original research work done by me. I also declare that no material contained in the thesis has been published earlier in any manner.

Place: Hyderabad

Date:

G. SNIGDHA

I.D.No. RAM/2020-106

ACKNOWLEDGEMENT

*I express my sincere thanks to **Mamatha, Jayakar, Bhargavi, Swaroopa, Karthik, Srinika, Chandra Shekar** and the staff of the Water Technology Center for their timely cooperation and help during the P.G.Programme.*

I express my immense and wholehearted thanks to all my near for their cooperation and help during my study and research.

Finally, I profusely thank the Water Technology Center, Professor Jayashankar Telangana State Agricultural University (PJTSAU) for providing me with the opportunity to pursue an M.Sc. degree program.

Date: **(G. Snigdha)**

Place: Hyderabad

LIST OF CONTENTS

LIST OF TABLES

LIST OF ILLUSTRATIONS

LIST OF APPENDICES

LIST OF PLATES

LIST OF SYMBOLS AND ABBREVIATIONS

%	:	Per cent
*.prn	:	*Formatted Text (Space delimited)*
<	:	Less than
=	:	Is equal to
>	:	Greater than
A	:	leaf absorptivity
AMIC	:	Agricultural Marketing Intelligence Cell
amp	:	Annual Amplitude in mean monthly temperature
API	:	Application Programming Interface
APSIM	:	Agricultural Productive Systems Simulator
AVHRR	:	Advanced Very High-Resolution Radiometer
AWifS	:	Advanced Wide-Field Sensor
C	:	Carbon
°C	:	Degree Celsius
CAD	:	Computer aided design
CART	:	Classification and Regression Trees
CCC	:	Canopy Chlorophyll Content
CCE	:	Crop Cutting Experiments
CEC	:	Cation Exchange Capacity
CERES	:	Crop Environment Resource Synthesis
CHIRPS	:	Climate Hazards Group InfraRed Precipitation with Station data
CIgreen	:	Green chlorophyll index
Cl	:	Chlorophyll
CSM	:	Crop Simulation Model
CU	:	Cubist
CV	:	Coefficient of variation
CVI	:	Chlorophyll Vegetation Index
DAT	:	Days after transplantation
dB	:	Decibels
DCRFs	:	Dynamic Conditional Random Fields
DEM	:	Digital Elevation Model
DOA	:	Department of Agriculture

DOT	:	Day of transplantation
DVS	:	Development of vegetative stage
EO	:	Earth Observation
EPIC	:	Erosion productivity Impact Calculator
ERDAS	:	Earth Resources Data Analysis System
ERMES	:	An Earth observation Model based RicE information Service
ESA	:	European Space Agency
ET	:	Evapotranspiration
et al.,	:	and others
etc.,	:	and other similar
ETM+	:	Enhanced Thematic Mapper
FAO	:	Food and Agriculture Organisation
f_b	:	beam fraction
GBM	:	Gradient Boosting Model
GEE	:	Google Earth Engine
GEPIC	:	GIS-based environment policy integrated climate
GIDA	:	Ghana's Irrigation Development Authority
GIS	:	Geographical Information System
GPS	:	Global Positioning System
GRD	:	Ground Ranged Detected
GVI	:	Green Vegetation Index
ha	:	Hectare
IDE	:	Integrated Development Environment
IRRI	:	International Rice Research Institute
IRS-1C	:	Indian Remote Sensing Satellite -1C
ISBA	:	Interactions between Soil, Biosphere, and Atmosphere)
ISRIC	:	International Soil Reference and Information Centre
IW	:	Interferometric Wide Swath
K	:	Potassium
K^1	:	Extinction coefficient
kg	:	Kilogram
km	:	Kilometers
L ha	:	Lakh hectares
LAI	:	Leaf Area Index
LCC	:	Leaf Chlorophyll Content

LISS-III	:	Linear Imaging Self Scanner-III
LTM	:	Landsat Thematic Mapper
LULC	:	Land Use /Land Cover
m	:	Meter
MAE	:	Mean Absolute Error
MAPE	:	Mean Absolute Percent Error
maxt	:	Maximum temperature
Mg	:	Magnesium
mint	:	Minimum temperature
MJ	:	Mega Joule
MJm^{-2}	:	Mega Joule per Meter square
ML	:	Machine Learning
MLC	:	Maximum Likelihood Classification
Mm	:	Milli meter
MODIS	:	Moderate resolution image spectro-radiometer
MSI	:	Multi-Spectral Imagery
n	:	Sample size
N	:	Nitrogen
NABARD	:	National Bank for Agricultural and Rural Development
NARP	:	National Agricultural Research Project
NASA	:	National Aeronautics and Space Administration
NASS	:	National Agricultural Statistics Service
NBSSLUP	:	National Bureau of Soil Survey and Land Use Planning
NDVI	:	Normalised Difference Vegetative Index
NIR	:	Near Infra-Red
NN	:	Neural Network
NOAA	:	National Oceanic and Atmospheric Administration
NOAA	:	National Oceanic and Atmospheric Administration
NRMSE	:	Normalised Root Mean Square Error
OLI	:	Operational Land Imager
OSAVI	:	Optimised soil-adjusted vegetation index
PAR	:	Photosynthetically Active Radiation
PE	:	Percent Error
pH	:	Potential of Hydrogen
PROSAIL	:	PROSPECT-D and SAIL radiative transfer models

PSO	:	Particle Swarm Optimization
PVI	:	Perpendicular vegetation index
QA	:	Quality Assurance
r	:	Coefficient of Determination
R^2	:	Coefficient of Correlation
radn	:	Solar radiation
RAEZ	:	Refined Agro-Ecological Zones
RF	:	Random Forest
RMSE	:	Root Mean Square Error
RMSEP	:	Root Mean Square Percent Error
RS	:	Remote Sensing
S1	:	Sentinel-1
S2	:	Sentinel-2
SAR	:	Synthetic Aperture Radar
SAVI	:	Soil Adjusted Vegetation Index
SAVI	:	Soil Adjusted Vegetation Index
SD	:	Standard Deviation
SI	:	Stress Index
SMO	:	Sequential Minimal Optimisation
SMT	:	Spectral Matching Technique
SOM	:	Soil Organic Matter
SPI	:	Spectral Vegetation Indices
sq.km	:	Square Kilometres
SR	:	Simple Ratio
SRI	:	System of Rice Intensification
SVM	:	Support Vector Machine
SVM	:	Support Vector Machine
SVM	:	Support Vector Machine
SWAP	:	Soil-Water-Atmosphere-Plant
SWIR	:	Short Wave Infra-Red
T ha	:	Thousand hectares
t_{av}	:	Annual Average Ambient temperature
TCARI	:	Transformed Chlorophyll in Reflectance Index
TIRS	:	Thermal Infra-Red Sensor
TMC	:	Thousand Million Cubic Feet

TOA	:	Top of Atmosphere
TWRIS	:	Telangana Water Resource Information System
UN	:	United Nations
USA	:	United States of America
USDA	:	United States Department of Agriculture
USDA	:	US Department of Agriculture
USGS	:	United States Geological Survey
USGS	:	US Geological Survey
VH	:	Vertical transmit and Horizontal receive
VI	:	Vegetation Index
VV	:	Vertical transmit and Vertical receive
WDVI	:	Weighted Difference Vegetation Index
WEKA	:	Waikato Environment for Knowledge Analysis
Y_o	:	Observed yields
Y_s	:	Simulated yields
σ°	:	Backscatter coefficient
τ	:	ratio of transmitted and incident PAR

Name of the Author	:	**G. SNIGDHA**
Title of the thesis	:	**RICE YIELD ESTIMATION USING REMOTE SENSING AND CROP SIMULATION MODEL IN NALGONDA DISTRICT, TELANGANA**
Degree	:	**MASTER OF SCIENCE IN AGRICULTURE**
Faculty	:	**AGRICULTURE**
Discipline	:	**AGRONOMY (WATER MANAGEMENT)**
Major Advisor	:	**Dr. GUMMA MURALI KRISHNA**
University	:	**PROFESSOR JAYASHANKAR TELANGANA STATE AGRICULTURAL UNIVERSITY RAJENDRANAGAR, HYDERABAD - 500030**
Year of submission	:	**2022**

ABSTRACT

A study on "**Rice yield estimation using Remote Sensing and crop simulation model in Nalgonda district, Telangana**" was carried out during *kharif*, 2021.

Precise and real-time agricultural yield data at the national, international and regional levels is becoming increasingly crucial for global food security. Crop yield forecasting could be very useful in advanced crop planning, strategy creation, and management. Because of the importance of yield prediction in food security, the present study used the APSIM-ORYZA model and remote sensing to estimate rice yield. The core objective of this study was to develop a method to integrate remotely sensed data and APSIM model for rice yield estimation in Nalgonda district, Telangana. This study includes mapping of rice growing areas and execution of APSIM model, followed by integration of remote sensing and crop simulation model for rice yield prediction and verification using government statistics.

Based on stratification, two villages, Telakantigudem from Kangal mandal and Mallaram village from Kattangoor mandal in Nalgonda district were selected and ten fields from each village were chosen for the study to collect the measured LAI values with the help of ceptometer in the fields and the crop management data from the respected farmers. Crop classification was performed on Sentinel-1 and Sentinel-2 time series data using a Random Forest (RF) classifier and ground reference points collected from field surveys in the Google Earth Engine platform. The results demonstrated an overall accuracy of 92% and a kappa coefficient of 0.85, and rice area was validated with the crop coverage report (kharif, 2021) provided by the Department of Agriculture (DOA), Telangana state showed a relative variation of -0.16%.

Remote sensing products like VV, VH AND VH/VV from Sentinel-1 and NIR, Red and NDVI from Sentinel-2 were derived using GEE and were calibrated with the measured LAI data collected from farmers' fields. The result showed that there was a

significant relation (R^2=0.78) between NDVI and field LAI and hence it was considered for integration with the crop model output. Maps were derived showing spatial variation in crop extent, and leaf area index (LAI), which are crucial in yield assessment.

Execution of APSIM-ORYZA model was done using the weather parameters, soil parameters, genetic coefficients and crop management data. The evaluation of the model with simulated yield and observed yield in the farmers' fields showed linear regression of R^2 = 0.79, root mean square error (RMSE)=804 kg ha^{-1} and mean absolute error (MAE)=728 kg ha^{-1}. The overall spatially averaged model yield for the district showed 4925 kg ha^{-1} which is deviated by 2% from the average yield in the government statistics with 5024 kg ha^{-1}. The study showed that by assimilation of remotely sensed data with the crop models, crop yields before harvest could be successfully predicted.

Chapter I

INTRODUCTION

Rice is one of the most vital food crops and considered as a primary food for over half of the world's population, particularly in Asia (IRRI, 2006), and its cultivation is a key source of income for many billions of people worldwide. The world's rapidly rising population is fed by limited land and input resources, while the expense of cultivation and poverty rises. As a result, more food production is required, particularly in the case of rice, which is consumed in greater proportions globally. India is the second largest rice producer and cultivator in the world. Rice accounts for 42% of total food grains and 45% of total cereal production in India (Nikitha *et al*., 2018). In *Kharif* 2021–22, acreage in India increased by 0.20% from 41.33 M ha to 41.41 M ha. Telangana escalated its land area by 0.382 M ha, which was 2.12 M ha, during the previous year to 2.50 M ha in 2021. Within the state, Nalgonda has around 0.186 M ha of rice area (AMIC. 2022).

The growth and development of rice crop is intensely affected by diverse environmental conditions, ensuing in significant disparities in crop yields from year to year. Hence, precise and instantaneous information on crop yields at national, international and regional scales is becoming gradually more essential for overcoming food security in the world (Basso *et al*., 2013). Accurate yield predictions help farmers to make informed economic and management decisions to support famine prevention efforts and advanced crop planning.

Remote sensing (RS) is essential in crop classification, crop monitoring, and yield estimation. RS data is required in the field for agronomical research since soil, climate, and other physicochemical changes are highly fragile. It is a technique that uses space-borne sensors to collect repetitive (from minutes to days) and synoptic (from local to regional coverage) data on the spectral performance of crops in a changing environment (soil and atmosphere). These methods are essential for timely monitoring because they provide an accurate image of the agricultural sector with a high revisit frequency and accuracy (Shanmugapriya *et al*., 2019). RS data can be used for a variety of applications, including yield prediction that use biophysical variables extracted from remote sensing data, crop inventory, crop yield estimates, drought monitoring, flood damage evaluation, pest and disease infestation, and irrigated land monitoring and control. (Kasampalis *et al*., 2018). Processing a significant volume of satellite pictures taken by numerous sensors is necessary in order to produce high resolution crop maps for vast areas (>10,000 sq. km).

Freely available satellite images for vast areas can be easily accessed and processed using the cloud infrastructure offered by the Google Earth Engine (GEE). Additionally, the GEE offers a collection of cutting-edge classifiers for pixel-based categorization that may be applied to crop mapping (Shelestov *et al*., 2017). Analysis of RS data alone or along with other ancillary data permits the determination of crop yield prior to the harvest period and provides information on crop status and health (through NDVI and LAI) for the estimation of potential crop yield (Gumma *et al., 2022*).

Crop growth models can be used to estimate the best planting dates and assess weather hazards for crop management and decision making (Van and Donatelli. 2003). It is also possible to use crop growth models to predict performance to introduce a new crop in a locality (Moorthy *et al*., 2004). Different crop models were used to analyse the potential effects of climate change on crop yields in different regions (Challinor *et al*., 2004, Watson *et al*., 2015, Lobell *et al*., 2006).

The application of crop growth models over the vast areas for monitoring crop growth or projecting crop production is hampered by a lack of geographical information regarding model inputs. Remote sensing and crop growth modeling are two independent technologies developed to solve several agronomic concerns at the field and regional levels (Batchelor *et al*., 2002). A lot of research has been attempted to estimate the agricultural output using a process-based crop growth simulation model and satellite data. Some examples of such research using different crop models are APSIM (Ziliani *et al*., 2018; Yang *et al*., 2021; Masjedi *et al*., 2018), Aquacrop (Jin *et al*., 2016; Jin *et al*., 2020), DSSAT (Li *et al*., 2020; Son *et al*., 2020), ORYZA (Setiyono *et al*., 2018; Setiyono *et al*., 2019) and Rice-Grow model (Wang *et al*., 2014).

Agricultural Production Systems Simulator (APSIM) is a software application that combines numerous sub-models (or modules) to simulate crop growth, soil processes, and various management options from the standpoint of cropping systems (Masjedi *et al.,* 2018). The APSIM-ORYZA model has been developed (Zhang *et al*., 2004) for the APSIM framework (Keating *et al*., 2003) based upon the original ORYZA2000 model. It enables rice metabolism, like photosynthesis, phonological development, and productivity, to be modelled in ORYZA2000 by utilising the present APSIM suite of modules for water, nitrogen, and other soil processes and management issues. This system feature enables the examination of a continuous cropping system, carry-over effects, and field management options. (Zhang *et al*., 2007).

The integrative method of remotely sensed data with crop simulation models has been progressively adopted for crop yield estimation because of the ability of satellites to attain information over an extensive coverage at a high revisit frequency. For this, LAI derived from satellite data is interpolated daily to offer daily observations that correspond to the interactive time-step of crop models. Better prediction can be achieved through models by considering the factors that affect crop growth and yield. Information such as meteorological and climate data (surface temperature, rainfall, etc.), soil properties and farming practices are combined with spatially explicit remote sensing derived information such as slope and vegetation indices (NDVI) to model crop growth and eventual estimation of the crop yield (Dorigo *et al.,* 2007).

Therefore, keeping the above facts in view and to make yield estimation more accurate and precise, the study entitled "Rice Yield Estimation using Remote sensing and crop simulation model in Nalgonda district, Telangana" was undertaken with the following objectives:

1. Mapping of rice-growing areas in the study area by applying a crop classification algorithm on satellite imagery.
2. Derivation of remote sensing-based products to integrate with crop model output.
3. Execution of a crop simulation model to calculate yields with various remote sensing derived inputs.
4. Integration of remote sensing data with crop model data to estimate optimised rice yields.
5. Verification of yield estimates obtained from crop model against government yield statistics.

<h1 style="text-align:center">Chapter II</h1>

<h1 style="text-align:center">REVIEW OF LITERATURE</h1>

Crop simulation models need a lot of inputs, such as crop parameters, soil properties, meteorological parameters, and crop-specific management techniques. The absence of enough spatial information regarding model inputs makes it difficult to apply crop models on vast regions to analyse crop growth conditions or forecast crop yield. Additionally, it has been demonstrated that remote sensing technology based on satellite data is capable of delivering crop characteristics and real-time information on circumstances altering as a result of different weather phenomena. The inclusion of remote sensing data in crop yield simulations for calibrating or changing the input parameters to assure that satellite observed and modelled conditions are the same has also been demonstrated in earlier field-scale investigations.

As a result, an effort was made to examine the accessible and relevant research findings that are directly or indirectly connected to the main concern. Keeping the current investigation's aims in view, the reviews have been collated and presented in this chapter under the six key headings:

2.1   Crop yield estimation

2.2   Mapping of Crop areas using classification algorithm on satellite images

2.3   Derivation of remote sensing-based products

2.4   Crop growth simulation model for rice yield estimation

2.5   Integrating Remote sensing derivatives with Crop simulation model

2.6   Verification of estimated yield

2.1 Crop yield estimation

Crop yield estimation is an important stage in planning for a district's or the entire nation's food security. Consequently, it is essential to be able to predict yields with some degree of precision before to harvest so that, if poor yields be foreseen, appropriate interventions can be implemented. Crop simulation models, remote sensing, machine learning algorithms, and other techniques may all be used to estimate crop yield.

In Sahibganj district, Jharkhand (India), during the 2017 rainy season, Ranjan and Parida (2019), mapped paddy acreage and yield estimation using sentinel-based

optical and SAR data. The paddy acreage mapping was prepared using a dependable machine learning Random Forest (RF) classification technique. A linear regression yield model was developed to forecast yields. The major conclusions showed that 68.3–77.8 T ha of paddy were present, based on Sentinel-1A and Sentinel-2B satellite data.

Filippi *et al*., 2019 developed a method to predict grain crop yield using machine learning (random forest models) and multi-layered, multi-farm data sets. Several big farms in Western Australia were employed as case studies for this work, and yield monitor data from wheat, barley and canola crops from three distinct seasons (2013, 2014, and 2015) that covered between 11,000 and 17, 000 ha per year were used. The results showed that the models' cross-validated predictions of yield had a root mean square error of 0.36 to 0.42 t ha^{-1} and a Lin's concordance correlation coefficient of 0.89 to 0.92 at the field resolution.

In order to predict the sugarcane yield grade of a farmer plot, Charoen-Ung *et al*., 2018 employed a RF based technique using the train dataset and test dataset of 8,765 records and 3,756 records, respectively, gathered from a group of sugarcane plots surrounding a sugar mill in Thailand. Their approach has a 71.88 % accuracy rate. This suggests that the suggested technique can be utilised to support decision-making for the operation planning of sugar mills.

In Faisalabad, Punjab, Pakistan, Ahmad *et al*., 2018 developed a method for yield forecasting of spring maize using remote sensing and crop modeling. In order to anticipate maize output using a crop model at farmers' fields, a field survey of 64 farms was done to gather information on the initial field conditions and crop management data. The CERES-Maize calibration and evaluation findings revealed a mean absolute percent error (MAPE) range for all recorded variables of 0.35 to 6.71 %. While remote sensing indicated an RMSE of 397 kg ha^{-1}, crop model yield predictions findings were accurate with an RMSE of 255 kg ha^{-1}.

Khanal *et al*., 2018 used high resolution remotely sensed data and machine learning approaches for the spatial prediction of soil characteristics and corn production. Multispectral aerial images and topographic data, both collected in 2013, were combined with field-based data on five soil properties (soil organic matter (SOM), cation exchange capacity (CEC), magnesium (Mg), potassium (K), and pH), as well as yield monitor-based corn yield data from seven fields at the Molly Caren Farm near London, Ohio. Five machine learning algorithms—RF, Neural Network (NN), Support

Vector Machine (SVM) with radial and linear kernel functions, Gradient Boosting Model (GBM), and Cubist (CU)—were used to construct models for the prediction of soil characteristics and maize yield. RF consistently outperformed other models and had greater accuracy for corn yield ($R^2 = 0.53$; RMSE = 0.97 t ha^{-1}).

Gandhi *et al*., 2016 used the WEKA (Waikato Environment for Knowledge Analysis) tool and a dataset of 27 districts in the Indian state of Maharashtra to demonstrate the prediction of rice crop yield using one of the machine learning techniques, and Sequential minimal optimization (SMO). The experimental findings demonstrated that alternative classifiers, including as Naive Bayes, BayesNet, and Multilayer Perceptron, outperformed SMO classifier, which had previously been claimed to have the lowest accuracy, sensitivity, and specificity for the same data set. The algorithm obtained 78.76 %, 68.17 % sensitivity, and 83.97 % specificity. The experimental findings demonstrated that alternative approaches performed significantly better than SMO on the same dataset.

Nain *et al*., 2004 developed a methodology using a crop simulation model and a discrete technological trend for yield forecasting for broad area and then applied to the coherent wheat yield variability zones of Eastern Uttar Pradesh, India. The outcomes demonstrated that this method could reasonably capture year-to-year variations in wide area wheat output. For the mean yield of 2.072 t ha^{-1}, RMSE between observed and projected yield was reported as 0. 098 t ha^{-1} (4.72 %). In contrast to the calibration period, the RMSE was somewhat greater during the forecasting period.

2.2. Mapping of Crop areas using classification algorithm on satellite images:

Panjala *et al*., 2022 assessed the performance of various supervised machine learning (ML) classifiers in the GEE platform and Spectral Matching Technique (SMT) using Sentinel-2 10 m satellite imagery in specific crop type classification for the year 2018-19 (rabi season) for Jhansi District using supervised classifiers like Random Forest (RF), Support Vector Machine (SVM), and Classification and Regression Trees (CART) The results showed the accuracy for RF was 81.8%, SVM was 68.8%, CART was 64.9%, and SMT was 88%. Results from the RF classifier were remarkably similar to those from the SMT classification map. The study found that RF classification beats other classifiers taken into account in the study.

Kpienbaareh *et al*., 2021 tested the ability to map crop kinds and land cover in two small-holder agricultural regions using Sentinel-1 (S-1) radar data, Sentinel-2 (S-2)

optical data, S-2 and PlanetScope data fusion, and S-1 C2 matrix and S-1 H/α polarimetric decomposition. For the categorization studies, they employed a random forest algorithm combined with data digitised from Google Earth Pro and DigitalGlobe. Overall accuracies (>85%) and Kappa coefficients (>0.80) were higher as a result.

Gumma *et al*., 2020a used a Spectral Matching Technique (SMT) approach based on temporal NDVI signatures and crop phenology to assess the capabilities and limitations of mapping cultivated areas in the *rabi* season and corresponding cropping patterns using Sentinel-2 Normalized Difference Vegetation Index (NDVI) 15-day time-series at 10 m resolution. The temporal signatures of wheat, chickpea, and mustard were easily distinguished, resulting in an overall accuracy of 84%, with wheat and mustard achieving 86% and 94% accuracy, respectively.

Hegarty-Craver *et al*., 2020 created a high-fidelity ground-truth dataset from imagery acquired by unmanned aerial vehicles, which included large mono-cropped fields, small intercropped fields, and natural vegetation. They collected the imagery in three rounds of flights at six different agro-ecological zones to capture growing conditions, and it was used to train and test a random forest model for classifying cropped land in Google Earth Engine using freely available Sentinel-1 and Sentinel-2 data. The model achieved an overall accuracy of 83% and a maize-specific accuracy of 91%.

Bazzi *et al*., 2019 used Sentinel-1 SAR, VV/VH polarisation data to map rice crops in the Camargue region of Southern France. Rice crop area was classified using decision trees and Random Forest (RF) classification algorithms. Each approach's classified rice crop map was validated using national data. The overall accuracy acquired using a conventional decision tree was 96.3 %, whereas the overall accuracy gained using the RF classifier was 96.6%. The results showed that using RF and decision together improves classification accuracy

Using Sentinel-1 data from two separate sites, Xu *et al*., 2019a developed a new classification technique to identify different crop growing zones in (i) Wuqing District and (ii) Fuju City, China. This method made use of multitemporal backscattering coefficients. To characterise the phenology information of the relevant crop, temporal models were developed from multitemporal intensities for each class. The overall accuracies were all above 90%, with the exception of Site-1's VV band result, which

had an overall accuracy of 89.74%, only 2.3% lower than the VH band. The overall accuracies of the VH and VV bands in Site-2 were extremely close, with both being about 90%.

In the Tamil Nadu district of Tiruvarur, the rice crop area was estimated using Sentinel-1A SAR satellite data utilising VV and VH polarisation (Raman *et al*., 2019). The rice area was assessed to be 91,007 ha in VV polarisation with an overall accuracy of 79.5% and 0.59 kappa index, while the rice area was estimated to be 91,007 ha in VH polarisation with an overall accuracy of 82.1% and 0.64 kappa coefficient. The lower accuracy in VV polarisation was related to an underestimation of the direct seeded rice area, while the underestimation in VH polarisation was due to an underestimation of the transplanted rice area.

RF and SVM classification methods were used to delineate rice crops using multi-temporal Sentinel -1 C-band SAR data. (Son *et al*., 2018). Overall accuracy and Kappa coefficient acquired by RF were 86.1% and 0.72, respectively, slightly higher than SVM (overall accuracy of 83.4% and Kappa coefficient of 0.67).

Using time series Sentinel-1 and Sentinel-2 data, Cai *et al*., 2019 established an RF approach for mapping paddy rice in China. The classification results showed overall accuracy and Kappa coefficient greater than 95% and 0.93, respectively and stated that this approach can offer technological assistance for mapping rice in regions with a lot of cloud and rainy weather.

Kenduiywo *et al*., 2018 demonstrated the utility of Sentinel-1 multitemporal data for crop-type mapping. They used the framework of dynamic conditional random fields (DCRFs), which provides a flexible, robust, and low-cost classification approach. They used an ensemble classifier to generate an optimal map based on posterior class probabilities estimated from the image sequence. When subjected to high-dimensional images with fewer training data, the result showed high accuracy when compared to MLC-stack.

Onojeghuo *et al*., 2018 explored the use of multi-temporal Sentinel-1A data and Landsat-derived NDVI data during the rice crop growing season (May to October) to map the geographical distribution of paddy rice fields throughout areas of the Sanjiang plain in Northeast China. To map paddy rice fields, SVM and RF machine learning classification algorithms were applied to a co-registered set of ten dual polarisation (VH/VV) SAR and NDVI images that show crop phenological development. When the NDVI time-series data were combined with the different multi-temporal polarisation

channel combinations (i.e., VH, VV, and VH/VV), the findings demonstrated a considerable improvement in the overall classification. The RF algorithm applied to combined multi-temporal VH polarisation and NDVI data yielded high overall accuracy (95.2%) and for rice (96.7%). The dual polarisation (VH and VV) SAR data alone provided the best results for the SVM classifier, with classification accuracy for rice of 91.6% and overall accuracy for rice of 82.5%.

Van Tricht *et al*., 2018 created a crop map for Belgium using Sentinel-1 radar and Sentinel-2 optical imagery. They achieved this by creating Sentinel-1 12-day backscatter mosaics after incidence angle normalisation and smoothing Sentinel-2 normalised difference vegetation index (NDVI) images to produce 10-daily cloud-free mosaics. Using an optimised random forest classifier, they predicted the eight crop types with a maximum accuracy of 82% and a kappa coefficient of 0.77. Their findings revealed that a classification based on a combination of radar and optical imagery always outperformed a classification based on single-sensor inputs, and that classification performance increased throughout the season until July, when crop type differences were greatest.

On Google Earth Engine, Xiong *et al*., 2017 developed a method for mapping agricultural extent using Sentinel-2 data in conjunction with Landsat-8 data (GEE) of 2015-2016 for the whole African continent. Random Forest (RF) was utilised as the primary supervised classification technique, while Support Vector Machine (SVM) was used when Random Forest overfitting concerns occurred due to noise in the input training data in specific locations. The map-derived cropland area results were compared to UN FAO statistics. The cropland class had an overall accuracy of 94 %, with a producer accuracy of 85.9 % and a user accuracy of 68.5%, according to an independent accuracy assessment. For the nominal year 2015, Africa's total net cropland area (TNCA) was estimated to be 313 M ha.

Gumma *et al*., 2011a mapped rice area for six South Asian countries using MODIS time series data for the period 2000 to 2001.They have used composite images from the MODIS sensor to produce rice maps and rice characteristics (e.g., intensity of cropping, cropping calendar) taking data for the years 2000 to 2001 and by adopting spectral matching techniques, decision trees, and ideal temporal profile data banks to identify and classify rice areas over large spatial extents. A fuzzy classification accuracy assessment for the 2000-2001 rice-map product, based on field-plot data, demonstrated

accuracies from 67% to 100% for individual rice classes, with an overall accuracy of 80% for all classes.

Oliphant *et al*., 2019 used 30-m (1 pixel = 0.09 ha) data from Landsat 8 Operational Land Imager (OLI) and Landsat 7 Enhanced Thematic Mapper (ETM+) in their study. They developed a code and run a pixel-based random forest (RF) supervised machine learning algorithm on the Google Earth Engine (GEE) cloud computing environment to separate croplands from non-croplands. For the South and Northern Asian Countries areas which included 7 refined agro-ecological zones (RAEZ), the overall accuracy was 88.1% with a producer's accuracy of 81.6% and user's accuracy of 76.7%. For each of the 7 RAEZs overall accuracies varied from 83.2 to 96.4%.

Gumma *et al*., 2014 showed how hyper temporal moderate-resolution image spectro-radiometer (MODIS) data may be used to map the seasonal rice crop extension and area. They carried out research in Bangladesh, where rice can be harvested once, twice, or three times per year. When compared to field-plot data, the rice versus non-rice maps were more than 90% accurate in all three seasons. During the boro season, MODIS-derived rice area estimates were 6% higher than sub-national statistics, 7% higher during the aus season, and 3% higher during the aman. For the boro, aus, and aman seasons, the MODIS-derived sub-national areas explained 9%, 9%, and 96% of the variability at the district level, respectively.

Gumma *et al*., 2020bxu used Landsat satellite time-series big-data and machine learning algorithms (MLAs) on the Google Earth Engine (GEE) cloud computing platform to create a high spatial resolution (30 m or greater) baseline farmland extent product for South Asia for the year 2015. According to the results, the South Asia agricultural product had a producer accuracy of 89.9%, a user accuracy of 95.3 %, and an overall accuracy of 88.7%. When compared to national statistics from South Asian countries, the national and sub-national (districts) areas estimated from this agricultural extent product explained 80-96 % variability.

Gumma *et al*., 2016 used MODIS 250 m time-series data to map rainfed and irrigated rice-fallow farmland areas across South Asia, identifying where the agricultural system may be strengthened by the addition of a short-season crop during the fallow period. The accuracy of the maps was assessed using independent ground survey data and compared to accessible sub-national statistics. The accuracy of the agricultural fallow groups was between 75 and 82 % for both producers and users. For

rice classes, the total accuracy and kappa coefficient were estimated to be 82 % and 0.79, respectively. According to the study, South Asia has roughly 22.3 million hectares of ideal rice-fallow land, with 88.3 % in India, 0.5 % in Pakistan, 1.1 % in Sri Lanka, 8.7% in Bangladesh, 1.4 % in Nepal, and 0.02 % in Bhutan.

Gumma *et al*., 2011b mapped irrigated agricultural areas as well as other land use/land cover (LULC) classes in Ghana using Landsat Enhanced Thematic Mapper (ETM+) data and time-series Moderate Resolution Imaging Spectroradiometer (MODIS) data. The irrigated classes' fuzzy classification accuracy varied between 67 and 93 %. A remote sensing-derived irrigated area (32,421 ha) was 20–57% larger than irrigated areas reported by Ghana's Irrigation Development Authority (GIDA).

2.3 Derivation of Remote Sensing-based products

Bhargav 2021 have derived Remote Sensing products like VV, VH, VV/VH using Sentinel-1 and NDVI using Sentinel-2 for differentiation of rice ecosystems in Jogulamba Gadwal district, Telangana. Results indicated that linear regression analysis performed between the LAI and maximum NDVI showed R^2 values of 0.869 for direct seeded rice and 0.79 for transplanted rice.

Fan *et al*., 2009 determined linear relation between NDVI and LAI and reported a correlation of 0.79, with the measured insitu NDVI and LAI values in semi-arid grassland in Inner Mongolia, China during the growing season in 2005 and 2006.

Goswami *et al*., 2015, investigated relationships between NDVI, Biomass, and LAI for six key plant species near Barrow, Alaska, and reported that NDVI was correlated with LAI with an R^2 of 0.70.

Clevers *et al*., 2017 used Sentinel-2 satellite images to test the hypothesis that LAI, leaf chlorophyll content (LCC), and canopy chlorophyll content (CCC) of a potato crop may be calculated using vegetation indices. For that, they calculated the WDVI using Sentinel-2 TOC spectral measurements to predict the LAI. Sentinel-2 results showed that the weighted difference vegetation index (WDVI) with bands at 10 m spatial resolution can be utilised to estimate the LAI (R^2 of 0.809; RMSEP of 0.36).

Xavier and Vettorazzi, 2004 investigated the link between Leaf Area Index and Spectral Vegetation Indices for different land covers in a subtropical rural watershed (in Piracicaba, State of Sao Paulo, Brazil), to use the best relationship to build an LAI map

for the watershed. Spectral Vegetation Indices produced from Landsat-7 ETMz data included the Simple Ratio (SR), NDVI, and Soil Adjusted Vegetation Index (SAVI). For all vegetation types, the LAI–SVI connections were comparable, and the prospective model provided the best fit. The LAI–NDVI correlation (R^2 0.72) was found to be statistically similar to the LAI–SR correlation (R^2 0.70). LAI–SAVI produced a poor correlation (R^2 0.56).

Rastogi *et al*., 2000 calculated the Leaf Area Index (LAI) for two wheat-growing regions in India (Karnal and Delhi) using data from the Linear Imaging Self Scanner-III (LISS-III) onboard the Indian Remote Sensing Satellite-1C (IRS-1C). In addition to red and near-infrared (NIR) readings above the vegetation canopy, the model only requires a priori crop specific attenuation constants. These constants for wheat were computed using published and field ground reflectance measurements. When applied to 36 fields using ground estimates of LAI, the model gave an RMSE of 1.28 and 1.07 for the Karnal and Delhi sites, respectively.

Campos-Taberner *et al*., 2018 compared and validated various LAI satellite products from operational services and customised solutions based on novel Earth Observation (EO) data such as Landsat-7/8 and Sentinel-2A. The comparison was made to evaluate the overall quality of LAI estimates for rice, which are used as a fundamental input in various scale (regional to local) operational crop monitoring systems, such as those developed as part of the "An Earth obseRvation Model based RicE information Service" (ERMES) project. In all seasons, the results revealed good consistency between Landsat-7/8 LAI estimations and ground measurements, with high correlations (R^2 0.89) and low root mean squared errors (RMSE 0.75).

Future directions for enhanced evapotranspiration modelling: Assimilation of remote sensing data into crop simulation models and SVAT models has been researched by Olioso *et al*., 2005. They calculated LAI from NDVI using microwave data and then incorporated the information into ISBA and ISBA-Ags (Interactions between Soil, Biosphere, and Atmosphere) (Ags holds for net assimilation and stomatal conductance). ISBA-Ags simulations were also corrected using the estimated LAI from NDVI. The simulated LAI was compared to the NDVI-estimated LAI over the course of the soybean crop cycle. Results showed that the use of remote sensing data to correct the time variation of LAI had only a minor effect on LAI values as well as ET and water

reserve simulations. In the case of the entire rectification, ET outcomes improved marginally.

Ines *et al*., 2013 developed a data assimilation-crop modelling framework that uses sequential data assimilation to include remotely sensed soil moisture and leaf area index (LAI) into a crop model. They employed the MODIS leaf area index (LAI). They processed LAI from 2003 to 2009 for testing and assessment of the data assimilation-crop modelling system. Assimilation of MODIS-LAI resulted in a minor improvement in simulated yields compared to the open-loop simulation ($R^2 = 0.51$), including a tiny reduction in a systematic error.

2.4 APSIM-ORYZA for Rice Simulation

Biswas *et al*., 2021 studied the effect of transplanting date on (consumptive water footprints) CWFs of paddy by using field experimental data and APSIM-ORYZA for Kharagpur, West Bengal State of India. In *kharif* and *rabi* of 2015–2016 and 2016–2017, medium duration rice variety (IR–36) was chosen and grown using AWD and CON (convential) irrigation techniques while utilising the current transplanting dates (i.e. 16 July in *kharif* and 14 January in *rabi*). The impact of different transplanting dates on paddy yield, ETC, and CWFs predicted, demonstrated that AWD practise saved 22-29% more seasonal water than CON practise at a cost of 2-4% lower output. The grain production predicted calibration was found to be closely matched with the observed for both CON and AWD practises (R2=0.96, RMSE=400 kg ha^{-1}).

Radanielson *et al.,* 2018 used the APSIM model and Oryza V3 to see the effect of salinity on rice growth and grain yield. It has been concluded that both the models resulted in good accuracy for simulating biomass, LAI, and grain yield. Variability of simulated yield under stressed and non-stressed conditions showed an RMSE, of 191 kg ha^{-1} and 222 kg ha^{-1}, respectively, for ORYZA v3 and APSIM-Oryza where these values were inbound with the experimental results. These findings reveal that model can be used for simulating yields under different scenarios.

Amarasingha *et al.,* 2015 used the APSIM model to simulate crop and water productivity under diverse agro-climatic conditions and different water management methods (rainfed with supplemental irrigation) in Srilanka. Results reveal that the model simulated grain yield with an R^2 of 0.97 and RMSE 484 kg ha^{-1}. When the onset of rainfall is delayed, crop modeling scenarios using the validated APSIM model showed an increased dependence on supplementary irrigation for rice cultivation.

Alternatively, in years when an early onset was observed, late planting in the season reduced the use of rainwater by 95% while increasing the irrigation water requirement by 11% compared with planting at rainfall onset.

Fernanado *et al*., 2015 validated the APSIM-ORYZA module for two long duration rice varieties, Bg403 and Bg379-2 (4months maturity). The results shown a strong fit (R^2 of 0.88 and 0.77, respectively, and CV of 9.9% and 14.4%, respectively) for observed rice yield and and claimed that yield was lower when grown under rainfed conditions than under irrigation for both kinds.

Subhash *et al*., 2015 examined the APSIM model's capability to simulate the impacts of various irrigation regimes on yield, irrigation water requirement, and irrigation water productivity (WPi) of rice, wheat, and RW (rice-wheat) system in upper-gangetic plains of India. Long-term simulated wheat yields showed a lesser dropping trend at an average rate of 48 kg ha-1 yr^{-1} ($R^2 = 0.48$, p<0.05), and long-term simulated rice yields showed a continuously declining trend at an average rate of 120 kg ha^{-1} yr^{-1} ($R^2 = 0.94$, p<0.05). The RW system with the rice irrigation regime (IR) of 8 days of alternating wetting and drying (AWD) and five irrigations for wheat with a yield penalty of 25.5% showed the greatest WPi of 8.31 kg ha^{-1} mm^{-1}.

Kumar *et al*., 2014 used the APSIM agricultural simulation model to investigate the effect of transplanting dates on rice production and water productivity in Faizabad, located in the middle Indo Gangetic Plains (IGP). Using soil, crop, and meteorological data from the research site, the model was initially parameterized for the study site. The calibrated model was then used to simulate yield and water productivity for six possible transplanting dates over an 11-year period. Based on the findings of the simulation, 10 June was determined to be the best day to transplant rice in Faizabad due to the crop's greater yield, lower coefficient of variation (CV), and higher water productivity on that day compared to alternative delayed transplantation dates.

Suriadi *et al*., 2009 used rice-rice-soybean crop sequence data from a field experiment conducted at the Assessment Institute for Agricultural Technology, Indonesia in 2007-2008 to evaluate the efficacy of APSIM-ORYZA with and without nitrogen limitation. N fertiliser was administered at three rates to rice: 0 kg N ha^{-1} (F0), 70 kg N ha^{-1} (F1), and 140 kg N ha^{-1} (F2), as well as three rates for soybean: 0 kg N ha^{-1} (S1), 12 kg N ha^{-1} (S1), and 24 kg N ha^{-1} (S2). From the results, it was showed that the model accurately predicted the dynamics of crop variables (phenological phases, yield, and biomass), soil

factors, and water variables (ponded water depth, pH, temperature and daily infiltration rate). For both the first (wet) and second (dry) rice seasons, simulated biomass resembled the pattern of rice growth when nitrogen was not a limiting factor (F2), with minor over-prediction under both F1 and F0 treatments.

Zhang *et al*., 2007 used APSIM to know the effect of different nitrogen levels and transplanting time on yields. The model predicted yields were compared with the observed yields. Results show an RMSE of 242 kg ha^{-1}. It has been concluded that model results were acceptable for simulating different varieties in a continuous rice cropping system over the long term.

2.5 Integrating Remote sensing derivatives with Crop simulation model

Clevers *et al*., 1996 employed optical and microwave remote sensing data for crop growth monitoring and estimated LAI using a basic reflectance model from optical data and a simple backscattering model from radar data for sugarbeet crop. To calibrate the crop growth model to actual growing circumstances, the remote sensing models were inverted to get LAI estimations during the growing season for using it in calibrating the crop model to actual growing conditions. Results showed that simultaneous optical and radar observations did not increase estimations of LAI over optical data alone.

Hong *et al*., 2004 estimated leaf area index (LAI) as a function of image-derived vegetation indices, and compared measured and estimated LAI to crop model simulation results during the 2001 growing season in two central Missouri experimental fields, one with corn (Zea mays L.) and the other with soybeans (Glycine max L.) (Glycine max L.). The CERES-Maize and CROPGRO-Soybean models were calibrated using measured soil moisture and yield data and then used to replicate LAI throughout the growing season. At all corn monitoring sites, the CERES-Maize model over-predicted LAI. For most soybean monitoring sites, simulated LAI using CROPGRO-Soybean was similar to observed and image-estimated LAI. The results suggested that crop growth model predictions might be improved by incorporating image-estimated LAI.

Bouman (1995) developed two methods for combining remote sensing data with crop growth models. In the first, optical remote sensing-derived estimates of light interception (ground cover, LAI) are utilised as a forcing function in the models. Crop growth models are augmented with remote sensing sub-models in the second method, which simulates time-series of optical and radar remote sensing signals. The crop

growth model is re-calibrated to match simulated with observed remote sensing data once these simulated signals are matched to measured signals. The suggested methods improved the accuracy of wheat and sugar beet crop growth and yield simulations.

Fang *et al*., 2011 integrated MODIS LAI and vegetation index products with the CSM–CERES–Maize model for corn yield estimation in Indiana, USA. The remotely sensed data was used to build the CSM–CERES–Maize model's parameters. Results indicated that the predicted corn yield correlated very well with the US Department of Agriculture (USDA) National Agricultural Statistics Service (NASS) data. The best results were obtained when both the MODIS vegetation index and the LAI products were used, and the relative deviations from the NASS data were less than 3.5%.

By integrating field, weather, and satellite data with crop simulation models, Milesi *et al*., 2022 calculated yields of bajra and rice at Gram Panchayat scale in Firozabad district of Uttar Pradesh and Kendujhar district of Odisha, respectively. In both crops, a comparison of modelled yields with CCE yields revealed that the model performed well (rice: R^2 = 0.80, root-mean-square error (RMSE) = 411 kg ha^{-1}, mean absolute error (MAE) = 359 kg ha^{-1}, percent error (PE) = 7, observed mean = 1500 kg ha^{-1}; Bajra: r = 0.84, RMSE = 309 kg ha^{-1}, MAE = 262 kg ha^{-1}, PE = -1).

Muslim *et al.*, 2015 used a GIS-based environment policy integrated climate (GEPIC) model to estimate paddy rice yield at the regional level. According to the simulated yield, the projected production is 4305.55 kg ha^{-1}. Plains crop cultivars such as Jhelum, K-39, Chenab, China 1039, China-1007, and Shalimar rice-1 had an average yield of 4783.3 kg ha^{-1}. Meanwhile, yields of 4102.2 kg ha^{-1} were obtained in high altitude locations using cultivars such as Kohsaar, K-78 (Barkat), and K-332. The measured and simulated yields matched well, with R^2=0.95 and RMSE=132.24 kg ha^{-1}, respectively.

Zhao *et al*., 2020 tested the potential for indices derived from Sentinel-2 data to estimate dryland wheat yields at the field scale and the potential for enhanced predictability by incorporating a modelled crop water stress index (SI) with the observations taken from 103 study fields over the 2016 and 2017 cropping seasons across North-eastern Australia. Vegetation indices derived from Sentinel-2 showed moderately high accuracy in yield prediction and explained over 70% of the yield variability. The model combined with optimized soil-adjusted vegetation index (OSAVI), Chlorophyll (CI) and Stress index (SI) generated a much higher correlation, with R^2 = 0.91 and RMSE = 0.54 t ha^{-1}. When validating the models on an independent set of fields, this model also showed high correlation (R^2 = 0.93, RMSE = 0.64 t ha^{-1}).

Tripathy *et al*., 2013 attempted to include remotely sensed input data into the mechanistic crop simulation model World Food Studies (WOFOST) for in-season wheat yield forecasts in India's Punjab state. The leaf area index (LAI) produced from remotely sensed data was utilised to forecast spatial yield in the WOFOST simulation model. LAI was calculated from AWiFS NDVI data using an empirical model developed with the assistance of ground observations (Nigam et al. 2007). Using a correction factor, LAI from remotely sensed data at a near-peak vegetative stage was put into the model (Chaudhari *et al*. 2010). Results showed that all growth parameters' values decreased after forcing. The LAI was lowered from 5.7 to 2.7 m^2 and the above-ground biomass from 6 to 3 t ha^{-1}. The actual yield per grid was determined using these modifications to simulated growth factors.

Jing-Feng *et al*., 2002 created a new model (Rice-SRS) that is based on the ORYZA1 model and modified to accept remote sensing data from various sources. The model is capable of accepting three types of NDVI data: NOAA AVHRR (LAC) - NDVI, NOAA AVHRR (GAC) - NDVI, and radiometric measurements - NDVI. The integration of NOAA AVHRR (LAC) data and the Rice-SRS simulation model resulted in correct estimations for rice yield in the Shaoxing area, with the estimated error reduced to 1. 027 %, 0. 794 %, and (-0.787 %) for early, single, and late season, respectively. Using NDVI data from NOAA AVHRR (GAC) as input in Rice-SRS can result in a good estimate of rice production with an average inaccuracy (- 7.43%).

Doraiswamy *et al*., 2005 evaluated the quality of the MODIS 250 m resolution data for retrieval of crop biophysical parameters that could be integrated into crop yield simulation models. The spatial distribution of LAI was done across the study area (McLean County, Illinois, USA) over three stages of crop development of corn and soybean to estimate the simulated yields of the model across the study area. Results showed by comparing model yield results with NASS/USDA reported county level yields showed that the distribution of model yields was within an acceptable range of the reported yields computed from statistical ground sampling at the state level.

Doraiswamy *et al*., 2004 monitored vegetation changes that are used indirectly to assess crop condition and yields at the field level using LANDSAT and MODIS. The spatial distribution of LAI was done to estimate yields across the Walnut Creek watershed, Ames and Iowa. Results showed that the mean of simulated yields for corn was lower than reported yields by about 3% and soybean yields were higher by 6.6% compared to NASS reported yields.

Satya Priya and Ryosuke Shibasak, (2001) have simulated spatial crop yield using GIS-based crop production model spatial EPIC model developed from EPIC (Erosion productivity Impact Calculator) model. Spatial distribution of productivity was done across India. Yield simulation of the rainfed maize varied from 0.4 to 3.5 t ha^{-1}. The difference between the reported and simulated means was smallest for Rice than the wheat and greatest for maize.

Yongqiang Zhang and Martin Wegehenkel (2006), integrated MODIS data into a simple model for the spatially distributed simulation of soil water content and evapotranspiration. The good performance of the model was documented by comparing the measured and simulated discharged rates and analyzing the correlation between ET$_a$ rates and LAI in the Ucker catchment in Northeastern Germany.

Muslim *et al*., 2015 estimated paddy rice yield at the regional level using GIS-based environment policy integrated climate (GEPIC) model. The simulated yield showed that estimated production to be 4305.55 kg ha^{-1}. The crop varieties like Jhelum, K-39, Chenab, China 1039, China-1007, and Shalimar rice grown in plains recorded average yield of 4783.3 kg ha^{-1} Meanwhile, high altitude areas with varieties like Kohsaar, K-78 (Barkat), and K-332 recorded yield of 4102.2 kg ha^{-1} The observed and simulated yield showed a good match with R^2=0.95, RMSE=132.24 kg ha^{-1}, respectively.

2.6 Verification of the estimated yield

Setiyono *et al*., 2019 methodology of SAR data incorporation into crop yield simulation and comprehensive validation of yield forecast and estimates in the Tamil Nadu, India. Remote sensing data assimilation into a crop model effectively captures the responses of rice crops to environmental conditions over large spatial coverage, which otherwise is practically impossible to achieve. A process-based crop simulation model is used in the system to ensure that climate information is captured, and this provides the capacity to deliver a mid-season yield forecast for national planning and policy for rice. In this case, SAR-based yield estimates for the 2014–15 Samba season ranged from 3.12 to 3.87 t ha^{-1}, with NRMSE against official yield statistics of 15% and RMSE of 552 kg ha^{-1}.

Srilatha (2020) calculated the acreage and production of soybean crops in Telangana's Nizamabad district. The validation results revealed that the yield was strongly associated with ground-observed yield data, with a coefficient of determination (R^2) value of 0.93, and with a high RMSE of 567 kg ha^{-1}.

Son *et al*., 2016 developed a methodology to incorporate remotely sensed data into a crop simulation model (DSSAT) for estimating rice yield in Taiwan. Using the particle swarm optimization (PSO) technique, the data assimilation was processed to incorporate biophysical characteristics into the DSSAT model for estimating rice yield. Results of the yield estimation were when compared to the government's yield statistics showed the RMSE of 11.7% and the mean absolute error of 9.7 %, respectively.

Chapter III

MATERIAL AND METHODS

This chapter deals with the details of the study area, remote sensing techniques, description of the Crop Simulation Model (CSM) and its application in yield estimation. The details of materials used and the methodology adopted for the Estimation of Rice yield in the Nalgonda district of Telangana state are described below:

3.1 GENERAL DESCRIPTION OF THE STUDY AREA

3.1.1 Experimental Site and Location

Telangana state is located on the Deccan Plateau and is bordered to the north by Maharashtra, to the northeast by Chhattisgarh, to the northwest by Karnataka, to the west by the Rayalaseema area, and the southeast by the coastal Andhra region. The region is drained by two main rivers, the Godavari and Krishna, as well as minor rivers including the Bhima, Manjira, and Musi. The climate is primarily hot and dry and falls under a semi-arid region.

The Nalgonda District lies in the southern part of the Telangana region between 16º25' N & 17º50' N and 78º40' E & 80º05' E. It has the highest number of mandals in the state i.e., 31 in total. The borders of the district were covered by Suryapet, Sangareddy, Yadadri, and Nagarkurnool districts, and the state boundary of Andhra Pradesh. The geographical area of the district is 7,122 sq. km. It is representative of the southern plateau and hills under India's agro-climatic zone. Approximately 75% of the population depends directly or indirectly on Agriculture in the Nalgonda district. Paddy and cotton are two major growing crops with a net irrigated area of 76000 ha.

3.1.1.1 Selection of villages and farmers: Two major paddy cultivating mandals i.e, Kanagal and Kattangoor were selected in Nalgonda district as study areas that explicit the conditions of Nalgonda district. They were selected based on the previous season's rice crop map, the soil map with the data taken from NBSSLUP, and the Rainfall map which was constructed using the 20 years of rainfall data from USGS Earth Explorer for the Nalgonda district. These maps were analysed and two rice-growing mandals were selected having low and high rainfall under Alfisols. The Mandal Agriculture Officers of respective mandals, Kangal and Kattangoor helped in the identification of Telakantigudem village in Kangal and Mallaram village in Kattangoor (Fig 3.1). From each village, 10 paddy cultivating farmers were selected randomly which are at a distance

of a minimum of 200 m, so that no two fields can collide into a single pixel in the satellite image. Thus, total sample size of 20 has been considered for the study.
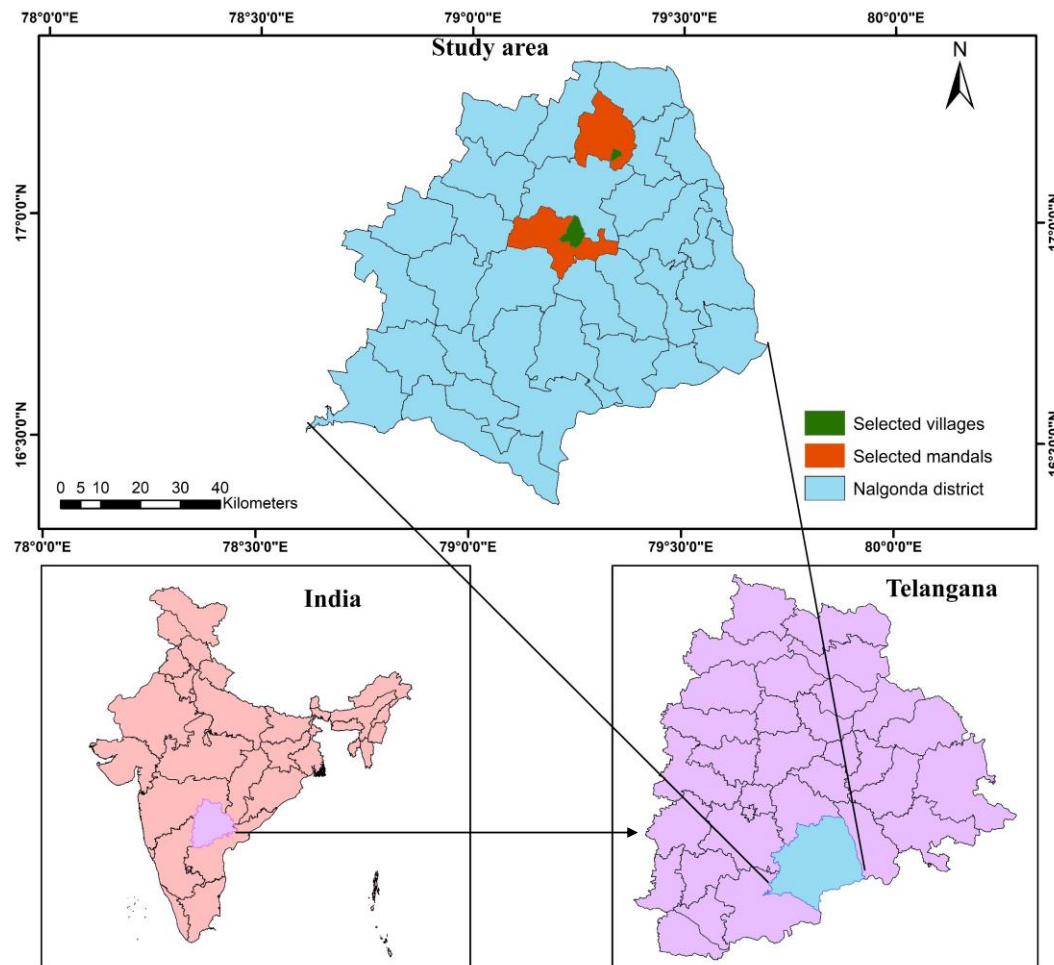
Fig 3.1 Study area map representing the selected villages in the Nalgonda district

3.1.2 Climate and Weather conditions

In Nalgonda, the wet season is oppressive and overcast, the dry season is humid and mostly clear, and it is hot, year-round. Over the years, the temperature typically varies from 17.2°C to 40°C and is rarely below 14.4°C or above 43.3°C.

The average annual rainfall of the district is 751 mm, which ranges from 2.0 mm in February to 171 mm in July. Fig 3.2 represents the soil map of Nalgonda districts generated with 20 years of rainfall data from USGS Earth Explorer (https://e4ftl01.cr.usgs.gov/MOLA/MYD13Q1.006/)

. The rainfall for the 2021 *kharif* crop period for Kangal and Kattangoor Manda are shown in Fig 3.3 respectively where Kanagal mandal showed more amount of rainfall than Kattangoor mandal.
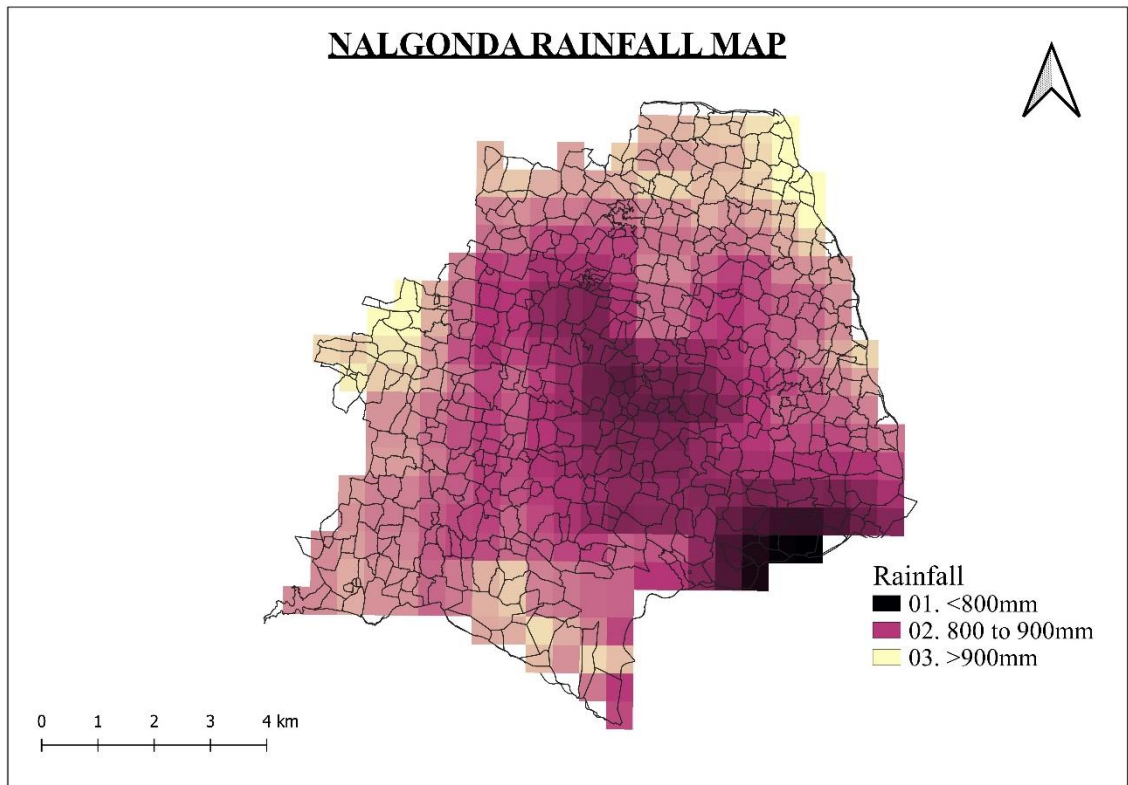
Fig 3.2. Rainfall map of Nalgonda district using 20 years data from USGS Earth Explorer
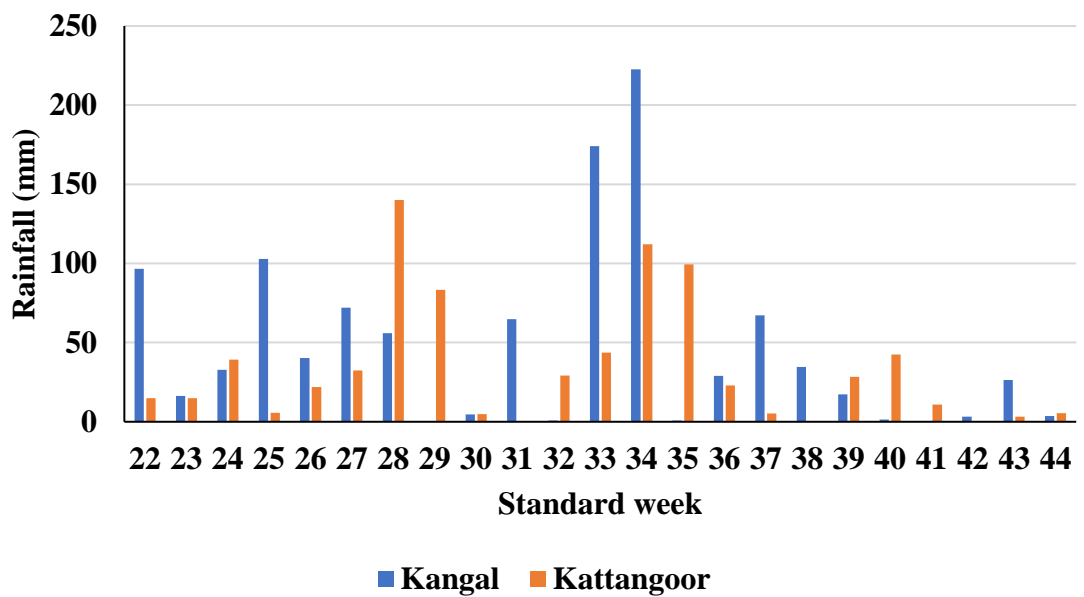
Fig 3.3. Rainfall distribution of Kangal and Kattangoor for standard week

3.1.3 Soils of Nalgonda

The soil comprises red soil, black soil, alkaline soil, and alluvium. The red soil constitutes 85 % of the area. Black soil is found over the limestone area, in the southeast part. Alkaline soil occurs as limited patches in the central part. Alluvial soil occurs along Alair, Musi and Kargal rivers. Soil map prepared using the
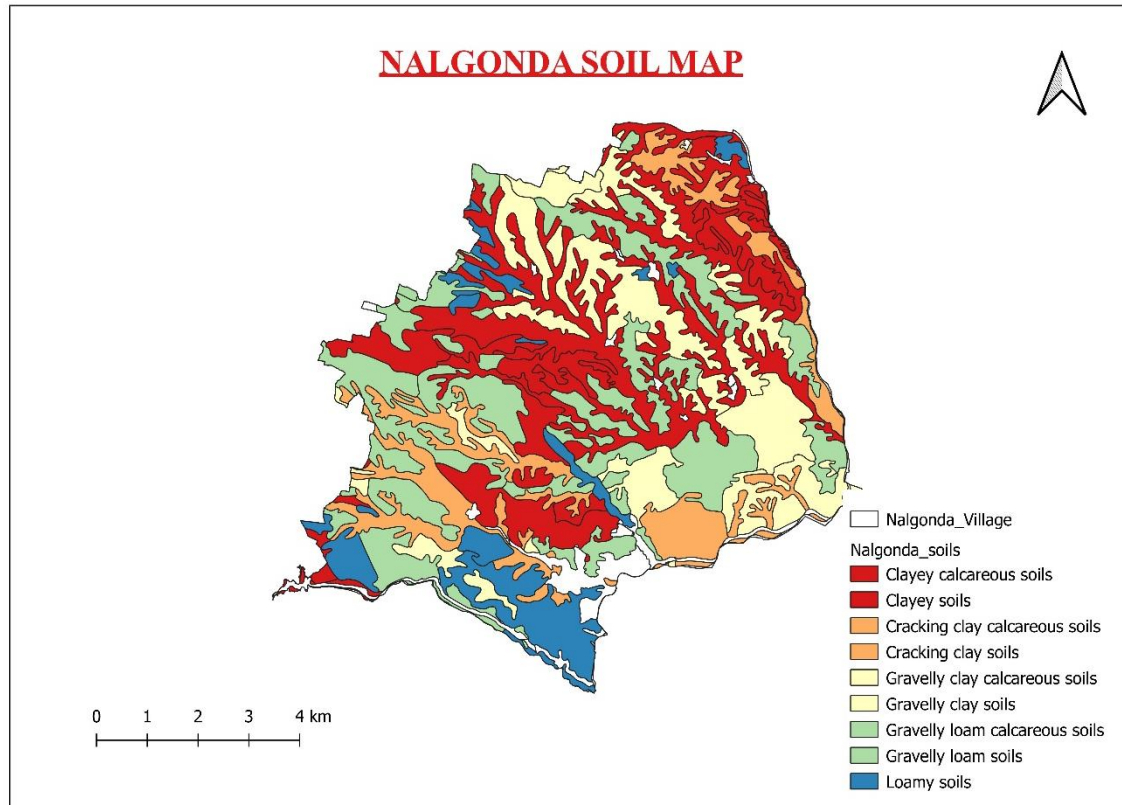
Fig 3.4. Soil map of Nalgonda using NBSS&LUP data

3.2 INSTRUMENTS USED

3.2.1 Ceptometer LP-80

The AccuPAR LP-80 Ceptometer (Plate 1) is a portable and lightweight instrument with a group of Photosynthetically Active Radiation (PAR) sensors for the measurement of the leaf area index (LAI). It allows the user to measure canopy intercepted PAR and accurately calculates LAI at any site within a plant canopy. The in-built PAR sensor in AccuPAR LP-80 measures above and below canopy PAR simultaneously to estimate the intercepted PAR. The ceptometer can be operated in clear, partly cloudy, or overcast sky conditions to get accurate PAR and LAI data. It can also function with temperatures from - 30ºC to 50ºC, and relative humidity up to 100%. The LP-80 uses the Eq. (1) to calculate LAI:

$$L = \frac{\left[\left(1 - \frac{1}{2K}\right)fb - 1\right]ln\tau}{A(1 - 0.47fb)}$$

(3.1)

Where K = extinction coefficient

f_b = beam fraction (ratio between diffuse and beam radiation)

A = leaf absorptivity

τ = ratio of transmitted and incident PAR

Ceptometer LP-80 was used for recording the LAI and also above and below canopy PAR readings for rice crop fields in the 20 fields.

Plate 1. AccuPAR/LAI Ceptometer

3.3 SOFTWARE USED

3.3.1 Arc map 10.7.1

ESRI®ArcMap is the application for creating and altering geographic and tabular data, in addition to mapmaking and map-based analysis. Shapefiles, coverages, and geodatabases can all be edited with ArcMap's single-user interface. ArcMap includes advanced, CAD-based editing capabilities that allow rapidly and efficiently creating features while retaining the spatial integrity of the GIS information.

In this study, Arc Map was used for mapping the spatial distribution of LAI and yields by integrating remote sensing and the APSIM model with the spatial analyst tool and also used for calculating the zonal statistics.

3.3.2 ERDAS IMAGINE 16.5.1

ERDAS IMAGINE is a raster-based programme that is simple to use and is intended primarily to extract information from images. In this study, ERDAS IMAGINE was used for the accuracy assessment of the rice classification.

3.4 Google Earth Engine Platform

GEE is a computing platform that allows users to run geospatial analysis on Google's infrastructure. The GEE computing engine supports both JavaScript and Python application programming interfaces (APIs), allowing developers to quickly create algorithms that run in parallel on Google's data processing systems. Data from Landsat 4, 5, 7, and 8 processed by the US Geological Survey (USGS), many MODIS products, including global composites, recent imagery from Sentinel-1, 2, and three satellites, and much more may be found in the GEE.

The Code Editor (code.earthengine.google.com) is a web-based IDE (Integrated Development Environment) for writing and running scripts. The components of the Code Editor are illustrated in Plate 2.

In this study, GEE was used for mapping rice growing areas in the Nalgonda district by using a supervised classification algorithm and for deriving remote sensing products for integrating with the APSIM-Oryza model output.
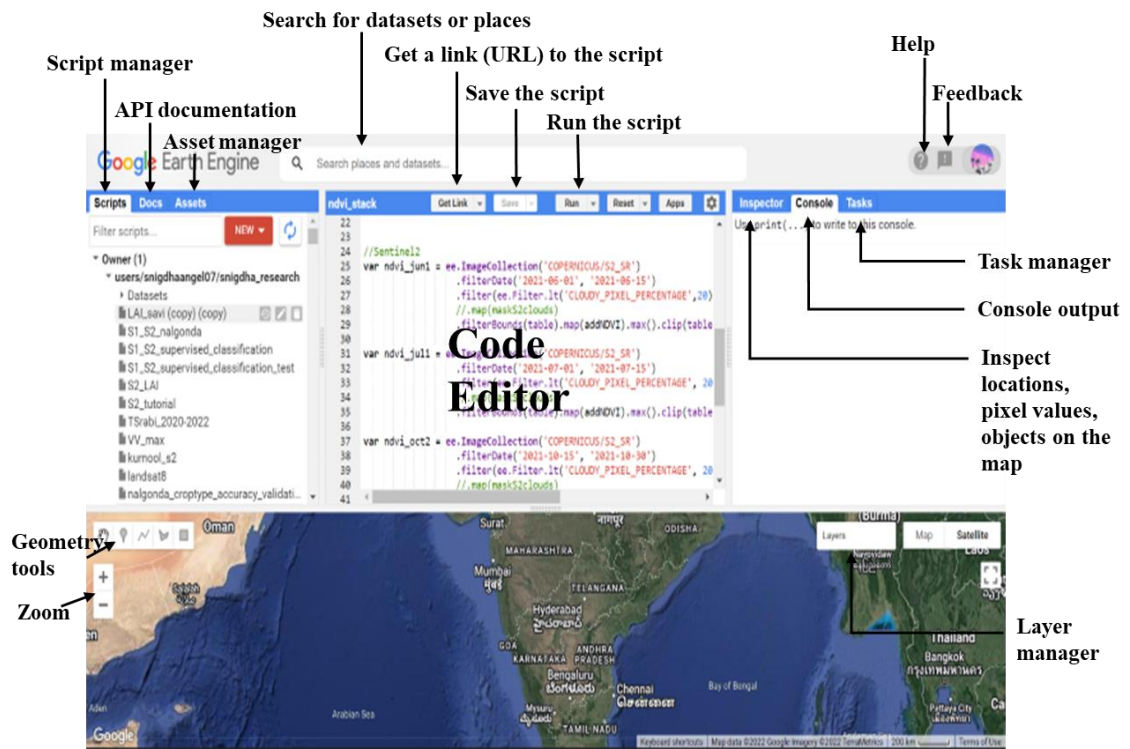
Plate 2. Components of the Google Earth Engine Code

3.5 Satellite Data Used

The satellite images used in this study were derived in GEE using coding. The sensor specifications of Sentinel-1 and Sentinel-2 are shown in Table 3.2

Table 3.1. Specifications of Sentinel-1 and Sentinel-2

	Sentinel-1	Sentinel-2
Spectral range	3.75-7.5 cm	0.47-0.6 µm
Resolution	5×20 m	10, 20, 60 m
Orbital altitude	693 km	786 km
Sensor complement	C-SAR	MSI
Wavelength	1cm to 1mm	1 micron

3.5.1 Sentinel-1

Sentinel-1 data have the advantages of being all-weather capable, having a high spatial resolution (up to 10 m), and being publicly available, which makes them valuable for mapping non-rice crops as well when there is a lack of optical data identification (Jain *et al*., 2019; Milesi and Kukunuri, 2022). The default acquisition of Sentinel-1(SAR) data was done in Interferometric Wide swath (IW) mode in dual-polarization. VV and VH bands (vertical transmit/vertical receive—VV and vertical transmit/horizontal receive— VH) of the Sentinel-1 (GRD) data in Interferometric Wide Swath (IW) mode were used for this study.

3.5.2 Sentinel-2 Data

Sentinel-2 (S2) is a mission for wide-area, high-resolution, multispectral imagery, with a global 5-day revisit frequency. It offers information useful for determining the condition and change of the plant, soil, and water cover. A time series of monthly maximum NDVI for the months of June to October 2021, cloud-screened, was created using data from Sentinel-2 bands 4 (red wavelength) and 8 (NIR wavelength), both at 10-m spatial resolution. The cropland mask created from the supplementary data was improved in the study district using the monthly Sentinel-2 NDVI data.

NDVI: Normalized Difference Vegetation Index (NDVI) is a vegetation index computed using red and Near Infrared (NIR) bands, which indicates the greenness of a pixel. It varies between -1 and +1, with values closer to +1 indicating high greenness. For practical applications, NDVI values greater than 0.3 indicate the presence of vegetation. The NDVI product is used to separate crops from non-crop. Normalized Difference Vegetation Index (NDVI) was calculated using Eq. (3.2).

$$NDVI = (NIR - Red) / (NIR + Red) \qquad (3.2)$$

3.6 Simulation Model Used: APSIM

The Agricultural Production Systems Simulator (APSIM) dynamic simulation model is capable of predicting the growth and productivity of plant species based on plant genetics, environmental conditions, and management practices (Masjedi *et al*., 2018).

The APSIM framework allows a detailed specification of farmer management practices, decision-trees, and the simulation of associated soil water and salinity dynamics, together with the interactions between rice and other crops, allowing for a much broader assessment of cropping system performance which can be provided by ORYZA V3 (Radanielson *et al*., 2018).

APSIM -Oryza is a model for rice growth simulation that has been increasingly employed in related studies due to the widely established APSIM platform (Amarasingha *et al.,* 2015; Gaydon *et al.,* 2017; Holzworth *et al.,* 2014; Radanielson *et al.,* 2018). APSIM-crop Oryza's growth process was inspired by the Oryza2000 model (https://sites.google.com/a/irri.org/oryza2000/, Bouman *et al.,* 2001; Bouman and Van Laar, 2006; Li *et al.,* 2017, Keating *et al*., 2003). The model's primary goals are to accurately replicate rice growth and development while also addressing major management issues such as fertilization, transplanting times, and field management procedures. It enables rice physiology, including photosynthesis, phenological

development, and yield, to be modeled in ORYZA2000 while utilizing the existing APSIM suite of modules for water, nitrogen, and other soil processes and management challenges. This system feature enables the examination of a continuous cropping system, carry-over effects, and field management options (Zhang *et al*., 2007).

3.6.1 Input Data for the Simulation Model

Basic biophysical data- These data are required to parameterize the model and allow it to run. These include basic weather, soil, and crop parameters, as shown in Table 3.2.

Table 3.2. Input data and their variables for simulation model (APSIM-ORYZA)

Input data	Variables
Site data	Longitude (East or West), Latitude (North or South) and Altitude (m).
Weather data	Solar radiation (MJm^{-2}) daily maximum and minimum temperature (°C), annual average ambient temperature (t_{av}, °C), and annual amplitude in mean monthly temperature (amp, °C).
Soil data	Soil pH, soil organic carbon, soil texture, coarse fragments, cation exchange capacity, bulk density, field capacity, wilting point, texture, and hydraulic conductivity
Crop data	Variety, genotype coefficient
Management data	Fertilizer application rate (e.g., N, P, K), irrigation date and amount, cropping calendar (e.g., sowing and harvesting times), plant population, transplanting date, and row spacing

3.7 METHODOLOGY

The methodology used to evaluate the performance of APSIM in estimating the Rice yield in the Nalgonda district is divided into five sections:

1. Mapping of rice-growing areas in the study area by applying crop classification algorithm on satellite imagery.
2. Derivation of remote sensing-based products to integrate with crop model output.

3. Execution of crop simulation model to calculate yields with various remote sensing derived inputs.

4. Integration of remote sensing data with crop model data to estimate optimised rice yields.

5. Verification of yield estimates obtained from crop model against government yield statistics.

3.7.1 Ground truth data collection

Field visits were planned and conducted according to the time of satellite pass and weather conditions. The ground truth points were collected for mapping rice areas using supervised classification in GEE. A total of 107 ground reference points were collected. GPS points were taken in each field and LAI values were recorded by using Ceptometer. Fig 3.5 depicts the ground reference points collected for mapping rice cultivated areas.

3.7.1.1 Farmers Interview: Farmers' interview (Plate 3) was conducted during the visits to the farmers' fields. A questionnaire (Appendix A) was followed for every farmer with the details like the name of the farmer, contact number, area of rice cultivated, the previous crop cultivated, variety of rice, soil type, soil nutrient status, date of transplantation, irrigation and its source, amount and type of fertilizer applied, pest and disease, date of harvesting and yield obtained. The field IDs were given as T1 to T10 for the village Telakantigudem and M1 to M10 for the Mallaram village represented in Plate 4.

As represented in Table 3.3, at Telakantigudem village out of 10 farmers 8 farmers cultivated MTU-1010 variety and the other two farmers have sown KNM-118 and BPT-5204. The transplanting dates ranged from 24 July to 3 August 2021. The rate of nitrogen applied ranged from 120 to 160 kg ha^{-1}. The observed yield recorded from the farmers varied mostly between 4500 to 6500 kg ha^{-1}.

In Mallaram village as denoted in Table 3.4, different cultivars were sown like MTU-1010, IR-64, JGL-24423, BPT 5204, and RNR-15048. The transplantation was done between 20 July and 9 August. The rate of nitrogen applied ranged from 115 to 180 kg ha^{-1}. Recorded yield data from the farmers varied from 3600 to 6100 kg ha^{-1}.

Plate 3. Interaction with the farmers for the collection of crop management data
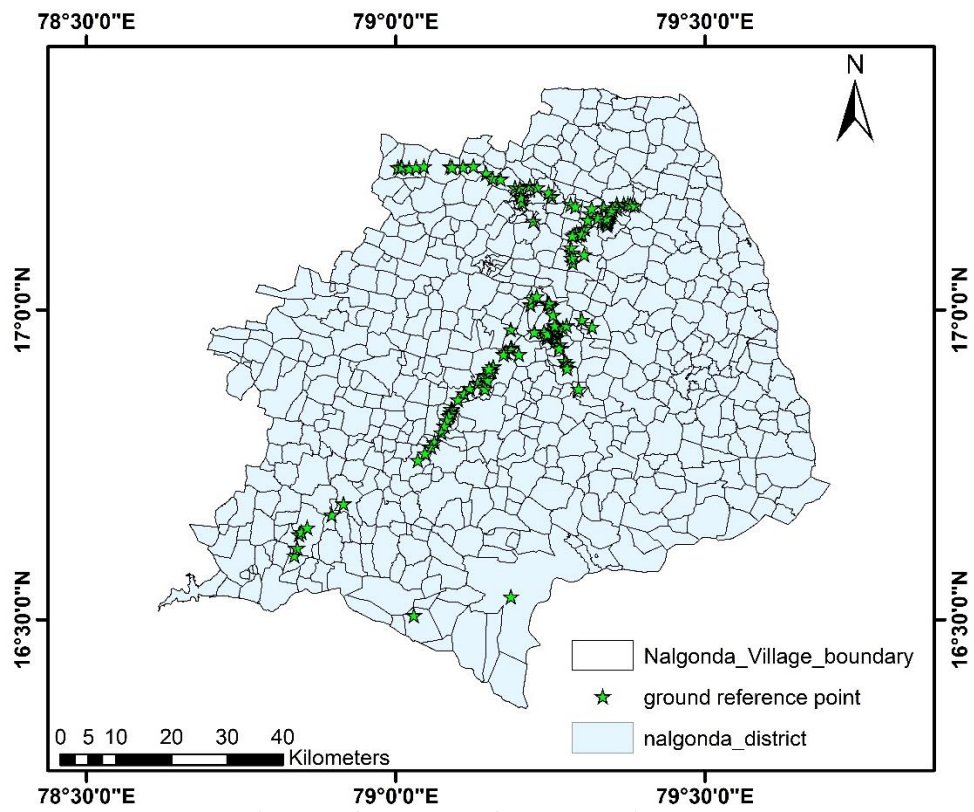
Fig 3.5. Ground reference points collected

Table 3.3. Ground truth data collected at Telakantigudem village during the field visits

Field-ID	Variety	DOT	Nitrogen applied (kg ha^{-1})	Observed yield (kg ha^{-1})
T1	MTU 1153	27 July 2021	127	6500
T2	MTU 1010	30 July 2021	160	5500
T3	MTU 1010	24 July 2021	128	6000
T4	MTU 1010	3 Aug 2021	160	3600
T5	MTU 1010	1 Aug 2021	120	5300
T6	MTU 1010	24 July 2021	122	5800
T7	KNM 118	30 July 2021	108	4500
T8	MTU 1010	30 July 2021	108	4600
T9	MTU 1010	30 July 2021	124	5100
T10	BPT 5204	24 July 2021	140	6300

Table 3.4. Ground truth data collected at Mallaram village during the field visits

Field-ID	Variety	DOT	Nitrogen applied (kg ha^{-1})	Observed yield (kg ha^{-1})
M1	MTU 1010	25 July 2021	127	4400
M2	IR 64	27 July 2021	115	6100
M3	JGL 24423	24 July 2021	180	4600
M4	BPT 5204	20 July 2021	130	4400
M5	MTU 1010	24 July 2021	100	4500
M6	RNR 15048	4 Aug 2021	160	3800
M7	MTU 1010	3 Aug 2021	160	4100
M8	MTU 1010	27 July 2021	130	3920
M9	BPT 5204	9 Aug 2021	122	3600
M10	BPT 5204	24 July 2021	130	3650
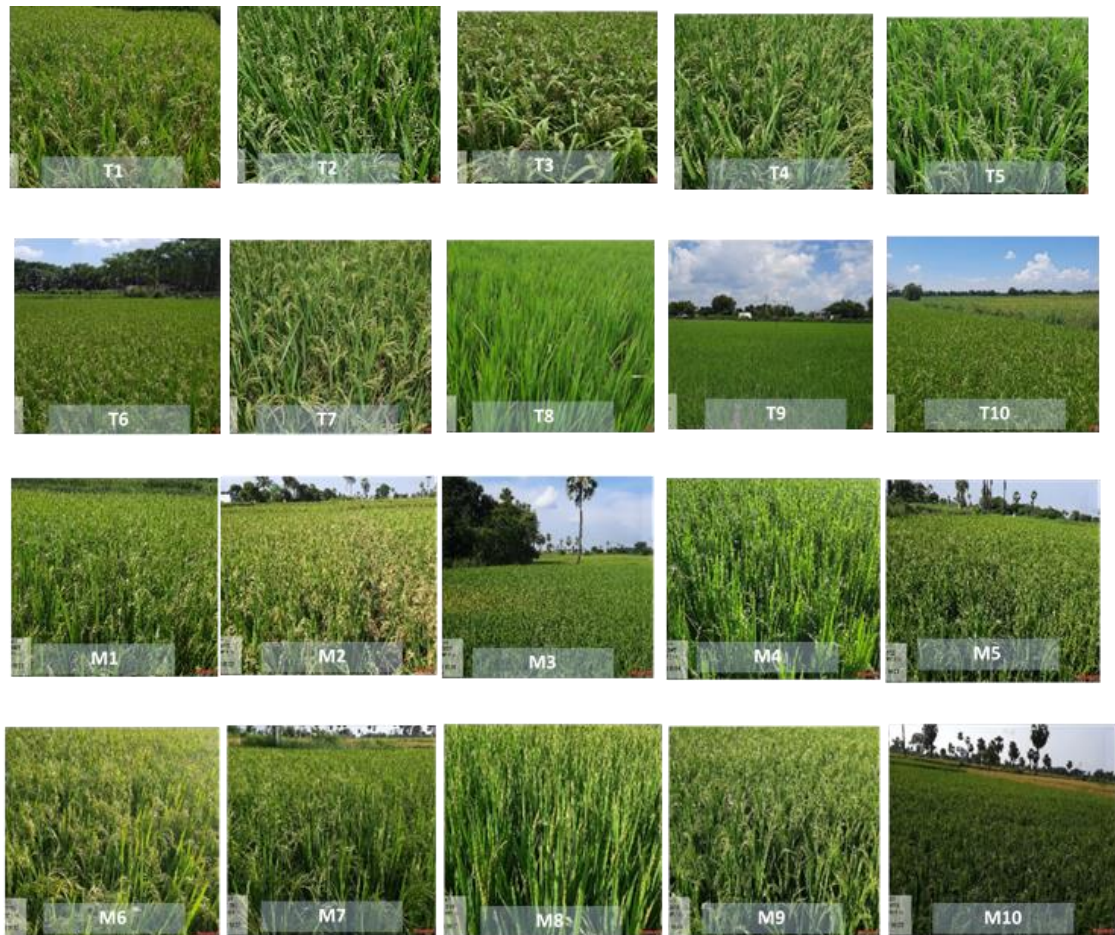
Plate 4. Images of the selected fields in the study area

3.7.1.2 Measuring LAI with Accupar LP-80 Ceptometer

LAI was estimated using Accupar LP-80 Ceptometer placing it above and below the plant canopy at two points in every field. The average of the values is considered the main value of the field. The readings were taken when PAR is above 400 nm as the Ceptometer cannot calculate LAI under PAR below 400nm. LAI values were recorded at two visits on Oct-8th and Oct-26th when the crops were under panicle initiation to maturity stage. Plate 6 represents the points of the fields in which ground LAI data was recorded. The factory-calibrated external PAR sensor was utilized to calibrate the LP-80 probe before each measurement session, guaranteeing that the PAR response between the external sensor and the probe is the same. To lessen the impact of unintentional leaf movements four readings were taken at each position (Pokovai *et al*., 2019). Locations were chosen with the intention that the row direction would not coincide with the direction of the sun at that time of day. Plate 5 represents the images of recording field LAI using a Ceptometer.

Plate 5. Field LAI recorded in the selected fields at Telakantigudem and Mallaram villages.
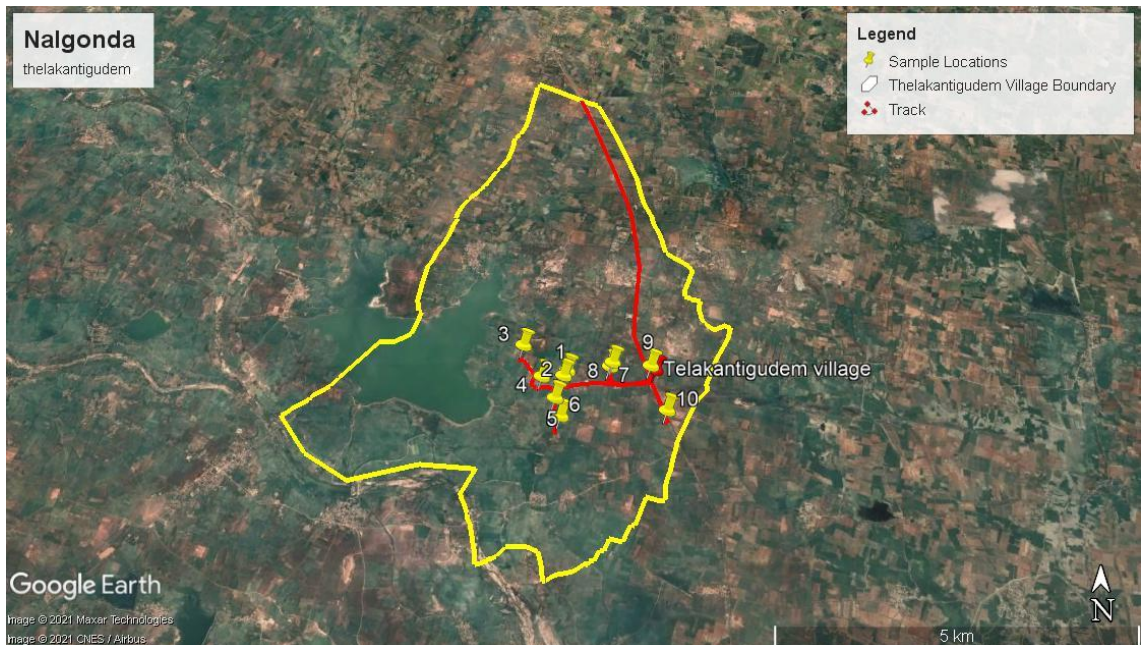
Plate 6. Nalgonda LAI Ground Data Collection

3.7.2 Mapping of Rice growing areas

The methodology used for the classification of rice growing areas is represented in Fig 3.6. GEE was chosen to process and classify the Sentinel-2 and Sentinel-1 data

because the quality of S-2 data is assured with cloud masks and user-friendly functions for image processing and classification. Moreover, the main advantage of GEE is its cloud computing capability which reduces the need for the user to have hardware and software capabilities. Table 3.5 demonstrate the satellite data and their bands used in the study.
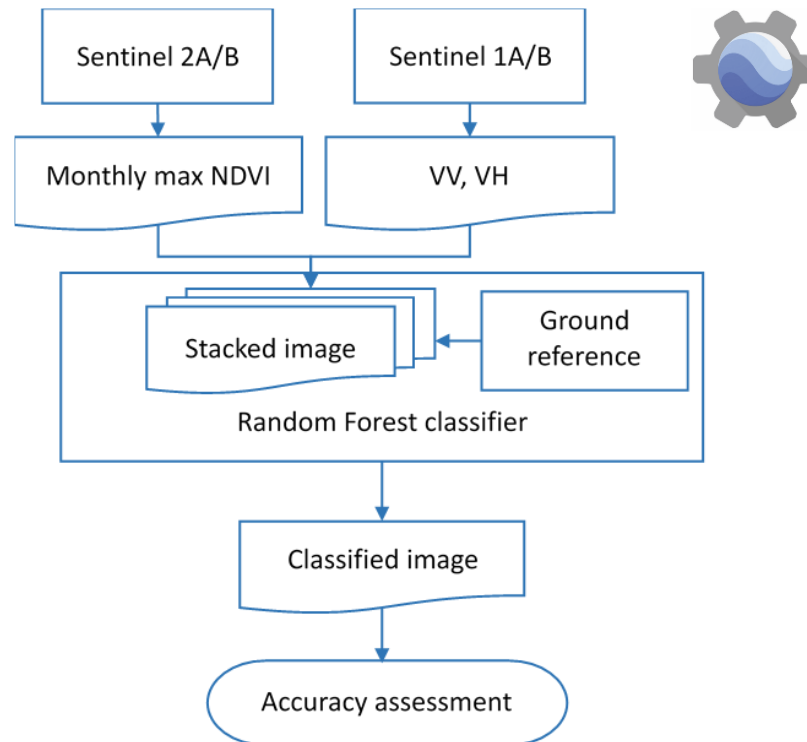
Fig 3.6 Schematic diagram showing the methodology for rice area estimation using GEE

The procedure for mapping of rice areas for *kharif,* 2021 in the Nalgonda district by combining Sentinel-1 and Sentinel-2 data has been adapted as shown in Fig.3.7 (Milesi and Kukunuri, 2022). GEE was used for satellite data processing and classification (Gumma *et al*., 2020, Gumma *et al*., 2022). The collection of Sentinel-1 of GEE provides data from a dual-polarization C-band Synthetic Aperture Radar (SAR) instrument. Imagery in the Earth Engine 'COPERNICUS/S1_GRD' Sentinel-1 ImageCollection consists of Ground Range Detected (GRD) scenes processed to backscatter coefficient ($\sigma°$) in decibels (dB). VV and VH of Sentinel-1 and NDVI of Sentinel-2 were derived and stacked. The stacked composite image was passed through a supervised classification by giving the training data with 107 ground reference points which were pointed in Google earth, were given and an RF classifier was used. Accuracy assessment was carried out using the ground truth data for the RF algorithm.

Table 3.5. Satellite data and their bands with their importance used in the study

Satellite imagery	Bands	Spatial resolution(m)	Importance
SENTINEL-1	VV and VH	5×20	Helps to quantify the variability in the temporal dynamics of the crop
SENTINEL-2	Band4 (Red)	10	helps in classifying the vegetation
	Band8 (NIR)	10	

3.7.2.1 Random Forest Classifier: Random Forest, as the name implies, is a classifier that uses several decision trees on different subsets of the provided dataset and averages them to increase the dataset's predictive accuracy. Instead of depending on a single decision tree, the random forest uses forecasts from each tree and predicts the result based on the votes of the majority of predictions. Higher accuracy and overfitting are prevented by the larger number of trees in the forest. It takes less training time as compared to other algorithms. It predicts output with high accuracy, even for a large dataset it runs efficiently. It can also maintain accuracy when a large proportion of data is missing.

3.7.2.2 Accuracy assessment: Accuracy assessment is an essential step in the processing of remote sensing data. It determines the user's information value of the resultant data. The overall accuracy of the classified image is determined by comparing how each pixel is classified to the definite land cover conditions acquired from the ground truth data. Producer accuracy is a measure of how well real-world land cover types can be classified. The likelihood of a categorized pixel matching the land cover type of its corresponding real-world location is measured by the user's accuracy (MacLean and Longalton, 2012). The kappa's coefficient and error matrix have become basic means of evaluation of image classification accuracy**.** In this study, accuracy assessment was performed using ERDAS IMAGINE, which uses an error matrix.

3.7.3 Derivation of RS-Based Products to Integrate with Crop Model Output.

Sentinel-1 data was used for deriving RS products like VV, VH, VH/VV and Sentinel-2 data for deriving Band 8 (NIR), Band 4 (Red) and NDVI. These products were derived using javascript code in GEE by applying the filter date according to the visit dates made to the field which were planned as per the satellite passing dates. These products were compared to the field LAI to examine the correlation. Among these

products, based on their correlation to the field LAI, NDVI was used for deriving the spatial LAI map by integrating with the model output.

3.7.4 Execution of APSIM Model

The APSIM user interface is organized into four panels: a main toolbar at the top, a simulation tree on the left that lists all the components in the loaded file, a module properties pane on the right, and a bar at the bottom that lists available toolboxes.

Based on daily climate data (solar radiation, maximum and minimum temperatures, rainfall), APSIM-Oryza can simulate soil water, C, and N dynamics and their interactions within crop/management systems. In response to various environmental factors such as solar radiation, temperature, nitrogen fertilizer management, and soil water content, the APSIM-Oryza simulates biomass production, rice phenology, nitrogen accumulation, leaf area development, and yield (Bouman *et al*., 2001, Zhang *et al*., 2004).

3.7.4.1 Preparation of Weather File or Met File

The met file (Plate 7) must contain a minimum of three constants: latitude, t_{av} (annual amplitude in mean monthly temperature), and amp (annual average ambient temperature). A year and day column, solar radiation (MJm^{-2}), the maximum and minimum temperatures ($° C$), and rainfall were also required in the met file. The headings for these columns were used as year and day (or date), radn, maxt, mint, and rain. In this study rainfall data for 1 year (2021) from the AWS located in the Kattangoor and Kanagal mandals of the Nalgonda district were acquired separately. The minimum and maximum daily temperatures, and solar radiation were taken from NASA Power (https://power.larc.nasa.gov/data-access-viewer/). The annual average ambient temperature was calculated by averaging the maximum and minimum temperatures of the day and annual amplitude in mean monthly temperature was obtained by averaging the mean daily temperature of each month over the entire data period resulting in twelve mean temperatures and then subtracting the minimum of these values from the maximum. t_{av} is obtained by averaging the twelve mean monthly temperatures. (https://www.apsim.info). The file was initially prepared in EXCEL, where it was saved as a Formatted Text (Space delimited) (*.prn) file with the .met file extension.

3.7.4.2 Simulation of transplanted rice under ponded conditions

a) Pond Depth

To simulate the ponded conditions Pond depth component was applied to the manager folder (from "Rice Management Toolbox" -> Rice-> "Manager (Pond depth)". In that component, the start date for ponding was given as the transplanted date and the end date as ten days before the harvesting date for all the 20 farmers' field conditions.

b) Soil Water and SOIL N module

The soil water module necessitates soil bulk density, saturated water content, soil water at field capacity and wilting point in the soil layers that make up the profile, crop-specific parameters that determine root extension. SOILN includes pH, organic carbon, electric conductivity EC, CEC, and exchangeable sodium percentage. These were edited as per the data collected from ISRIC 2.0 with 250 m as shown in Table 3.6. The soil component window is represented in Plate 9.

c) Cultivar file generation

For adding new cultivars, the "ini" component was used from the Standard Toolbox under the Structural folder onto the crop module. A new cultivar was created by copying and pasting the cultivar in the document next to the current cultivar. The cultivar's name was changed to recorded cultivars sown from the farmers and the genetic coefficients were given as per Swain *et al*., 2007 considering the long and medium duration varieties of rice grown and maintaining document's XML structure.

d) Rice Transplant Aman

Rice transplant Aman (from "Rice Management Toolbox" -> Rice-> "Manager (Rice-Transplant Aman)" was the component used in APSIM-ORYZA for simulating the crop sown during June to July. This component requires the information such as start and end of sowing dates, duration of seedbed, number of plants on hills, fertiliser type and amount of fertiliser at transplanting as shown in Plate 8.

e) Fertiliser Application

Fertilise on growth stage component was added to the Manager Folder (from "Rice Management Toolbox" -> Rice-> "Manager (Fertilise on growth stage)". Split application of nitrogen was adopted based on the data recorded from the respective farmers at three stages of rice, at the time of transplanting, end of juvenile (DVS=0.4), and at the panicle initiation stage (DVS=0.65).

f) Generating Output file

In the output component, output variables that were needed for the study such as biomass, LAI and yield were added and the frequency of output was selected as harvesting time and also as daily. The simulation was saved and executed the model by clicking on run option at the top of the interface. Plate 10 shows the sample of output file generated in APSIM.

Table 3.6. Input variables and parameters for major physiological processes simulated in APSIM-ORYZA

Simulation	Input variables and parameters	Source	Module
Phenology	Meteorological data: daily max. and min Temp, rainfall, solar radiation	Automatic Weather Station and NASA Power	'Oryza' module in APSIM
Soil water balance and soil nitrogen supply	Water availability in soil profiles	Default values in APSIM	'SoilWat2' module in APSIM
	Soil N supply is determined from the ground truth data from the farmers	Farmers	'Oryza' module in APSIM
Irrigation, fertilizer application, and other field management	Irrigation (depth of ponding water), application levels of nitrogen fertilizer, and transplanting dates	Farmers	Oryza module in APSIM
Physical and chemical properties of soil	Bulk density, pH, soil organic carbon, Electric conductivity, cation exchange capacity	ISRIC 2.0 (https://www.isric.org)	Apsoil module in APSIM
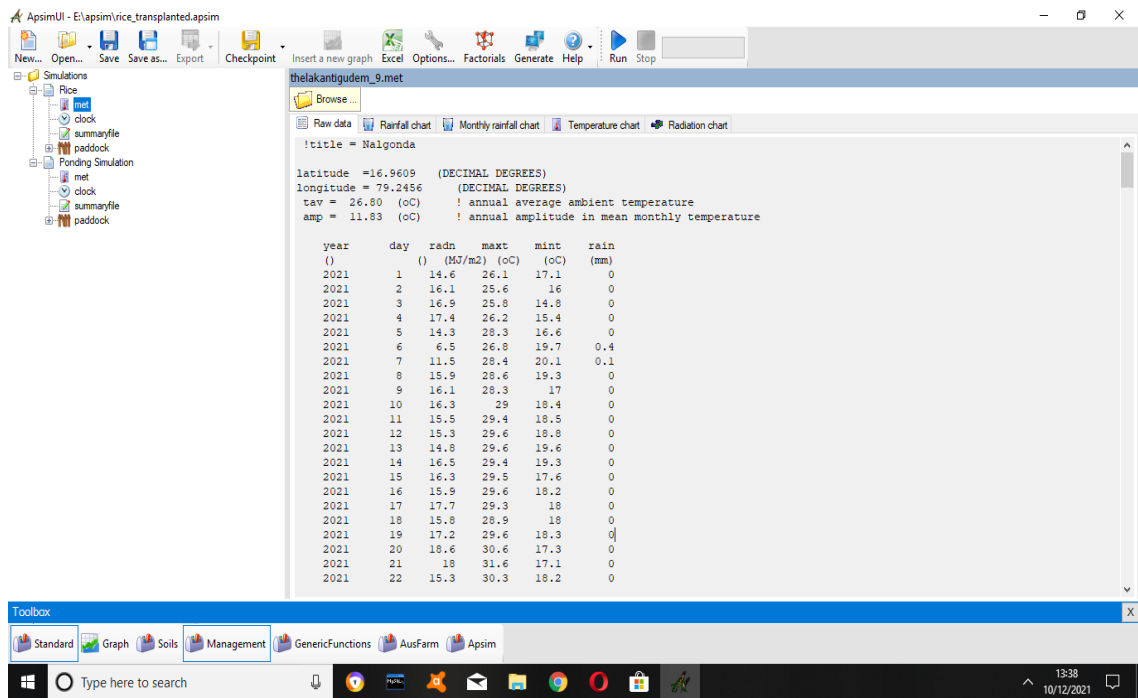
Plate 7: A sample of the weather file in the APSIM model
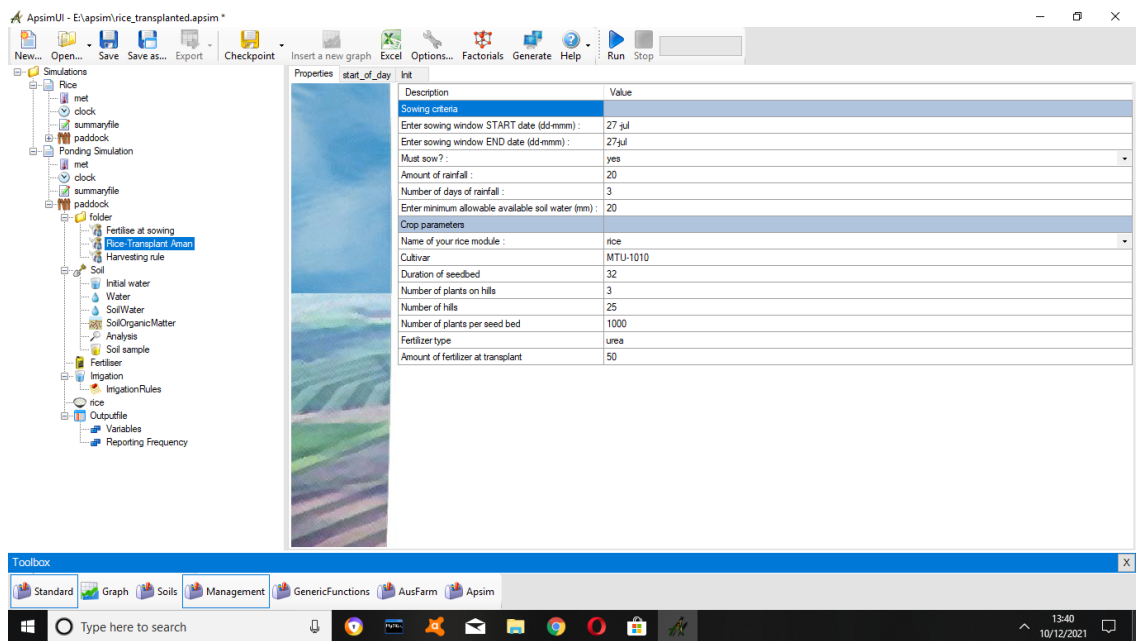
Plate 8: Window showing the details of transplanted rice component in APSIM model
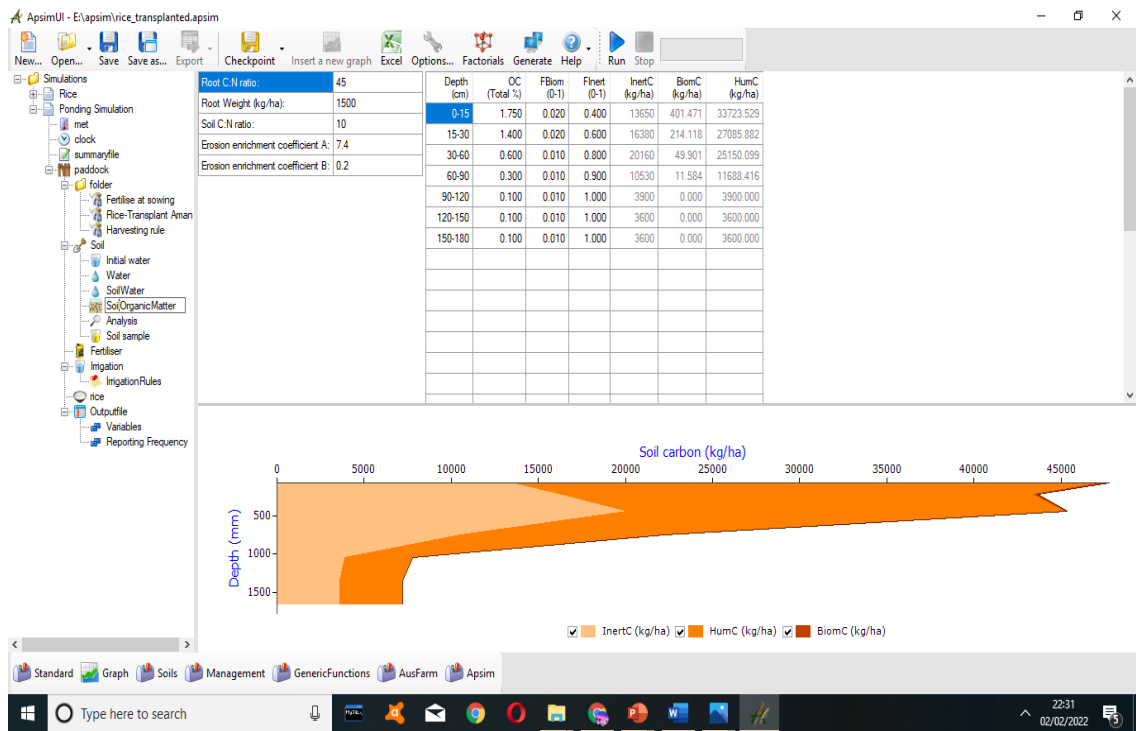
Plate 9: Window showing the details of soil component file in APSIM
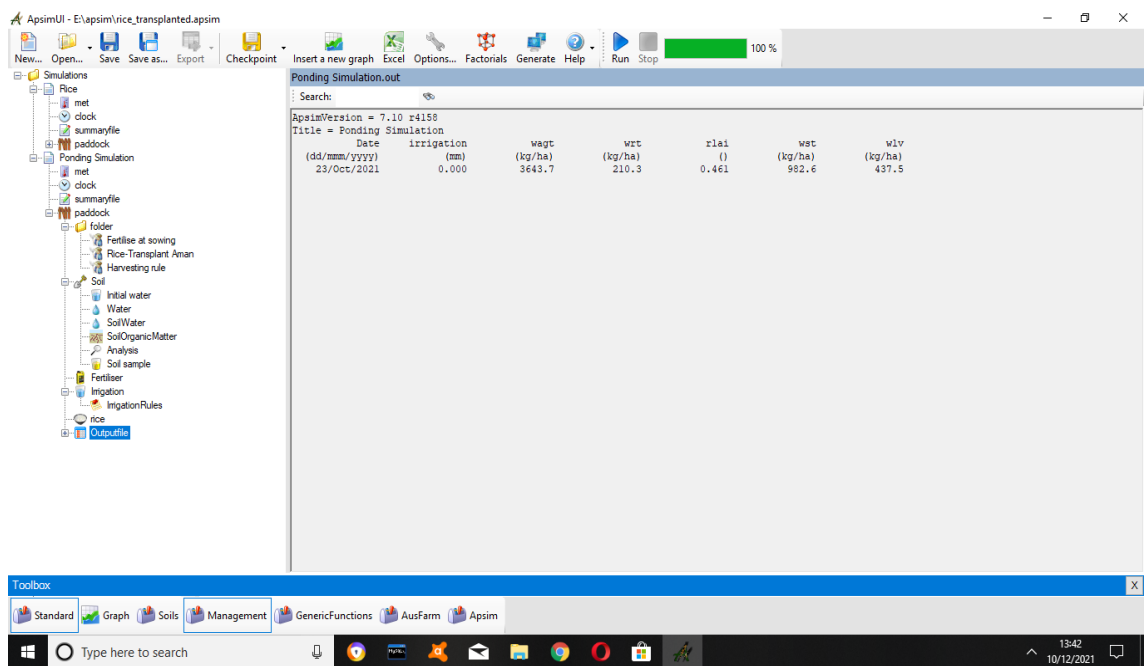
Plate 10: A sample of the output file in the APSIM model

3.7.5 Model evaluation using the statistical measures:

The model's performance was evaluated using both a graphical comparison of results and statistical analyses. The statistical measures included root mean square error (RMSE), root mean absolute error (MAE), standard deviation (SD), and coefficient of variation (CV). (Bouman and van Laar, 2006; Zhang *et al*., 2007). RMSE is a good measure of

how accurately the model predicts the response. It's the most important criterion for fit as the main purpose of the model is prediction. The RMSE and MAE were calculated using Eq. (3.3) and (3.4).

$$RMSE = \{\Sigma(Y_s - Y_o)^2 / n\}^{0.5} \qquad\qquad (3.3)$$

$$MAE = \Sigma(Y_s - Y_o)/n \qquad\qquad (3.4)$$

In the above cases, Y_s is the simulated yields, Y_o is the observed yields and n is the sample size.
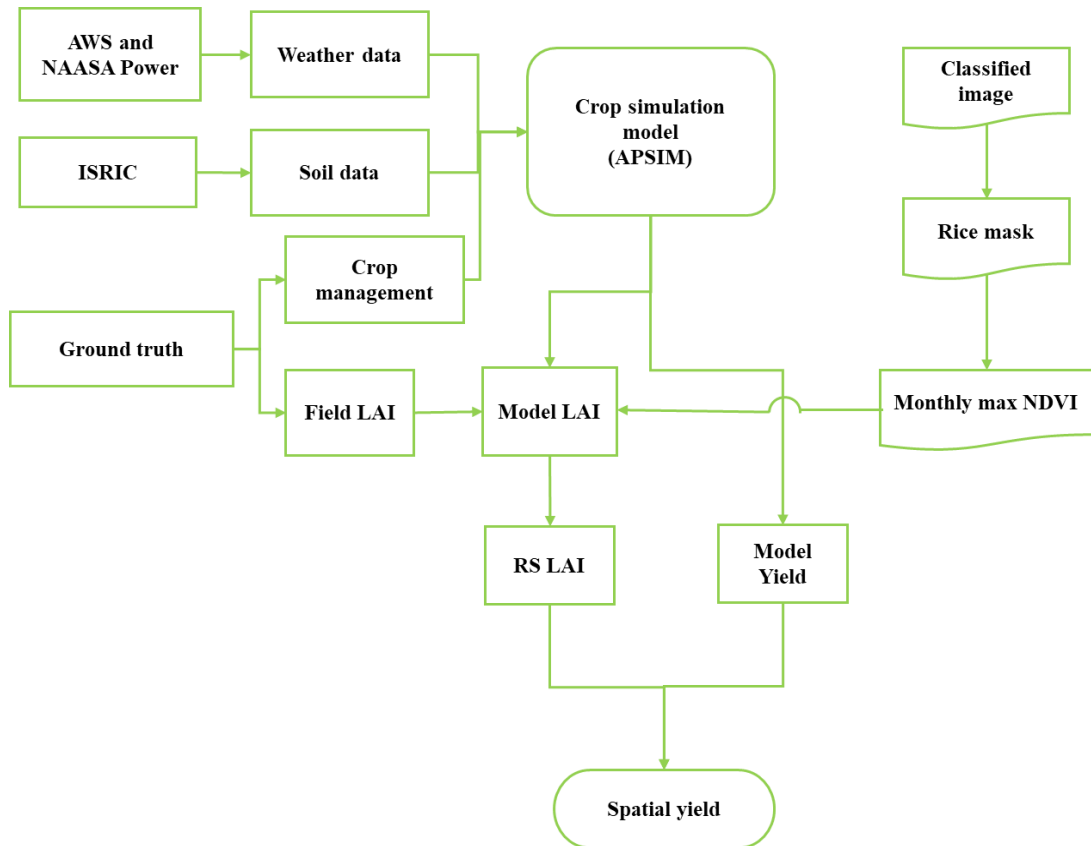
Fig 3.7 Schematic diagram for calculating the spatial rice yield estimation using RS data integrating with the simulation model

3.7.6 Integration of remote sensing data with crop model data to estimate optimized rice yields.

The rice mask from the crop map which was generated using the supervised classification was used to mask out the other vegetation and uncertain areas. The noise obtained in the classified rice mask was reduced by giving the NDVI threshold of above 0.4 value and it was used for further process of the spatial distribution of yield. Fig 3.7 represents the methodology used for integrating Remote Sensing products into the model for spatial yield distribution for the whole district.

3.7.6.1 Comparision of field LAI to model LAI: To determine the correctness of the model in simulating the LAI, the field LAI and model LAI were compared. After the correlation and the linear relation were known further proceeding to integrate the model LAI with the Remote Sensing derived NDVI was integrated.

3.7.6.2 Comparision of NDVI to model simulated LAI and biomass: Model outputs like LAI and biomass were considered to integrate with the Remote Sensing products. For that, model LAI and model biomass were compared with the Remote Sensing derived NDVI and based on the correlation, LAI was further considered.

3.7.6.3 Generation of spatial LAI map: Based on the linear relationship between the model LAI and the NDVI obtained by correlation, the linear equation was used on the NDVI image to generate a spatial LAI map for the Nalgonda district.

3.7.6.4 Generation of Spatial rice yield map: For generating the spatial rice yield map for the Nalgonda district, model LAI and yield were compared. The correlation and the linear relation were obtained and the linear equation was applied to the spatial LAI map.

3.7.7 Validation of yield estimates obtained from crop model against government yield statistics.

The yield obtained from the spatial distribution over the Nalgonda district was verified with the government yield from Telangana statistical abstract 2021 (https://www.telangana.gov.in/)

<div align="center">

Chapter IV

RESULTS AND DISCUSSION

</div>

This chapter presents the experimental results from the current study, "Rice yield estimation using Remote Sensing and crop simulation model in Nalgonda district, Telangana" which was conducted during *kharif* 2021. The findings of this research were given in the form of tables, graphs, and images. This chapter attempts to assess and explain the significant observations and conclusions of the current investigation under the following sub-headings.

4.1 LAI Estimation at the Field Using Ceptometer

4.1.1 Ceptometer readings at Telakantigudem village: The LAI readings of the crop cultivars obtained in the farmer fields of Telakantigudem for DAT are represented in Table 4.1. Only one farmer out of ten was seen to sow long-duration varieties like BPT-5204; instead, most medium-duration varieties like MTU-1010 were sown. The crops were at their maximum stages of tillering, heading, flowering, and maturity during the visits made to the fields. The medium duration variety was observed to have LAI ceptometer readings ranging from 4.75 to 5.21 during the flowering stage at 60 to 70 DAT, 4.43 to 4.52 during the grain formation stage at 71 to 80 DAT, 2.9 and 3.86 during the maturity stage at 81-90 DAT, and 2.5 to 2.7 above 90 DAT at harvesting. The long duration, BPT-5204, recorded 4.52 at the heading stage, i.e., 10-80 DAT, and 3.74 at the maturity stage, i.e., above 90 DAT. The LAI was observed to decrease from the reproductive stage as the leaf area decreased due to leaf drying.

4.1.2 Ceptometer readings at Mallaram village: The LAI readings of the crop cultivars acquired in the Telakantigudem farmer fields for DAT are shown in Table 4.2. Medium duration cultivars such as MTU-1010, RNR-15048, and IR-64, as well as long duration varieties such as BPT-5204 and JGL-24423, were mostly sown. The crops were at their peak stages of tillering, heading, flowering, and maturity when the fields were visited. The medium duration variety displayed LAI ceptometer readings between 3.64 and 4.1 during the flowering stage at 60 to 70 DAT, between 3.4 and 4.91 during the grain formation stage at 71 to 80 DAT, between 2.55 and 4.38 at the maturity stage, or at 81-90 DAT, and between 2.61 and 3.45 at the harvesting stage above 90 DAT. Long durations like BPT-5204 and JGL-24423 recorded 4.1 to 4.9 in the heading stage, or at 70 to 80 DAT, and 2.75 to 3.2 at the maturity stage, or above 90 DAT.

Table 4.1. Recorded LAI values at Telakantigudem village during the visits using Ceptometer

Field-ID	Variety	Julian day-281 (Oct 8th)		Julian day-299 (Oct 26th)	
		DAT	LAI-1	DAT	LAI-2
T1	MTU 1153	73	4.43	91	3.38
T2	MTU 1010	70	5.09	88	3.47
T3	MTU 1010	76	4.47	94	2.50
T4	MTU 1010	66	4.91	84	3.64
T5	MTU 1010	68	4.75	86	3.65
T6	MTU 1010	76	4.48	94	2.70
T7	KNM 118	70	4.81	88	3.02
T8	MTU 1010	70	5.01	88	2.90
T9	MTU 1010	70	5.21	88	3.86
T10	BPT 5204	76	4.52	94	3.74

It is difficult to determine if the instrument overestimates or underestimates the reference (direct) LAI measurement method based on the scant research that assessed ceptometer performance in crops. In contrast to other factors, Hyer and Goetz (2004) found that ceptometer-based LAI readings are more sensitive to incident PAR than any other factor, with a 10% shift in PAR leading to a 4–20 fold rise in LAI values.

Table 4.2. Recorded LAI values at Mallaram village during the visits using Ceptometer

Field-ID	Variety	Julian day-281 (Oct 8th)		Julian day-299 (Oct 26th)	
		DAT	LAI-1	DAT	LAI-2
M1	MTU 1010	75	3.40	93	2.61
M2	IR 64	74	3.54	92	3.04
M3	JGL 24423	76	4.3	94	2.95
M4	BPT 5204	80	4.1	98	3.2
M5	MTU 1010	76	4.5	94	3.23
M6	RNR 15048	65	4.1	83	4.38
M7	MTU 1010	66	3.64	84	2.55
M8	MTU 1010	74	4.8	92	3.45
M9	BPT 5204	60	3.92	78	4.35
M10	BPT 5204	76	4.91	94	2.75

4.2 Mapping of Rice Growing Areas

The mapping of rice growing areas was done in GEE using RF algorithm of supervised classification (Fig 4.1). Similarly Panjala *et al*., 2022, Bazzi *et al*., 2019, Son *et al*., 2018 and Xiong *et al*., 2017 used RF classification algorithm for mapping crop extent. The rice-growing areas of the Nalgonda district were depicted in the classified map was 1.56 L ha, which was comparable to the area indicated by the government statistics of 1.8 L ha for *kharif* 2021 (https://agri.telangana.gov.in/) with the deviation of -0.16%.

The bright green colour showed the presence of rice which is mainly observed in the command areas with the Nagarjuna Sagar canal and in the areas where irrigation

source is available mainly by the Krishna river in the Nalgonda district. The dark green colour in the map represented the area a with other crops sown which included majorly cotton and other crops such as groundnut, pulses, etc. The waterbody was represented by the dark blue colour and the built up was represented by the red colour and the grey colour displays the regions with the other LULC classes such as scrubland, forest areas, wasteland etc.
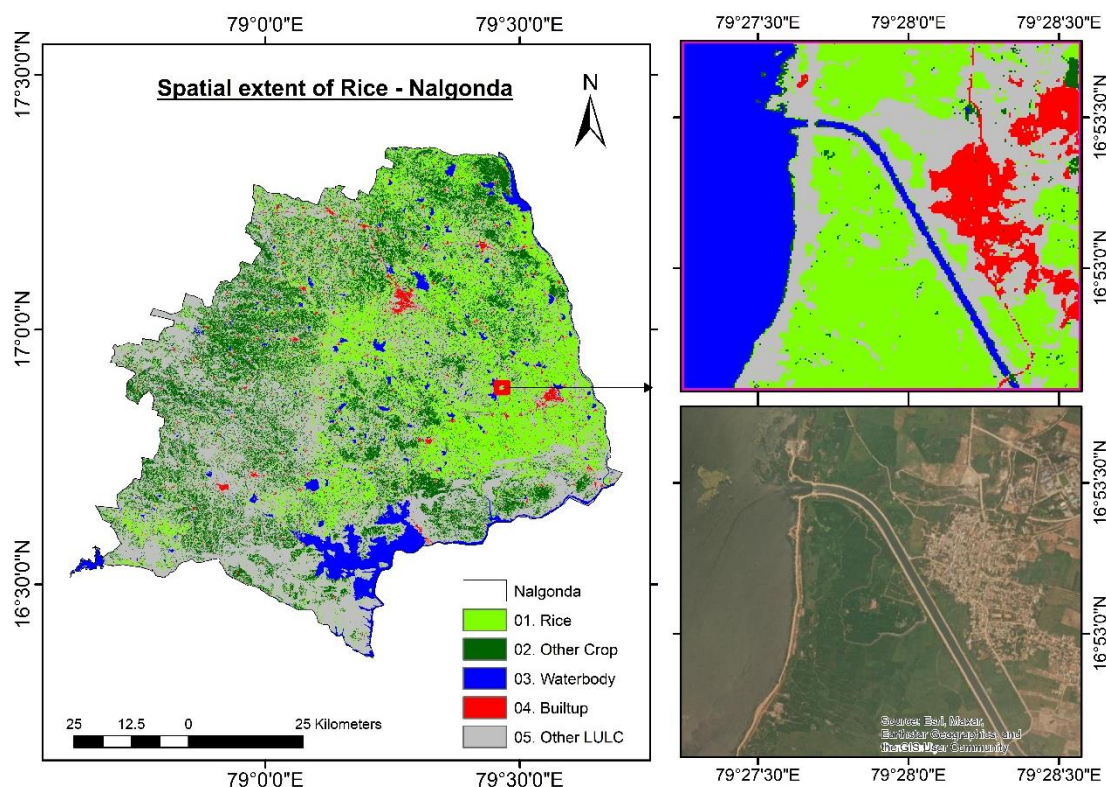
Fig 4.1. Mapping of the rice areas in Nalgonda district during *kharif* 2021

Table 4.3. Area of the respected classes from the classified map

Class	Area (L ha)
Rice	1.56
Other Crop	1.55
Waterbody	0.37
Built up	0.13
Other LULC	3.50
Total	7.11

According to the areas of the classes shown in Table 4.3, other land use and land cover occupied the largest amount of space (1.56 L ha), followed by rice with 3.5 Lha. About

1.55 L ha of the district's land was used for crops other than rice, while 0.37 and 0.13 L ha of water bodies and built up, respectively.

4.2.1 Accuracy assessment: The accuracy assessment performed for the classified image showed that the confusion matrix of the RF classified image achieved good accuracy in both user and producer accuracy, with a kappa coefficient of 0.894 and an overall accuracy of around 92 % (Table 4.4) whereas Hegarty-Craver *et al*., 2020 achieved an overall accuracy of 83% by using the similar approach by using a combination of Sentinel-1 and Sentinel-2 data and RF classifier. Due to almost identical signatures in some regions, some other Lssss which included shrubs is falsely categorised as a rice crop.The waterbody has shown 100% accuracy in both users and producers accuracy as they have contrast signatures when compared to the other classes.

Built up showed 100% users accuracy and 88% producers accuracy as identical signature with other LULC class. Other LULC class has shown 77% and 95% of users accuracy and producers accuracy respectively.

Table 4.4. **Confusion matrix showing classification accuracy in Nalgonda district**

Classified data	Rice	Other crop	Waterbody	Builtup	Other LULC	Totals	Users Accuracy (%)
Rice	46	1	0	0	0	47	97.8
Other crop	0	12	0	0	1	13	92.3
Waterbody	0	0	11	0	0	11	100
Builtup	0	0	0	8	0	8	100
Other LULC	5	0	0	1	21	27	77.7
Totals	51	13	11	9	22	106	
Producers accuracy (%)	90.2	92.3	100	88.8	95.4		
Overall accuracy (OA)		92.5%					
Kappa coefficient		0.894					

Other prior research has shown that utilising an RF algorithm on Sentinel -1 and Sentinel -2 offered technological assistance for mapping rice in regions with a lot of clouds and rainy weather (Cai *et al*., 2019). Bazzi *et al*., 2019 achieved an overall accuracy of 96.6% for mapping rice fields across the Camargue region of southern France using the Sentinel-1time-series and for mapping the spatial distribution of paddy rice fields throughout

sections of the Sanjiang plain in Northeast China using Sentinel-1A and Landsat-derived NDVI data and an RF classifier, Onojeghuo *et al.*, 2018 achieved an overall accuracy of 95.2% and a paddy accuracy of 96.7%.

4.3 Derivation of RS Products

4.3.1 Sentinel-1 derived indices: RS products like VV, VH, VH/VV, band4, band 8, and NDVI were used to compare the field LAI values that were measured at farmer fields using a ceptometer for the visiting day, further integrating it with the model output also. Using Sentinel-1, VV, VH, and VH/VV backscattering values were derived with the GEE code for the same dates on which the ground LAI was collected (Oct-8 and Oct-26) based on the date of satellite passing and weather conditions. In the comparison of VV with the ground LAI, the correlation observed was 0.29 and for VH and VH/VV, the correlations observed were 0.30 and 0.20 respectively as shown in Fig 4.2. The correlation of Sentinel-1 generated products was found to be less than 30, which indicates that they are not well aligned with the ground LAI.

4.3.2 Sentinel-2 derived indices: Sentinel-2 products like band4 (red), band8 (NIR) and NDVI reflected values were derived in GEE by applying the filter dates according to the visit dates when ceptometer values were recorded. The comparision was made between RS products and field LAI values to determine the linear relationship between them, and the correlations obtained for band4, band8 and NDVI were R^2 of 0.44, 0.41, 0.78, respectively as enhanced in Fig 4.3. As the NDVI showed the best fit with LAI having a correlation of above 75, it was used for integrating with the model output to estimate spatial yield as it is also the most commonly used RS indices for analyzing crop growth and estimating crop yield. Fan *et al.*, 2009 determined linear relation between NDVI and LAI and reported a correlation of 0.79, with the measured in-situ NDVI and LAI values in semi-arid grassland in Inner Mongolia, China during the growing season in 2005 and 2006. Goswami *et al.*, 2015, reported that NDVI was correlated with LAI showing an R^2 of 0.70 for six key plant species near Barrow, Alaska.
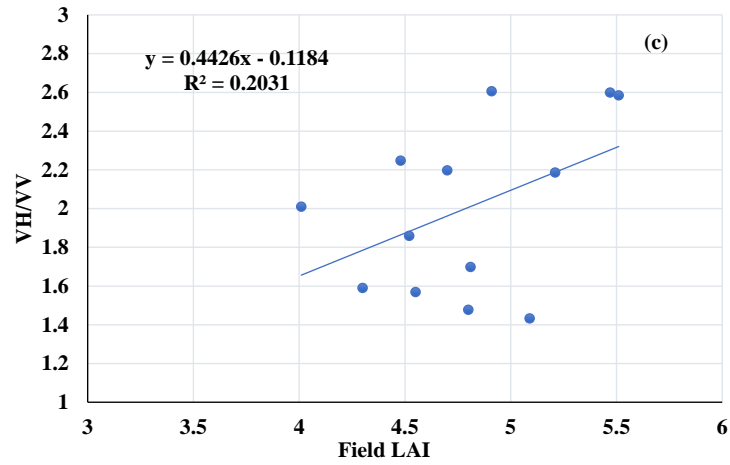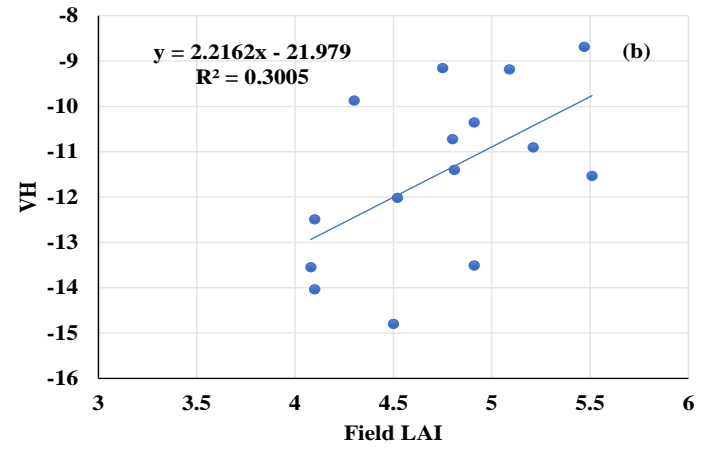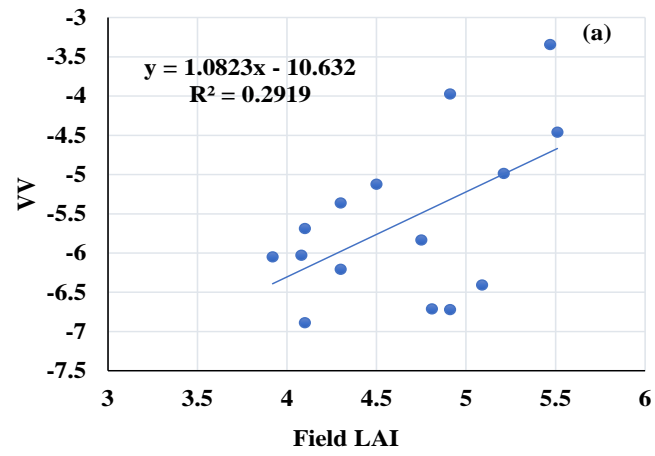
Fig 4.2. Comparison of a) VV, b) VH, c) VH/VV derived using Sentinel-1 to the field LAI collected for the visit day (Oct-8)
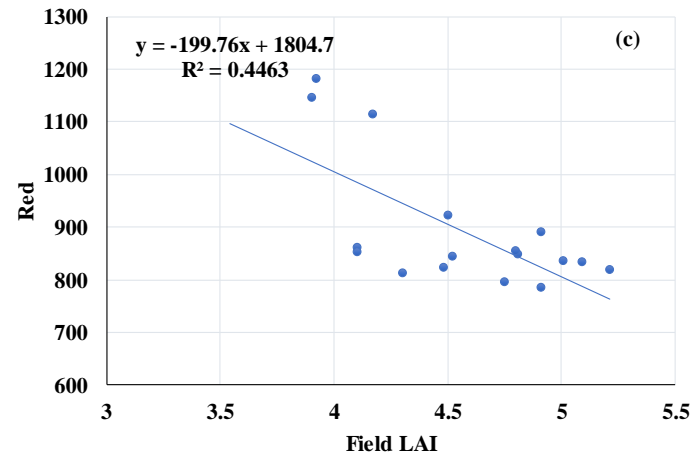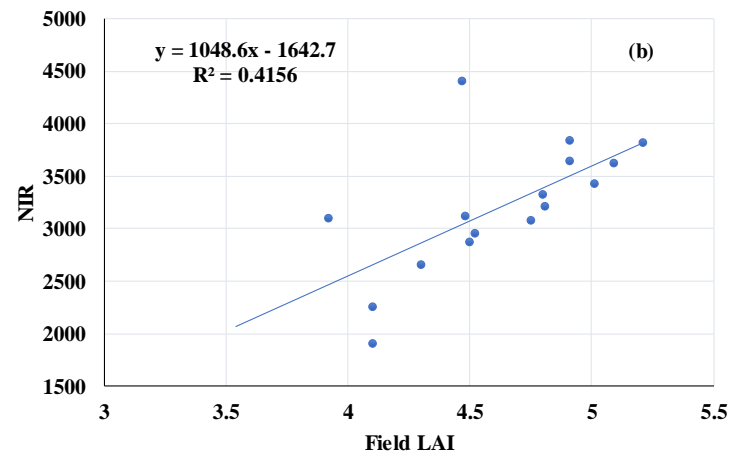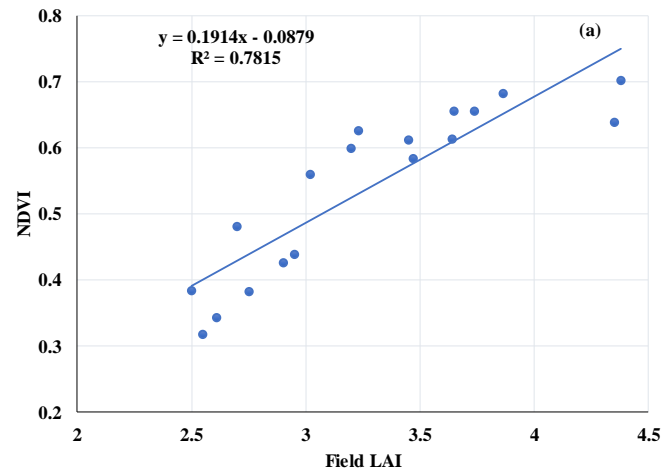
Fig 4.3. Comparison of Sentinel-2 products : a) NDVI, b) NIR and c) Red to the field LAI collected for the visit day (Oct-8)

Bhargav, 2021 reported the correlation between NDVI, LAI and yield for direct seeded rice and transplanted rice with R^2 of 0.78 in Jogulamba Gadwal district, Telangana. Xiao *et al*., 2002, observed a linear correlation (R^2=0.78) in Jiangning County, Jiangsu Province of China during the rice growing season (July to October) of 1999.

4.4 Crop Simulation by APSIM-ORYZA Model

4.4.1 Simulation of Grain yield

4.4.1.1 Yield simulation of Telakantigudem village fields: The APSIM-ORYZA was executed to estimate yields using two different weather files for the two villages, a different soil component file for each village, and 10 different treatments for each village as the transplanting dates and nitrogen amounts varied for all the chosen farmers' fields. The simulated yields ranged from 4400 to 6320 kg ha^{-1}, in Telakantigudem village, while the observed yields produced in the farmers' fields ranged from 3600 to 6500 kg ha^{-1}. The observed and simulated yields at Telakantigudem village observed were good yields. In Fig 4.4, the observed yields are visually compared to the model simulated yields of Telakantigudem village.

4.5.1.2 Yield simulation of Mallaram village fields: The simulated yields ranged from 3600 to 6100 kg ha^{-1}, in Mallaram village, while the observed yields produced in the farmers' fields ranged from 4500 to 5550 kg ha^{-1}. In Fig 4.5, the observed yields are visually compared to the model simulated yields of Mallaram village. A large difference was observed in the simulated yields to the observed yields in the Mallaram village when compared to the Telankantiguden village because the rainfall was low in the village, but the model considered little chance of water stress occurring in the crop as the field was fully irrigated with a maximum ponding depth of 100 mm in the model.

4.4.2 Deviation of simulated yields from the observed yields:

4.4.2.1 Deviation of simulated yields of Telakantigudem fields: The highest observed yield was in the T5 field and the lowest observed yield was in T4 field with a variation of 3000 kg ha^{-1}. The highest simulated yield with 6392 kg ha^{-1} was observed in the T5 field and the lowest yield with 4496 kg ha^{-1} in the T4 field with a variation of 1900 kg ha^{-1} of yield among the ten fields. According to Table 4.6, the difference ranged between 19.9 kg ha^{-1} and 1300 kg ha^{-1}, where the mean of the observed and simulated yields noticed was 5320 kg ha^{-1} and 5904 kg ha^{-1} and the SD and CV for the observed and simulated yields depicted were 899, 648 and 17, 11 respectively.

4.4.2.2 Deviation of simulated yields of Mallaram fields: The highest observed yield was in the M2 field and the lowest observed yield was in the M10 field with a variation of 2400 kg ha^{-1}. The highest simulated yield with 5554 kg ha^{-1} was observed in the M2 field and the lowest yield with 4513 kg ha^{-1} in the M9 field with a variation of 1040 kg ha^{-1} of yield among the ten fields. According to Table 4.5, the difference ranged between -545 kg ha^{-1} and 1239 kg ha^{-1}, where the mean of the observed and simulated yields noticed was 3863 kg ha^{-1} and 4498 kg ha^{-1} and the SD and CV for the observed and simulated yields depicted were 737, 339 and 19, 7 respectively.

In certain fields, the model simulated higher yields than real yields, whereas, in others, it simulated lower yields. The greater yields simulated were because the model doesn't account for abiotic stress like nutrient deficiencies or biotic stress like pest and disease attacks. The reduced yields could be due to the model's failure to account for the application of additional micronutrients and other major nutrients like phosphorus and potassium, and the spatial variability of ISRIC data (250m) on soil nutrient status. It was found that the model responded more favourably to the early transplantation and to the recommended dose of nitrogen (120 kg ha^{-1}). The major drawback of simulation models such as APSIM is that they require a huge number of input parameters and some of the required inputs are not easy to measure, such as soil initial nutrients.
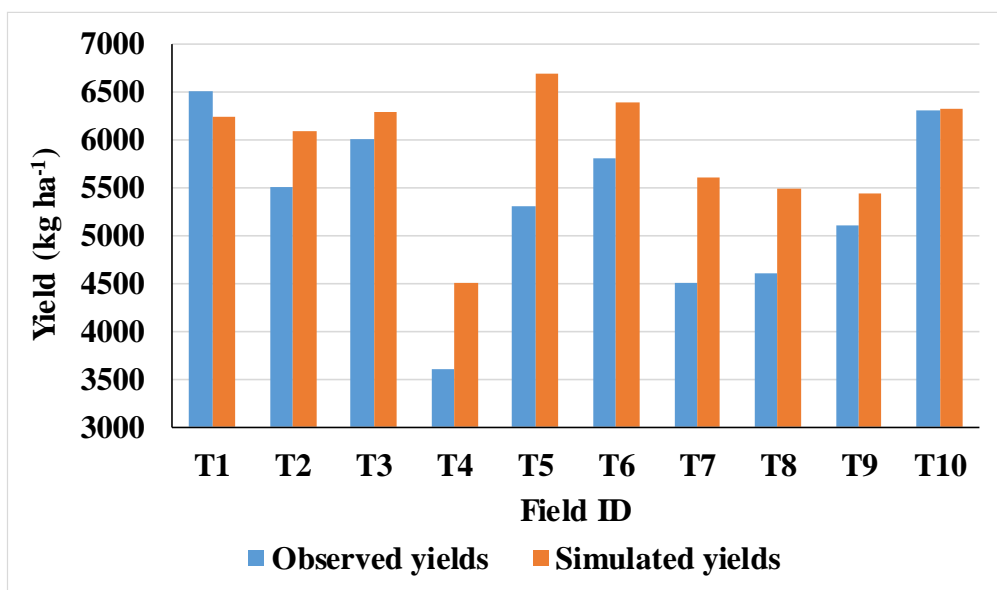
Fig 4.4. Simulated and observed yields of Telakantigudem village

Table 4.5. Comparison of observed and simulated rice yields of Telakantigudem village

Field ID	Observed yields (kg ha^{-1})	Simulated Yields (kg ha^{-1})	Deviation (kg ha^{-1})
T1	6500	6240	-259
T2	5500	6085	585
T3	6000	6285	285
T4	3600	4496	896
T5	5300	6600	1300
T6	5800	6392	592
T7	4500	5597	1097
T8	4600	5494	894
T9	5100	5442	342
T10	6300	6319	19
Mean	5320	5904	584
SD	899	648	
CV	17	11	
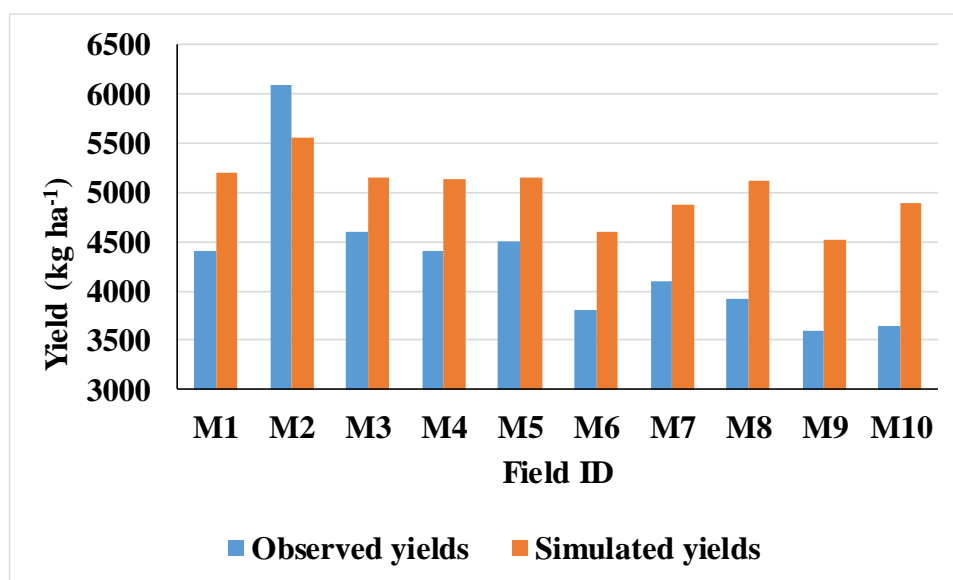
Fig 4.5. Simulated and observed yields of Mallaram village

Table 4.6. Comparison of observed and simulated rice yields of Mallaram village

Field ID	Observed yields (kg ha^{-1})	Simulated Yields (kg ha^{-1})	Deviation (kg ha^{-1})
M1	4400	5195	795
M2	6100	5554	-545
M3	4600	5150	550
M4	4400	5133	733
M5	4500	5150	650
M6	3800	4594	794
M7	4100	4880	780
M8	3920	5114	1194
M9	3600	4513	913
M10	3650	4889	1239
Mean	3867	4498	710
SD	737	339	
CV	19	7	

4.4.3 Evaluation of model: The linear regression's coefficient of determination (R^2) value was 0.795, resulting in smaller differences between the simulated and observed yields, as shown in Fig 4.6. The RMSE of the simulated yields was 785 kg ha^{-1}, which is lower than the standard deviation, indicating a better simulation of the model. Simulated yields had an MAE value of 708 kg ha^{-1}. All of these indications indicate that the model performed well while modelling the medium duration variety production in a transplanted rice ecosystem during the *kharif* of 2021. The RMSE of the simulated yields was 804 kg ha^{-1} and an MAE value of 728 kg ha^{-1}. All of these indications suggest that the model performed well while modelling the medium duration variety production in a transplanted rice ecosystem during the *kharif* of 2021.

$$y = 0.65x + 2321.5$$
$$R^2 = 0.795$$
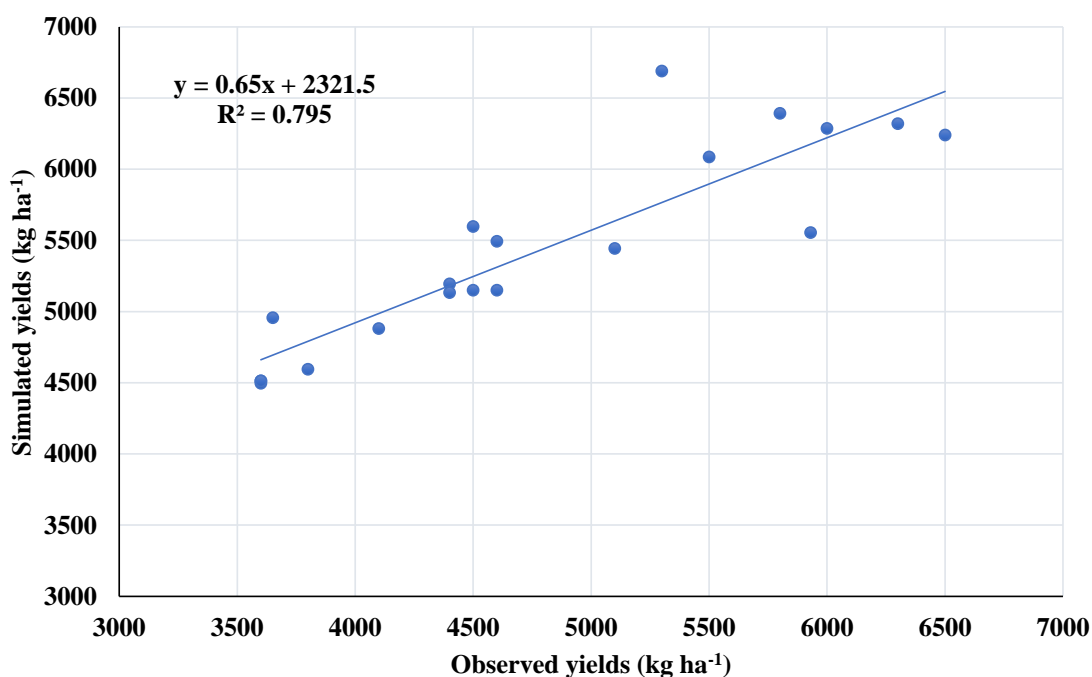
Fig 4.6. Correlation between the observed yields and simulated yields of Telakantigudem and Mallaram villages.

The results show the conformity with the findings of Biswas *et al*., 2021(R^2=0.85, RMSE<400 kg ha^{-1}), Amarasingha *et al*., 2015 ($R^2 > 0.97$, RMSE = 484 kg ha^{-1}) , Radanielson *et al*., 2018 (RMSE of 222 kg ha^{-1}), Zhang *et al*., 2007 (R^2= 0.76, RMSE = 515 kg ha^{-1}). The disparity can be attributed to the fact that models are by definition simplifications of reality, and some processes may be over-simplified or even incorrectly portrayed to effectively explain practical field scenarios. The difference in the simulated and measured yields is due to the reasons that may be because of the use of the default values from the APSIM-ORYZA model, as the photoperiod sensitivity parameters for the Telangana varieties could not be calibrated due to lack of data (Bouman *et al*., 2001). To accurately model the yields of photoperiod-sensitive varieties in Telangana, the photoperiod sensitivity characteristics required are to be calibrated.

4.5 Integration of RS Derived Products and Model Output

Among the RS products derived, NDVI was used to integrate with model output as it is most commonly used to analyze crop growth and to estimate crop yield and the correlation between the derived NDVI and ground LAI was found to be more (75%) than the other products such as VV, VH, VH/VV, NIR (band8) and red (band4) (Fig 4.2). NDVI is a typical RS measurement that describes the difference between visible and near-infrared reflectance of plant cover. The quantity of chlorophyll and other pigments exposed to the satellite's view influences NDVI. The values of the NDVI range from -1

to 1. Zero and below relate to surfaces that are not covered by vegetation. The density and vitality of the plants increase with increasing NDVI values. The NDVI derived using RS was compared with the model output parameters like biomass and LAI and based on the correlation, LAI was used to estimate the spatial rice yield of the Nalgonda district.

4.5.1 Comparision of field LAI to model LAI: Instead of conducting CCEs in this study, validation against government stats was raised as an objection. So, there was no CCE yield to compare to the field LAI, model LAI was used to compare with the model yield, to generate a spatial rice yield map.
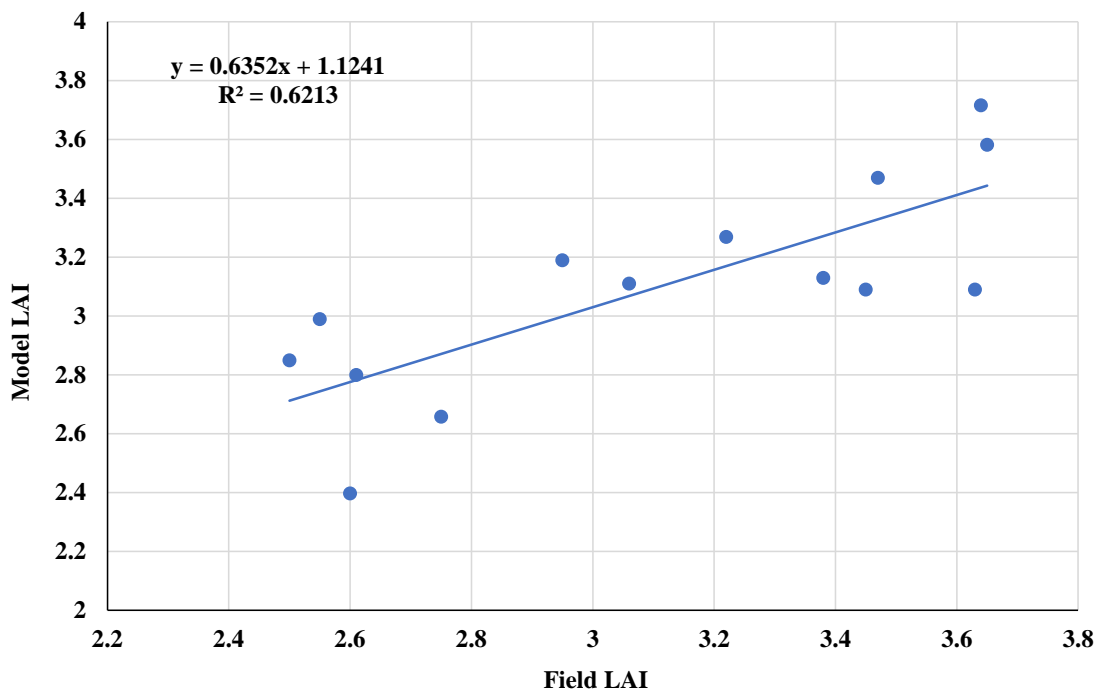
Fig 4.7. Comparison of field LAI and model LAI

The model simulated LAI and the field LAI during the reproductive stage of the crop was compared to determine how accurately the model simulated the LAI for the crop under different transplanting dates and different nitrogen rates. The correlation was found to be greater than 0.60 as shown in Fig 4.7, indicating a good fit between them. Therefore the model simulated LAI was used for generating the spatial LAI map.

4.5.2 Comparison of NDVI and Model LAI: The maximum NDVI derived using RS was compared to the maximum LAI simulated by the model for the crop and the

correlation was about 0.78 between them (Fig 4.8). Since the NDVI showed more correlation to the model LAI than model biomass, model LAI was used for determining the spatial rice yield.

The chart shows a scatter plot with y-axis labeled $NDVI_{max}$ ranging from 0.72 to 0.84, and x-axis labeled LAI_{max} ranging from 2.5 to 5. The regression equation is:

$$y = 0.043x + 0.6148$$
$$R^2 = 0.6457$$
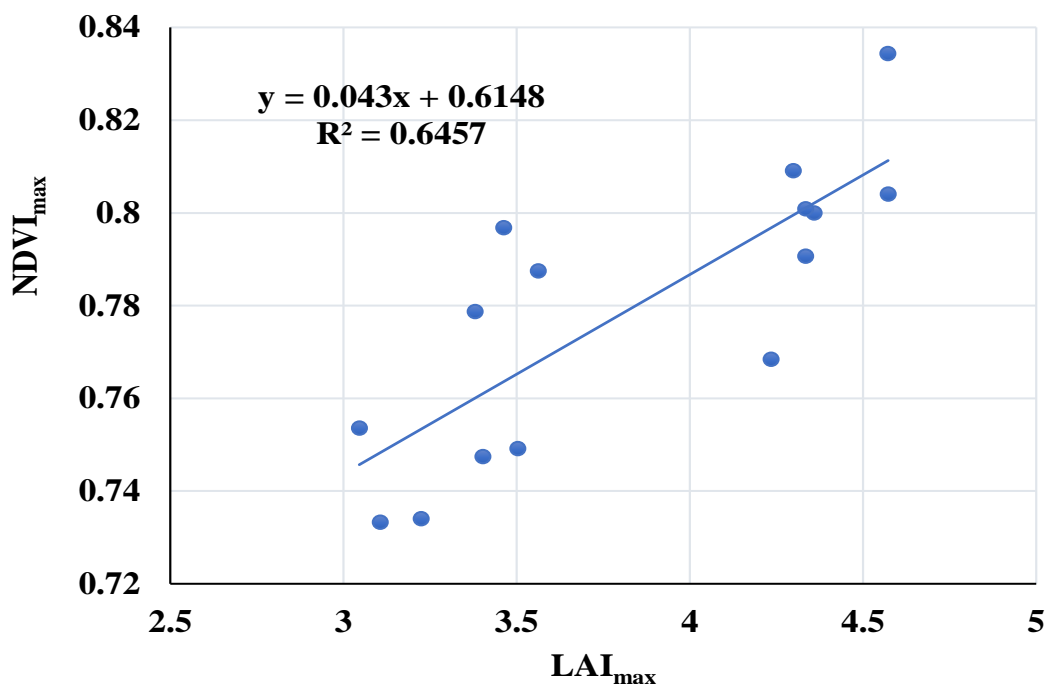
Fig 4.8. Comparison of Model simulated maximum LAI and the maximum NDVI of the crop

4.5.3 Comparison of NDVI and model Biomass: Using the coding in GEE, the maximum NDVI for the crop for each field was derived by applying the filter date over the entire crop period from June 2021 to October 2021. The maximum NDVI of the season was compared to the total biomass of the crop simulated by the model. The correlation between them was shown about 0.60 as in Fig 4.9. Hence based on the comparisions between the model LAI and model biomass to the NDVI, it was found that model LAI has shown the best fit with the NDVI. therefore model LAI was considered to correlate with the yields simulated so that the spatial rice yields map can be generated.
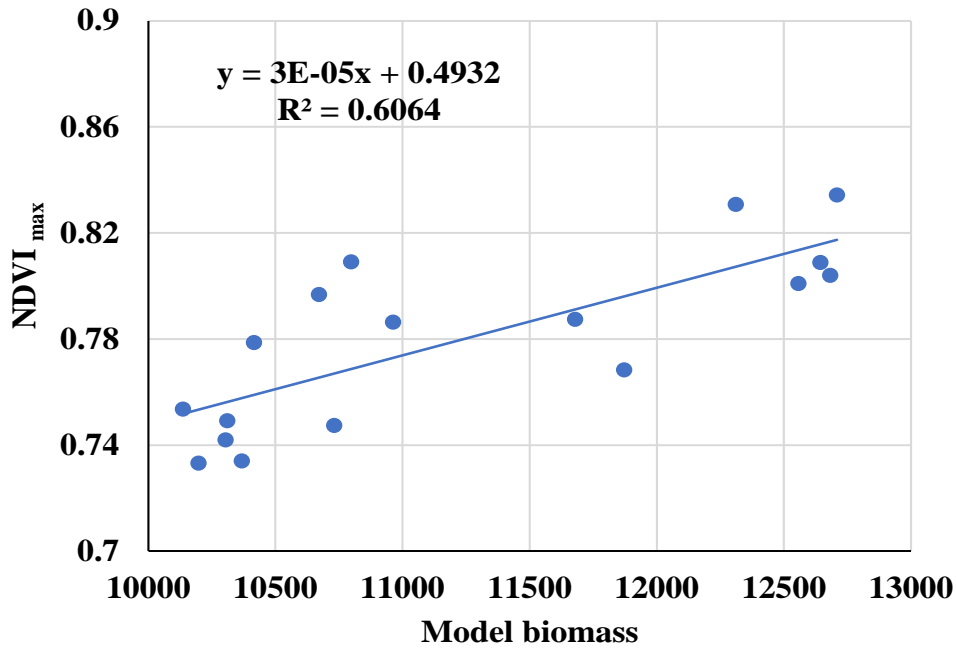
Fig 4.9. Comparison of NDVI and Biomass

4.5.4 Generating a spatial LAI map for the Nalgonda district: For generation of spatial LAI map, the NDVI image was masked with the rice mask which was generated using the supervised classification. The noise in the masked image was removed by giving the NDVI threshold of above 0.4 indicating the rice growing areas. For deriving RS LAI, the linear equation (Eq.4.1) obtained by the correlation of NDVI and model LAI was used.

$$LAI = 15.028 \times NDVI_{max} - 7.8835 \qquad\qquad (4.1)$$

From that, spatial LAI map was constructed as shown in Fig 4.10 where maximum LAI was shown in the rice fields which come under command areas of Nagarjuna Sagar and Krishna river flowing areas. The Miryalaguda revenue division has occupied more area of rice and observed with maximum LAI followed by the Nalgonda division and the least was observed in the Devarakonda revenue division.
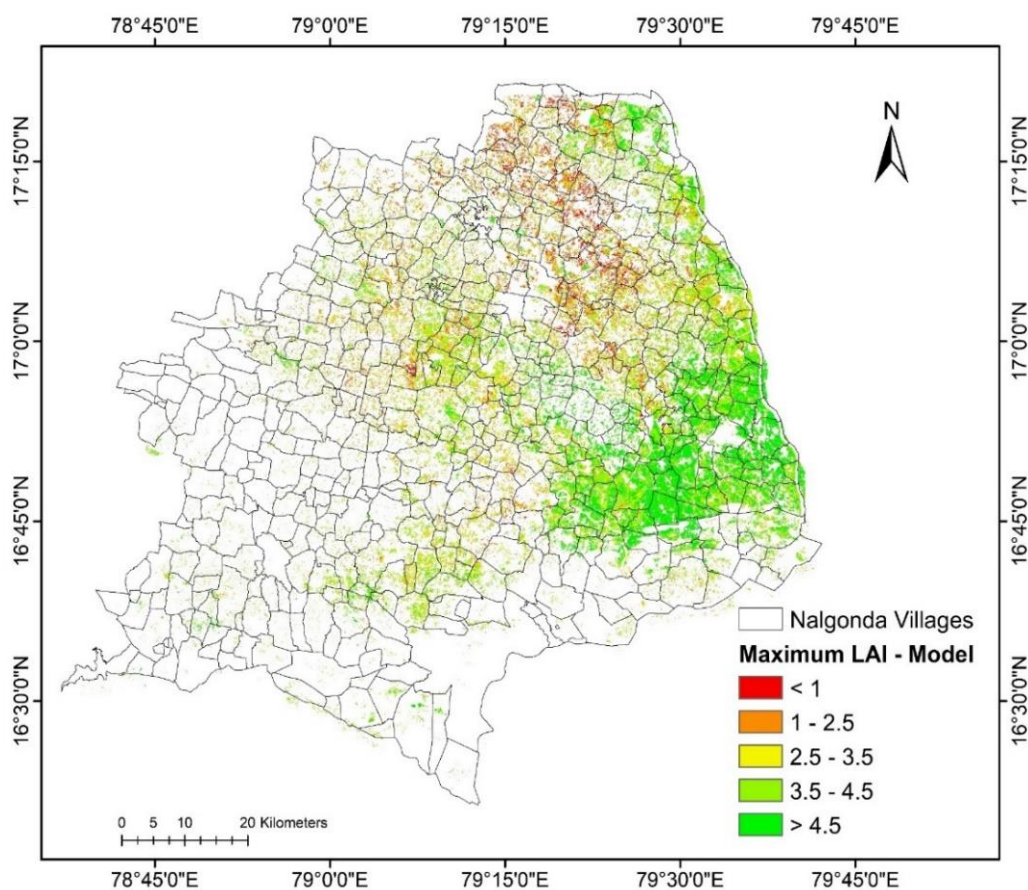
Fig 4.10. Spatial distribution of RS derived LAI over the Nalgonda district

4.5.5 Generating a spatial rice yield map for the Nalgonda district: The spatial LAI map and the linear equation between the model LAI and the model yield was used to generate spatial rice yield map of the Nalgonda district. The correlation between the LAI and the yield simulated by the model was more than 0.80 (Fig 4.11) and linear equation (Eq 4.2) obtained from the correlation was applied on the spatial LAI map to generate spatial rice yield map.

$$\text{Yield} = 4.0835 \times \text{LAI}_{\text{max}} + 1.0745 \tag{4.2}$$
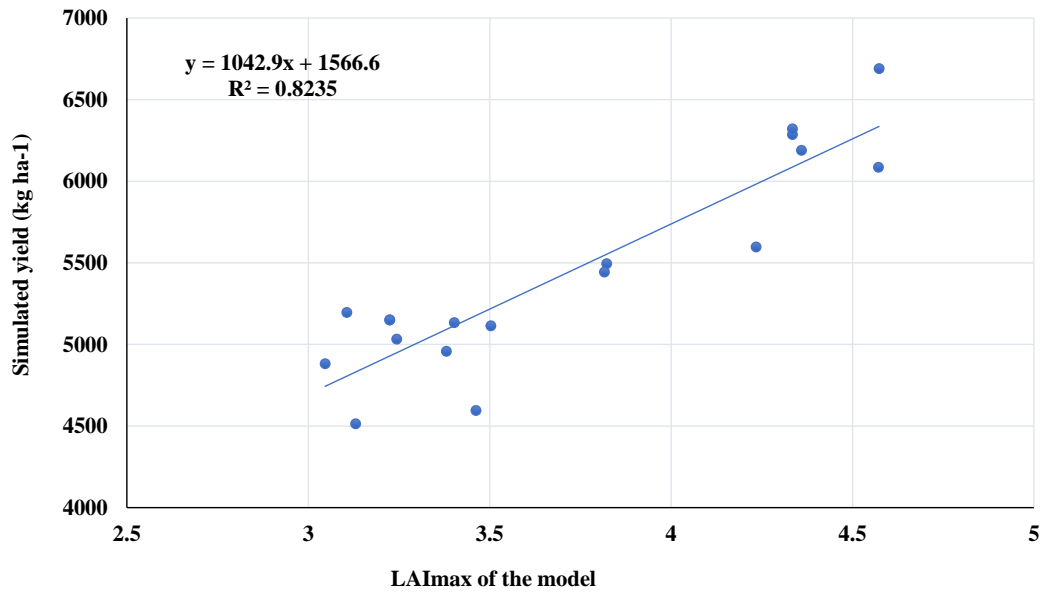
Fig 4.11 Comparison of maximum LAI of the model to the simulated yield of the model

The spatially distributed rice yield map as characterized in Fig 4.12 displayed the higher yields with more than 5500 kg ha^{-1} in the Miryalaguda division of the district where maximum LAI was distributed since they come under the Nagarjunasagar canal command regions, and water for irrigation is readily available in absence of rainfall. The spatial yield distribution map was in similarity to the LAI distribution map signifying that LAI has the direct relation with the growth and yield of the crop.
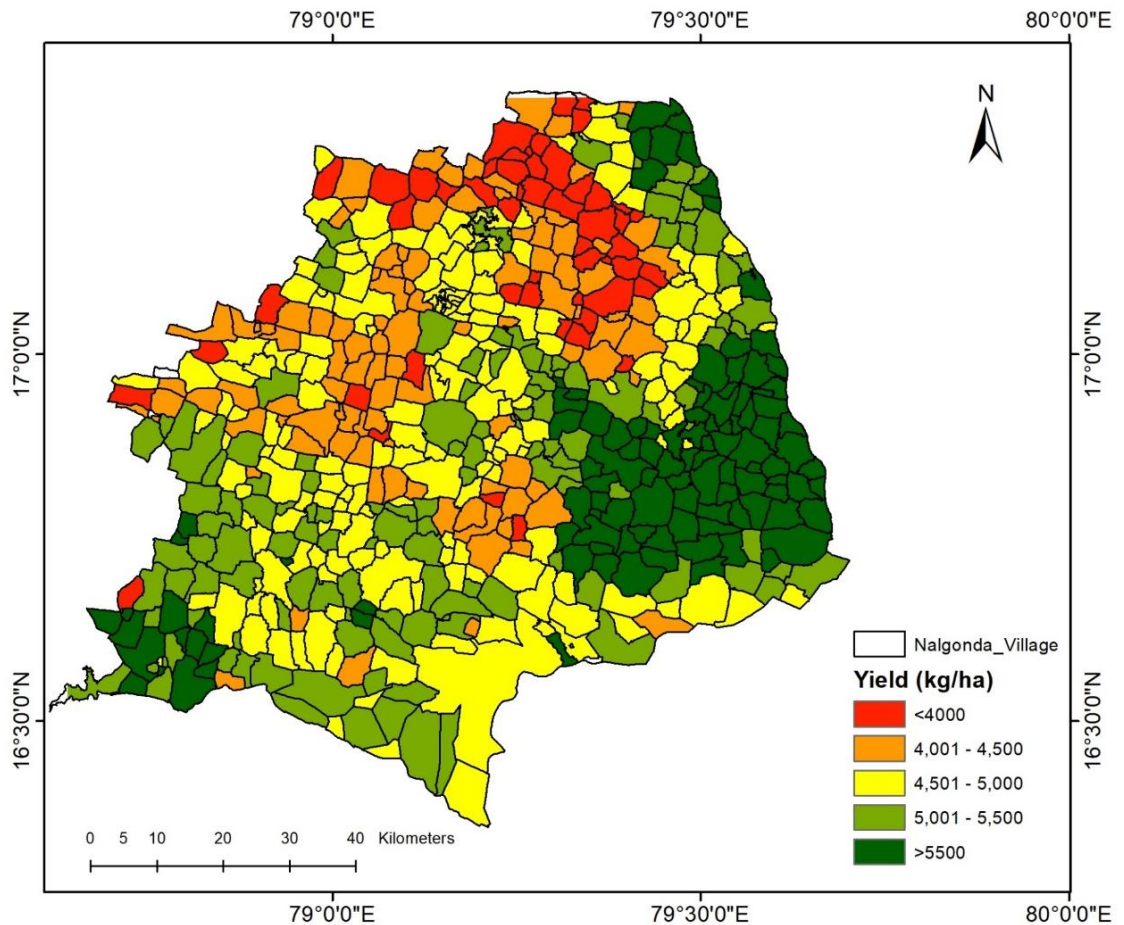
Fig 4.12 Spatial distribution of rice yield over the Nalgonda district at village level

4.6 Validation of spatially distributed model yield against the government statistics

Zonal statistics was generated on the spatial rice yield map to determine the mean yield of the of the whole district. The model mean yield for the whole district was found to be 4925 kg ha^{-1} where as the government statistics of Nalgonda district taken from the Telangana statistical abstract 2021 (telangana.gov.in./), rice yield was 5024 kg ha^{-1} resulting in 2% deviation.

<h1 style="text-align: center">Chapter V</h1>

<h1 style="text-align: center">SUMMARY AND CONCLUSION</h1>

The present study entitled "**Rice yield estimation using Remote Sensing and crop simulation model in Nalgonda district, Telangana**" was carried out during the *kharif*, 2021. Predicting crop yield is crucial in addressing emerging challenges in food security, particularly in an era of global climate change. Accurate yield predictions not only help farmers make informed economic and management decisions but also support famine prevention efforts. Crop modeling is a way of transferring the research knowledge of a system to farmers/ users. It can also be used to evaluate the economic impacts on agricultural land and crop and improve the quality of production, yield of the crop, and minimize the impact of pests through crop management applications and agronomic decision making. RS can provide missing spatial information required by crop models for improved yield prediction. Therefore, a combined approach using a crop simulation model and RS was used in this study.

Rice is the major crop grown in the Nalgonda district followed by cotton. To extrapolate the whole Nalgonda district conditions, the selection of the study area was done based on the variations in the rainfall and soil conditions. Thus, the villages of Mallaram from Kattangoor mandal, with low rainfall, and Telakantigudem from Kangal mandal, with high rainfall were chosen. Ground truth data were collected for acquiring ground reference points, measured LAI values in the farmer fields from both villages using a ceptometer and the crop management data from the farmers.

To map the rice growing areas in the Nalgonda district during *kharif* 2021, supervised classification was performed in the GEE combining Optical and SAR data, as optical data limits to provide information on lower levels of canopy and SAR data is not affected by atmospheric conditions and can acquire data for day and night. The monthly composite of VV and VH bands of the Sentinel-1 (GRD) data in Interferometric Wide Swath (IW) mode and the monthly maximum composite of NDVI of the Sentinel-2 data for the months June to October were used for this study. The stack was prepared and ground reference points were trained on the stacked image and the RF classification algorithm was applied to the composite image with the trained data. The accuracy assessment was carried out for the RF algorithm showed an overall accuracy of 92.5% and a kappa coefficient of 0.89 and a rice accuracy of

97%. From the result, it was observed that the RF classifier performed well in the supervised classification of rice-growing areas.

To integrate with the crop model output, RS products considered were VV, VH, VH/VV of Sentinel-1 data and NIR, Red and NDVI of Sentinel-2 data. These values were independently determined for the fields that were chosen and the visited dates that were scheduled based on satellite passing dates and weather conditions. The derived products were correlated with the collected ground LAI and observed that Sentinel-1 products were not well aligned as the correlations observed were less than 30%. From the Sentinel-2 products, NIR and Red bands showed a correlation of less than 50, while NDVI showed a correlation of above 75%. Thus, it was used for integrating with the model output to estimate spatial yield as it is also the most commonly used RS indices for analyzing crop growth and estimating crop yield.

Execution of APSIM-ORYZA was performed using the basic input parameters such as weather data including rainfall, maximum and minimum temperature and solar radiation collected from the AWS and NASA power, soil parameters from ISRIC data, crop management data from the respective farmers and genetic coefficient data taken from the previous studies (Swain et al., 2007) to run the model to simulate the growth and development of rice and its yield. The correlation between the observed and simulated yields showed an R^2 of 0.795 and the RMSE and MAE were found to be 785 and 705 kg ha^{-1} respectively. The differences in observed and simulated yields were caused by the models' failure to account for micronutrient application as well as biotic and abiotic stress in the field conditions.

Integration of RS and crop model was done based on the correlation between the NDVI and field LAI and the model LAI and field LAI. The correlation between the model LAI and field LAI was found to be more than 70%, hence the model LAI was used for integrating with the RS NDVI. The linear equation obtained between the NDVI and model LAI was used to generate a spatial LAI map using the NDVI image derived in GEE. Correlation between the model LAI and model yield showed R^2 of 82 and the linear equation was applied on the spatial LAI map to generate a spatial rice yield map. Rice average predicted yields were calculated at the district, mandal, and village levels by calculating zonal mean statistics after overlaying administrative mandal and village boundaries on a spatial variability yield distribution map. The district average predicted yield (4925 kg ha^{-1}) was validated against

the government statistics (5024 kg ha^{-1}) and found to be deviated by 2% demonstrating that integrating RS and crop simulation model increases the accuracy of the predicted yields.

CONCLUSIONS

- Mapping of rice growing areas using a classification algorithm on satellite imagery showed an accuracy of 92 % with the total rice area compared to the government statistics showed a deviation of -0.16 % for *kharif* 2021.
- RS products like VV, VH, VH/VV and NDVI, Band 8 and Band 4 using Sentinel-1 and Sentinel-2 were derived. NDVI was found to have the best fit with the field LAI with an R^2 of above 75%.
- The simulated yields obtained by executing the APSIM-ORYZA model, were generally close to the reported yields (R^2 of 0.79), suggesting that the model can be used to estimate rice yield under farmers' field conditions.
- The spatial distribution of rice yield over the Nalgonda district was obtained by integrating RS data with crop model, which demonstrated an improvement in estimated yield accuracy.
- The spatially distributed model mean yield of the district when compared to government yield statistics showed a 2% deviation.

FUTURE LINE OF WORK

- There is a requirement for calibration of input data parameters to match field conditions within some acceptable criteria.
- There is a requirement to improve the accuracy and consistency of remotely sensed information with an insight into accuracy requirements for operational purposes.
- The model needs further improvement for simulating rice yield in extreme weather events such as droughts, waterlogging, pests, diseases, and nutrients other than nitrogen.
- Additional non-destructive methods for measuring LAI can be used as the ceptometer may not provide reliable data.

LITERATURE CITED

Ahmad, I., Saeed, U., Fahad, M., Ullah, A., Habibur Rahman, M., Ahmad, A and Judge, J. 2018. Yield forecasting of spring maize using remote sensing and crop modeling in Faisalabad-Punjab Pakistan. *Journal of the Indian Society of Remote Sensing*. *46*(10): 1701-1711.

Amarasingha, R.P.R.K., Suriyagoda, L.D.B., Marambe, B., Gaydon, D.S., Galagedara, L.W., Punyawardena, R., Silva, G.L.L.P., Nidumolu, U and Howden, M. 2015. Simulation of crop and water productivity for rice (*Oryza sativa* L.) using APSIM under diverse agro-climatic conditions and water management techniques in Sri Lanka. *Agricultural Water Management*. *160*: 132-143.

AMIC. 2021. Agricultural Marketing Intelligence Cell, Department of Economics. College of Agriculture, Rajendranagar.

Basso, B., Cammarano, D and Carfagna, E. 2013. Review of crop yield forecasting methods and early warning systems. In *Proceedings of the first meeting of the scientific advisory committee of the global strategy to improve agricultural and rural statistics, FAO Headquarters, Rome, Italy* .18:19.

Batchelor, W.D., Basso, B and Paz, J.O. 2002. Examples of strategies to analyze spatial and temporal yield variability using crop models. *European Journal of Agronomy*. 18(1-2): 141-158

Bazzi, H., Baghdadi, N., El Hajj, M., Zribi, M., Minh, D.H.T., Ndikumana, E., Courault, D and Belhouchette, H. 2019. Mapping paddy rice using Sentinel-1 SAR time series in Camargue, France. *Remote Sensing*. *11*(7): 887.

Bhargav, M. 2021. Discrimination of rice ecosystem and yield estimation using temporal SAR (Synthetic Aperture radar) and optical RS (Remote Sensing) data in Jogulamba Gadwal district, Telangana. *MSc Thesis*. Professor Jayashankar Telangana State Agricultural University, Hyderabad, India

Biswas, A., Mailapalli, D.R and Raghuwanshi, N.S. 2021. APSIM-Oryza model for simulating paddy consumptive water footprints under alternate wetting and drying practice for Kharagpur, West Bengal, India. *Paddy and Water Environment*. *19*(3):481-498.

Bouman, B.A.M and Van Laar, H.H. 2006. Description and evaluation of the rice growth model ORYZA2000 under nitrogen-limited conditions. *Agricultural Systems*. *87*(3): 249-273.

Bouman, B.A.M. 1995. Crop modelling and remote sensing for yield prediction. *Netherlands Journal of Agricultural Science*. *43*(2): 143-161.

Cai, Y., Lin, H and Zhang, M., 2019. Mapping paddy rice by the object-based random forest method using time series Sentinel-1/Sentinel-2 data. *Advances in Space Research*. *64*(11):2233-2244.

Campos-Taberner, M., García-Haro, F.J., Busetto, L., Ranghetti, L., Martínez, B., Gilabert, M.A., Camps-Valls, G., Camacho, F and Boschetti, M. 2018. A critical comparison of remote sensing leaf area index estimates over rice-cultivated areas: From Sentinel-2 and Landsat-7/8 to MODIS, GEOV1 and EUMETSAT polar system. *Remote Sensing*. *10*(5): 763.

Challinor, A.J., Wheeler, T.R., Craufurd, P.Q., Slingo, J.M. and Grimes, D.I.F., 2004. Design and optimisation of a large-area process-based model for annual crops. *Agricultural and Forest Meteorology*. *124*(1-2): 99-120.

Charoen-Ung, P and Mittrapiyanuruk, P. 2018. Sugarcane Yield Grade Prediction using random forest with forward feature selection and hyper-parameter tuning. *In International Conference on Computing and Information Technology* (33-42). Springer, Cham.

Chaudhari, K.N., Tripathy, R.O.J.A.L.I.N and Patel, N.K. 2010. Spatial wheat yield prediction using crop simulation model, GIS, remote sensing and ground observed data. *Journal of Agrometeorology*. *12*(2): 174-180.

Choudhury, A and Jones, J. 2014. Crop yield prediction using time series models. *Journal of Economics and Economic Education Research*, *15*(3): 53-67.

Clevers, J.G., Kooistra, L and Van den Brande, M.M. 2017. Using Sentinel-2 data for retrieving LAI and leaf and canopy chlorophyll content of a potato crop. *Remote Sensing*. *9*(5): 405.

Clevers, J.G.P.W and Van Leeuwen, H.J.C. 1996. Combined use of optical and microwave remote sensing data for crop growth monitoring. *Remote sensing of Environment*. *56*(1): 42-51.

Cohen, J. 1960. A coefficient of agreement for nominal scales. *Educational and Psychological Measurement*. *20*(1): 37-46.

Congalton, R.G. 1991. A review of assessing the accuracy of classifications of remotely sensed data. *Remote Sensing of Environment*. *37*(1): 35-46.

Doraiswamy, P.C., Hatfield, J.L., Jackson, T.J., Akhmedov, B., Prueger, J and Stern, A. 2004. Crop condition and yield simulations using Landsat and MODIS. *Remote Sensing of Environment*. *92*(4): 548-559.

Doraiswamy, P.C., Sinclair, T.R., Hollinger, S., Akhmedov, B., Stern, A and Prueger, J. 2005. Application of MODIS derived parameters for regional crop yield assessment. *Remote Sensing of Environment*. *97*(2): 192-202.

Dorigo, W.A., Zurita-Milla, R., de Wit, A.J., Brazile, J., Singh, R and Schaepman, M.E. 2007. A review on reflective remote sensing and data assimilation techniques for enhanced agroecosystem modeling. *International Journal of Applied Earth Observation and Geoinformation*. 9(2): 165-193.

Fang, H., Liang, S and Hoogenboom, G. 2011. Integration of MODIS LAI and vegetation index products with the CSM–CERES–Maize model for corn yield estimation. *International Journal of Remote Sensing*. *32*(4): 1039-1065.

Fernando, M.E.K.K., Amerasekara, D.A.B.N., Amarasingha, R.K., Suriyagoda, L.D.B., Marambe, B., Galagedara, L.W., Silva, G.L.L.P., Punyawardena, R., Parsons, D and Meinke, H. 2015. Validation of APSIM for long duration rice varieties in different agro-climatic zones of Sri Lanka. In *17th Australian Society of Agronomy Conference*.1-4.

Filippi, P., Jones, E.J., Wimalathunge, N.S., Somarathna, P.D., Pozza, L.E., Ugbaje, S.U., Jephcott, T.G., Paterson, S.E., Whelan, B.M and Bishop, T.F. 2019. An approach to forecast grain crop yield using multi-layered, multi-farm data sets and machine learning. *Precision Agriculture*. *20*(5): 1015-1029.

Gandhi, N., Armstrong, L.J., Petkar, O and Tripathy, A.K., 2016. Rice crop yield prediction in India using support vector machines. In *2016 13th International Joint Conference on Computer Science and Software Engineering (JCSSE)* (1-5). IEEE.

Gaydon, D.S., Wang, E., Poulton, P.L., Ahmad, B., Ahmed, F., Akhter, S., Ali, I., Amarasingha, R.P.R.K., Chaki, A.K., Chen, C and Choudhury, B.U. 2017. Evaluation of the APSIM model in cropping systems of Asia. *Field Crops Research*. *204*: 52-75.

Gumma, M.K., Kadiyala, M.D.M., Panjala, P., Ray, S.S., Akuraju, V.R., Dubey, S., Smith, A.P., Das, R and Whitbread, A.M. 2022. Assimilation of remote sensing data into crop growth model for yield estimation: A case study from India. *Journal of the Indian Society of Remote Sensing*. *50*(2): 257-270.

Gumma, M.K., Nelson, A., Thenkabail, P.S and Singh, A.N. 2011a. Mapping rice areas of South Asia using MODIS multitemporal data. *Journal of Applied Remote Sensing*. 5(1): 053547.

Gumma, M.K., Thenkabail, P.S., Hideto, F., Nelson, A., Dheeravath, V., Busia, D and Rala, A. 2011b. Mapping irrigated areas of Ghana using fusion of 30 m and 250 m resolution remote-sensing data. *Remote Sensing*. *3*(4): 816-835.

Gumma, M.K., Thenkabail, P.S., Maunahan, A., Islam, S and Nelson, A. 2014. Mapping seasonal rice cropland extent and area in the high cropping intensity environment of Bangladesh using MODIS 500 m data for the year 2010. ISPRS *Journal of Photogrammetry and Remote Sensing*. 91: 98-113.

Gumma, M.K., Thenkabail, P.S., Teluguntla, P., Rao, M.N., Mohammed, I.A and Whitbread, A.M. 2016. Mapping rice-fallow cropland areas for short-season grain legumes intensification in South Asia using MODIS 250 m time-series data. *International Journal of Digital Earth*. 9(10): 981-1003.

Gumma, M.K., Thenkabail, P.S., Teluguntla, P.G., Oliphant, A., Xiong, J., Giri, C., Pyla, V., Dixit, S and Whitbread, A.M. 2020b. Agricultural cropland extent and areas of South Asia derived using Landsat satellite 30-m time-series big-data using random forest machine learning algorithms on the Google Earth Engine cloud. *GIScience & Remote Sensing*. 57(3): 302-322.

Gumma, M.K., Tummala, K., Dixit, S., Collivignarelli, F., Holecz, F., Kolli, R.N. and Whitbread, A.M. 2020a. Crop type identification and spatial mapping using Sentinel-2 satellite data with focus on field-level information. *Geocarto International*. 1-17.

Hegarty-Craver, M., Polly, J., O'Neil, M., Ujeneza, N., Rineer, J., Beach, R.H., Lapidus, D. and Temple, D.S. 2020. Remote crop mapping at scale: Using satellite imagery and UAV-acquired data as ground truth. *Remote Sensing*, 12(12):1984.

Holzworth, D.P., Huth, N.I., deVoil, P.G., Zurcher, E.J., Herrmann, N.I., McLean, G., Chenu, K., van Oosterom, E.J., Snow, V., Murphy, C and Moore, A.D. 2014. APSIM–evolution towards a new generation of agricultural systems simulation. *Environmental Modelling & Software*. *62*: 327-350.

Hong, S.Y., Sudduth, K.A., Kitchen, N.R., Fraisse, C.W., Palm, H.L and Wiebold, W.J. 2004. Comparison of remote sensing and crop growth models for estimating within-field LAI variability. *Korean Journal of Remote Sensing*. *20*(3): 175-188.

Hyer, E.J and Goetz, S.J. 2004. Comparison and sensitivity analysis of instruments and radiometric methods for LAI estimation: Assessments from a boreal forest site. *Agricultural and Forest Meteorology*. *122*(3-4):157-174.

Ines, A.V., Das, N.N., Hansen, J.W and Njoku, E.G. 2013. Assimilation of remotely sensed soil moisture and vegetation with a crop simulation model for maize yield prediction. *Remote Sensing of Environment*. *138*: 149-164.

IRRI. 2006. Rice varieties. IRRI knowledge bank. Los Banos.

Jensen, R., Gatrell, J., Boulton, J and Harper, B. 2004. Using remote sensing and geographic information systems to study urban quality of life and urban forest amenities. *Ecology and Society*. *9*(5).

Jin, X., Kumar, L., Li, Z., Xu, X., Yang, G and Wang, J. 2016. Estimation of winter wheat biomass and yield by combining the aquacrop model and field hyperspectral data. *Remote Sensing*. 8(12): 972.

Jin, X., Li, Z., Feng, H., Ren, Z and Li, S. 2020. Estimation of maize yield by assimilating biomass and canopy cover derived from hyperspectral data into the AquaCrop model. *Agricultural Water Management*. 227: 105846.

Jing-Feng, H., Shu-chuan, T., Abou-Ismail, O and Ren-chao, W. 2002. Rice yield estimation using remote sensing and simulation model. *Journal of Zhejiang University-SCIENCE A*. *3*(4): 461-466.

Kasampalis, D.A., Alexandridis, T.K., Deva, C., Challinor, A., Moshou, D and Zalidis, G. 2018. Contribution of remote sensing on crop models: a review. *Journal of Imaging*. *4*(4): 52.

Keating, B.A., Carberry, P.S., Hammer, G.L., Probert, M.E., Robertson, M.J., Holzworth, D., Huth, N.I., Hargreaves, J.N., Meinke, H., Hochman, Z and McLean, G. 2003. An overview of APSIM, a model designed for farming systems simulation. *European Journal of Agronomy*. *18*(3-4): 267-288.

Kenduiywo, B.K., Bargiel, D and Soergel, U. 2018. Crop-type mapping from a sequence of Sentinel-1 images. *International Journal of Remote Sensing*. 39(19): 6383-6404.

Khanal, S., Fulton, J., Klopfenstein, A., Douridas, N and Shearer, S. 2018. Integration of high resolution remotely sensed data and machine learning techniques for spatial prediction of soil properties and corn yield. *Computers and Electronics in Agriculture*. *153*: 213-225.

Kpienbaareh, D., Sun, X., Wang, J., Luginaah, I., Bezner Kerr, R., Lupafya, E and Dakishoni, L. 2021. Crop type and land cover mapping in northern Malawi using

the integration of sentinel-1, sentinel-2, and planetscope satellite data. *Remote Sensing*. 13(4): 700.

Kumar, V.P., Rao, V.U.M., Tripati, P.K and Venkateswarlu, B. 2014. The effect of rice transplanting date on rice-wheat cropping system performance in the middle IGP of India-A Simulation Study using APSIM. *Developing Capacity in Cropping Systems Modelling for South Asia*. 75-85.

Li, M., Du, Y., Zhang, F., Fan, J., Ning, Y., Cheng, H and Xiao, C. 2020. Modification of CSM-CROPGRO-Cotton model for simulating cotton growth and yield under various deficit irrigation strategies. *Computers and Electronics in Agriculture*. 179: 105843.

Li, T., Angeles, O., Marcaida III, M., Manalo, E., Manalili, M.P., Radanielson, A and Mohanty, S. 2017. From ORYZA2000 to ORYZA (v3): An improved simulation model for rice in drought and nitrogen-deficient environments. *Agricultural and Forest Meteorology*. *237*: 246-256.

Lobell, D.B., Field, C.B., Cahill, K.N and Bonfils, C. 2006. Impacts of future climate change on California perennial crop yields: Model projections with climate and crop uncertainties. *Agricultural and Forest Meteorology*, *141*(2-4): 208-218.

Lobell, D.B., Thau, D., Seifert, C., Engle, E and Little, B. 2015. A scalable satellite-based crop yield mapper. *Remote Sensing of Environment*. *164*: 324-333.

MacDonald, R.B and Hall, F.G., 1980. Global crop forecasting. *Science*. *208*(4445): 670-679.

MacLean, M.G and Congalton, R.G. 2012, March. Map accuracy assessment issues when using an object-oriented approach. In *Proceedings of the American Society for Photogrammetry and Remote Sensing 2012 Annual Conference, Sacramento, CA, USA* (19-23).

Masjedi, A., Zhao, J., Thompson, A.M., Yang, K.W., Flatt, J.E., Crawford, M.M., Ebert, D.S., Tuinstra, M.R., Hammer, G and Chapman, S. 2018. Sorghum biomass prediction using UAV-based remote sensing data and crop model simulation. In *IGARSS 2018-2018 IEEE International Geoscience and Remote Sensing Symposium.* (7719-7722).

Mayer, D.G and Butler, D.G. 1993. Statistical validation. *Ecological Modelling*. *68*(1-2): 21-32.

McCown, R.L., Hammer, G.L., Hargreaves, J.N.G., Holzworth, D.P and Freebairn, D.M. 1996. APSIM: a novel software system for model development, model testing and simulation in agricultural systems research. *Agricultural Systems*. *50*(3): 255-271.

Milesi, C and Kukunuri, M. 2022. Crop yield estimation at gram panchayat scale by integrating field, weather and satellite data with crop simulation models. *Journal of the Indian Society of Remote Sensing*. *50*(2): 239-255.

Moorthy, R.L., Hock-Guan, W., Wing-Cheong, N and Chung-Piaw, T. 2003. Cyclic deadlock prediction and avoidance for zone-controlled AGV system. *International Journal of Production Economics*. *83*(3): 309-324.

Murthy, V.R.K. 2004. Crop growth modeling and its applications in agricultural meteorology. *Satellite Remote Sensing and GIS Applications in Agricultural Meteorology*. *235*.

Muslim, M., Romshoo, S.A and Rather, A.Q. 2015. Paddy crop yield estimation in Kashmir Himalayan rice bowl using remote sensing and simulation model. *Environmental Monitoring and Assessment*. *187*(6): 1-12.

Nain, A.S., Dadhwal, V.K and Singh, T.P. 2004. Use of CERES-Wheat model for wheat yield forecast in central Indo-Gangetic Plains of India. *The Journal of Agricultural Science*. *142*(1): 59-70.

Nikitha, K., Sreenivas, G., Rani, P.L and Madhavi, A. 2018. Performance of photo sensitive rice cv. RNR 15048 (Telangana Sona) under varied nitrogen levels and environmental conditions. *International Journal of Current Microbiology and Applied Sciences*. *7*: 3602-3605.

Olioso, A., Inoue, Y., Ortega-Farias, S., Demarty, J., Wigneron, J.P., Braud, I., Jacob, F., Lecharpentier, P., Ottle, C., Calvet, J.C and Brisson, N. 2005. Future directions for advanced evapotranspiration modeling: Assimilation of remote sensing data into crop simulation models and SVAT models. *Irrigation and Drainage Systems*. *19*(3): 377-412.

Oliphant, A.J., Thenkabail, P.S., Teluguntla, P., Xiong, J., Gumma, M.K., Congalton, R.G and Yadav, K. 2019. Mapping cropland extent of Southeast and Northeast Asia using multi-year time-series Landsat 30-m data using a random forest classifier on the Google Earth Engine Cloud. *International Journal of Applied Earth Observation and Geoinformation*. 81: 110-124.

Onojeghuo, A.O., Blackburn, G.A., Wang, Q., Atkinson, P.M., Kindred, D and Miao, Y., 2018. Mapping paddy rice fields by applying machine learning algorithms to multi-temporal Sentinel-1A and Landsat data. *International Journal of Remote Sensing*. *39*(4):1042-1067.

Panjala, P., Gumma, M.K and Teluguntla, P. 2022. Machine learning approaches and Sentinel-2 data in crop type mapping. In *Data Science in Agriculture and Natural Resource Management* (161-180). Springer, Singapore.

Pokovai, K and Fodor, N. 2019. Adjusting ceptometer data to improve leaf area index measurements. *Agronomy. 9*(12):866.

Priya, S and Shibasaki, R. 2001. National spatial crop yield simulation using GIS-based crop production model. *Ecological Modelling. 136*(2-3): 113-129.

Radanielson, A.M., Gaydon, D.S., Li, T., Angeles, O and Roth, C.H. 2018. Modeling salinity effect on rice growth and grain yield with ORYZA v3 and APSIM-Oryza. *European Journal of Agronomy.* 100: 44-55.

Raman, M.G., Kaliaperumal, R., Pazhanivelan, S and Kannan, B. 2019. Rice area estimation using parameterized classification of sentinel 1A SAR data. *The International Archives of Photogrammetry, Remote Sensing and Spatial Information Sciences. 42*: 141-147.

Ranjan, A.K and Parida, B.R. 2019. Paddy acreage mapping and yield prediction using sentinel-based optical and SAR data in Sahibganj district, Jharkhand (India). *Spatial Information Research. 27*(4):399-410.

Rastogi, A., Kalra, N., Agarwal, P.K., Sharma, S.K., Harit, R.C., Navalgund, R.R and Dadhwal, V.K. 2000. Estimation of wheat leaf area index from IRS LISS-III data using Price model. *International Journal of Remote Sensing. 21*(15): 2943-2949.

Setiyono, T.D., Quicho, E.D., Gatti, L., Campos-Taberner, M., Busetto, L., Collivignarelli, F., García-Haro, F.J., Boschetti, M., Khan, N.I and Holecz, F. 2018. Spatial rice yield estimation based on MODIS and Sentinel-1 SAR data and ORYZA crop growth model. *Remote Sensing.* 10(2): 293.

Setiyono, T.D., Quicho, E.D., Holecz, F.H., Khan, N.I., Romuga, G., Maunahan, A., Garcia, C., Rala, A., Raviz, J., Collivignarelli, F and Gatti, L. 2019. Rice yield estimation using synthetic aperture radar (SAR) and the ORYZA crop growth model: development and application of the system in South and South-east Asian countries. *International Journal of Remote Sensing. 40*(21): 8093-8124.

Shanmugapriya, P., Rathika, S., Ramesh, T and Janaki, P. 2019. Applications of remote sensing in agriculture-A Review. *International Journal of Current Microbiology and Applied Sciences. 8*(1): 2270-2283.

Shelestov, A., Lavreniuk, M., Kussul, N., Novikov, A and Skakun, S. 2017. Exploring Google Earth Engine platform for big data processing: Classification of multi-temporal satellite imagery for crop mapping. *frontiers in Earth Science. 5*: 17.

Siyal, A.A., Dempewolf, J and Becker-Reshef, I. 2015. Rice yield estimation using Landsat ETM+ Data. *Journal of Applied Remote Sensing*. *9*(1): 095986.

Son, N.T., Chen, C.F., Chen, C.R and Minh, V.Q. 2018. Assessment of Sentinel-1A data for rice crop classification using random forests and support vector machines. *Geocarto International*. *33*(6): 587-601.

Son, N.T., Chen, C.F., Chen, C.R., Chang, L.Y and Chiang, S.H. 2016. Rice yield estimation through assimilating satellite data into a crop simumlation model. *International Archives of the Photogrammetry, Remote Sensing and Spatial Information Sciences*. *8*.

Son, N.T., Chen, C.F., Chen, C.R., Guo, H.Y., Cheng, Y.S., Chen, S.L., Lin, H.S and Chen, S.H. 2020. Machine learning approaches for rice crop yield predictions using time-series satellite data in Taiwan. *International Journal of Remote Sensing*. 41(20): 7868-7888.

Srilatha, V. 2020. Soybean area and yield estimation in Nizamabad district using temporal microwave and optical remote sensing data, *MSc Thesis*. Professor Jayashankar Telangana State Agricultural University, Rajendranagar, Hyderabad, India.

Subash, N., Shamim, M., Singh, V.K., Gangwar, B., Singh, B., Gaydon, D.S., Roth, C.H., Poulton, P.L and Sikka, A.K. 2015. Applicability of APSIM to capture the effectiveness of irrigation management decisions in rice-based cropping sequence in the Upper-Gangetic Plains of India. *Paddy and Water Environment*. *13*(4):325-335.

Suriadi, A., Gaydon, D., Abawi, Y and Misra, R.K. 2009, August. Capability of APSIM-Oryza to stimulate lowland rice-based farming systems under nitrogen treatments in a tropical climate. In *Farming Systems Design Symposium 2009 Proceedings*. 267-268. *International Environmental Modeling and Software Society (IEMSS)*.

Tripathy, R., Chaudhari, K.N., Mukherjee, J., Ray, S.S., Patel, N.K., Panigrahy, S and Parihar, J.S. 2013. Forecasting wheat yield in Punjab state of India by combining crop simulation model WOFOST and remotely sensed inputs. *Remote Sensing letters*. *4*(1): 19-28.

Van Diepen, C.V., Wolf, J.V., Van Keulen, H and Rappoldt, C. 1989. WOFOST: a simulation model of crop production. *Soil Use and Management*. *5*(1): 16-24.

Van Ittersum, M. and Donatelli, M. 2003. Modelling cropping systems-highlights of the symposium and preface to the special issues. *European Journal of Agronomy*. *18*(3-4): 187-197.

Van Tricht, K., Gobin, A., Gilliams, S. and Piccard, I. 2018. Synergistic use of radar Sentinel-1 and optical Sentinel-2 imagery for crop mapping: A case study for Belgium. *Remote Sensing*. 10(10): 1642.

Wang, H., Zhu, Y., Li, W., Cao, W and Tian, Y. 2014. Integrating remotely sensed leaf area index and leaf nitrogen accumulation with RiceGrow model based on particle swarm optimization algorithm for rice grain yield assessment. *Journal of Applied Remote Sensing*. 8(1): 083674.

Watson, J., Challinor, A.J., Fricker, T.E and Ferro, C.A. 2015. Comparing the effects of calibration and climate errors on a statistical crop model and a process-based crop model. *Climatic Change*. *132*(1): 93-109.price

Xavier, A.C and Vettorazzi, C.A. 2004. Mapping leaf area index through spectral vegetation indices in a subtropical watershed. *International Journal of Remote Sensing*. *25*(9): 1661-1672.

Xiong, J., Thenkabail, P.S., Tilton, J.C., Gumma, M.K., Teluguntla, P., Oliphant, A., Congalton, R.G., Yadav, K and Gorelick, N. 2017. Nominal 30-m cropland extent map of continental Africa by integrating pixel-based and object-based algorithms using Sentinel-2 and Landsat-8 data on Google Earth Engine. *Remote Sensing*. 9(10): 1065.

Xu, L., Zhang, H., Wang, C., Zhang, B and Liu, M. 2019. Crop classification based on temporal information using sentinel-1 SAR time-series data. *Remote Sensing*. 11(1): 53.

Xu, Y., Du, B., Zhang, L., Cerra, D., Pato, M., Carmona, E., Prasad, S., Yokoya, N., Hänsch, R and Le Saux, B. 2019. Advanced multi-sensor optical remote sensing for urban land use and land cover classification: Outcome of the 2018 IEEE GRSS data fusion contest. *IEEE Journal of Selected Topics in Applied Earth Observations and Remote Sensing*. *12*(6): 1709-1724.

Yang, J., Greenwood, D.J., Rowell, D.L., Wadsworth, G.A and Burns, I.G. 2000. Statistical methods for evaluating a crop nitrogen simulation model, N_ABLE. *Agricultural Systems*. *64*(1): 37-53.

Yang, K.W., Chapman, S., Carpenter, N., Hammer, G., McLean, G., Zheng, B., Chen, Y., Delp, E., Masjedi, A., Crawford, M and Ebert, D. 2021. Integrating crop growth models with remote sensing for predicting biomass yield of sorghum. *In Silico Plants*. *3*(1): 001.

Yang, X., Brown, H.E., Teixeira, E and Moot, D.J. 2021. Development of a lucerne model in APSIM next generation: 1 phenology and morphology of genotypes with different fall dormancies. *European Journal of Agronomy*. 130: 126372.

Yoshio Inoue, M. Susan Moran and Takeshi Horie. 1998. Analysis of spectral measurements in paddy field for predicting rice growth and yield based on a simple crop simulation model. *Plant Production Science*. 1(4): 269-279.

Zhang, X., Lee, J.H., Abawi, Y., Kim, Y.H., McClymont and Kim, H.D. 2007. Testing the simulation capability of APSIM-ORYZA under different levels of nitrogen fertiliser and transplanting time regimes in Korea. *Australian Journal of Experimental Agriculture*. *47*(12): 1446-1454.

Zhang, X., Meinke, H., DeVoil, P., van Laar, G., Bouman, B.A and Abawi, Y. 2004. Simulating growth and development of lowland rice in APSIM. In *Proceedings of 4th international crop science conference, Brisbane'*.

Zhang, Y and Wegehenkel, M. 2006. Integration of MODIS data into a simple model for the spatial distributed simulation of soil water content and evapotranspiration. *Remote Sensing of Environment*. *104*(4): 393-408.

Zhao, Y., Potgieter, A.B., Zhang, M., Wu, B and Hammer, G.L. 2020. Predicting wheat yield at the field scale by combining high-resolution Sentinel-2 satellite imagery and crop modelling. *Remote Sensing*. *12*(6): 1024.

Ziliani, M.G., Altaf, M.U., Aragon, B., Houborg, R., Franz, T.E., Lu, Y., Sheffield, J., Hoteit, I and McCabe, M.F. 2022. Early season prediction of within-field crop yield variability by assimilating CubeSat data into a crop model. *Agricultural and Forest Meteorology*. 313: 108736.

Ziliani, M.G., Ershadi, A., Zheng, B., Ait-El-Fquih, B., Altaf, M.U., Aragon, B., Hoteit, I., Franz, T.E., Chapman and McCabe, M. 2018. Corn-yield estimation through assimilation of remotely sensed LAI data into APSIM. In *AGU Fall Meeting Abstracts* (Vol. 2018: GC43I-1653).

https://e4ftl01.cr.usgs.gov/MOLA/MYD13Q1.006/

Pokovai, K and Fodor, N., 2019. Adjusting ceptometer data to improve leaf area index measurements. *Agronomy*. *9*(12):866.

https://www.isric.org

https://www.telangana.gov.in/

code.earthengine.google.com

https://sites.google.com/a/irri.org/oryza2000/

https://agri.telangana.gov.in/

Questionnaire followed to collect the data from the farmers

Farmer details Name and address Contact no	
Location of Plot	
Area of land holding	
Previous crop sown	
Soil type	
Soil nutrient status	
Variety name and duration	
Date of transplanting /sowing	
Irrigation details No. of irrigations Stages of irrigation	
Fertilizer details Rate of application Stage of application with quantity	
Organic amendments (if any applied)	
Pest and disease attack (if any) Name and quantity of insecticides/ pesticides used	
Date of harvesting	
Yield (Kg ha^{-1})	
Soil health card Details	
Other Comments	

APPENDIX-B

Day Wise Monthly Avg. Rainfall Report for the Month of January to December, 2021 (in mm) collected from AWS for Kattangoor Mandal

Days	Jan	Feb	Mar	Apr	May	Jun	Jul	Aug	Sep	Oct	Nov	Dec
1	0	0	0	0	0	18.2	0.7	0.0	1.3	4.7	9.2	0
2	0	0	0	0	0	0	34.9	0.0	0	0.0	15.9	0
3	0	0	0	0	0	39.7	0.3	0.3	54.2	0.0	1.2	0
4	0	0	0	0	0	7.4	0	0.0	0.3	0.0	0	0
5	0	0	0	0	0	0	0	0.0	54.9	0.0	0	0
6	0	0	0	0	0	2.4	0	0.0	7	0.0	0	0
7	0	0	0	0	0	0	0	0.0	10.7	0.0	0	0
8	0	0	0	0	0	0	5.8	0.0	0	0.0	0	0
9	0	0	0	0	0	0	0	4.6	0	8.3	0	0
10	0	0	0	0	0	0	9.6	0.0	0	9.0	0	7.4
11	0	0	0	0	0	3.7	0.3	0.0	0	0.0	0	0
12	0	0	0	0	25.4	0	24.5	0.0	0	0.0	0	0
13	0	0	0	0	0	92.9	0	51.6	0	0.0	3.5	0
14	0	0	0	0	0	16.3	35.7	0.0	0.7	0.0	0	0
15	0	0	0	13.4	0	0	8	0.0	0	0.0	0	0
16	0	0	0	0	0	0	4.3	13.2	0	0.0	0	0
17	0	0	0	0	0	0	2.9	33.5	0	1.3	15.5	0
18	0	0	0	0	0	0	18.6	0.7	0	0.0	0	0
19	0	0	0	0	4.1	0	2.6	0.0	0	0.0	2.7	0
20	0	0	0	0	0	0	0	0.0	1	0.0	1.3	0
21	0	0	0	0	0	0	4.7	0.0	27.9	0.0	6.6	0
22	0	0	0	0	0	0	35.9	0.0	11.7	0.0	1.2	0

23	0	0	0	15.7	0	3.5	15.4	0.0	4.3	0.0	0	0
24	0	0	0	0	0.9	7.2	0	0.0	0	0.0	0	0
25	0	0	0	0	0	0	0	21.2	0	0.0	16.4	0
26	0	0	0	0	0	0	0	25.7	30	0.0	0	0
27	0	0	0	0	0	22.1	0	12.1	3.1	0.0	0	0
28	0	0	0	0	0	66.9	0	12.5	29.8	0.0	0	0
29	0	--	0	0	0.5	0	0	3.9	0	0.0	0.9	0
30	0	--	0	0	0	0	0	98.6	0	0.0	0	0
31	0	--	0	--	0.3	--	0	13.4	--	3.1	--	0
Rainy Days	0	0	0	2	2	10	13	11	10	4	7	1
Avg Rainfall	0	0	0	29.1	31.2	280.3	204.2	291.3	236.9	26.4	74.4	7.4
Normal Rainfall	3.4	0.9	9	6.2	29.5	88.9	143.2	128.7	174	86.9	44.1	2.6
% Deviation	-100	-100	-100	369	6	215	43	126	36	-70	69	185
Status	No Rain	No Rain	No Rain	Excess	Normal	Excess	Excess	Excess	Excess	Scanty	Excess	Excess

Day Wise Monthly Avg. Rainfall Report for the Month of June to December, 2021 (in mm) collected from AWS for Kangal mandal

Days	Jun	Jul	Aug	Sep	Oct	Nov	Dec
1	18.2	0.7	0.0	1.3	4.7	9.2	0
2	0	34.9	0.0	0	0.0	15.9	0
3	39.7	0.3	0.3	54.2	0.0	1.2	0
4	7.4	0	0.0	0.3	0.0	0	0
5	0	0	0.0	54.9	0.0	0	0
6	2.4	0	0.0	7	0.0	0	0
7	0	0	0.0	10.7	0.0	0	0
8	0	5.8	0.0	0	0.0	0	8
9	0	0	4.6	0	8.3	0	0
10	0	9.6	0.0	0	9.0	0	7.4
11	3.7	0.3	0.0	0	0.0	0	0
12	0	24.5	0.0	0	0.0	0	0
13	92.9	0	51.6	0	0.0	3.5	0
14	16.3	35.7	0.0	0.7	0.0	0	0
15	0	8	0.0	0	0.0	0	0
16	0	4.3	13.2	0	0.0	0	0
17	0	2.9	33.5	0	1.3	15.5	0
18	0	18.6	0.7	0	0.0	0	8
19	0	2.6	0.0	0	0.0	2.7	9
20	0	0	0.0	1	0.0	1.3	0
21	0	4.7	0.0	27.9	0.0	6.6	0
22	0	35.9	0.0	11.7	0.0	1.2	0
23	3.5	15.4	0.0	4.3	0.0	0	0
24	7.2	0	0.0	0	0.0	0	0

25	0	0	21.2	0	0.0	16.4	0
26	0	0	25.7	30	0.0	0	0
27	22.1	0	12.1	3.1	0.0	0	0
28	66.9	0	12.5	29.8	0.0	0	0
29	0	0	3.9	0	0.0	0.9	0
30	0	0	98.6	0	0.0	0	0
31	--	0	13.4	--	3.1	--	0
Rainy Days	10	13	11	10	4	7	1
Avg. Rainfall	280.3	204.2	291.3	236.9	26.4	74.4	7.4
Normal Rainfall	88.9	143.2	128.7	174	86.9	44.1	2.6
% Deviation	215	43	126	36	-70	69	185
Status	Excess	Excess	Excess	Excess	Scanty	Excess	Excess

APPENDIX-C

GEE code for supervised classification

```
Map.addLayer(table2)
var collectionVV = ee.ImageCollection('COPERNICUS/S1_GRD')
   .filter(ee.Filter.eq('instrumentMode', 'IW'))
   .filter(ee.Filter.listContains('transmitterReceiverPolarisation', 'VV'))
   .filterBounds(roi) .select(['VV']);
   var VV1 = collectionVV.filterDate('2021-06-01', '2021-07-01').min();
   var VV2 = collectionVV.filterDate('2021-07-01', '2021-08-01').min();
   var VV3 = collectionVV.filterDate('2021-08-01', '2021-09-01').min();
   var VV4 = collectionVV.filterDate('2021-09-01', '2021-10-01').min();
   var VV5 = collectionVV.filterDate('2021-10-01', '2021-11-01').min();
print(collectionVV);
Map.addLayer(table);
var collectionVH = ee.ImageCollection('COPERNICUS/S1_GRD')
   .filter(ee.Filter.eq('instrumentMode', 'IW'))
   .filter(ee.Filter.listContains('transmitterReceiverPolarisation', 'VH'))
   .filterBounds(roi) .select(['VH']);
   var VH1 = collectionVH.filterDate('2021-06-01', '2021-07-01').min();
   var VH2 = collectionVH.filterDate('2021-07-01', '2021-08-01').min();
   var VH3 = collectionVH.filterDate('2021-08-01', '2021-09-01').min();
   var VH4 = collectionVH.filterDate('2021-09-01', '2021-10-01').min();
   var VH5 = collectionVH.filterDate('2021-10-01', '2021-11-01').min();
print(collectionVH);
Map.addLayer(roi)
function addNDVI(image) {
 var ndvi = image.normalizedDifference(['B8', 'B4']).rename('ndvi')
 return ndvi
}
var ndvi_Nalgonda = ee.ImageCollection('COPERNICUS/S2_SR')
          .filter(ee.Filter.lt('CLOUDY_PIXEL_PERCENTAGE', 20))
          .map(maskS2clouds)
           .filterBounds(roi);
```

```
  var ndvi1 = ndvi_Nalgonda.filterDate('2021-06-01', '2021-07-
01').map(addNDVI).max().clip(roi)

  var ndvi2 =ndvi_Nalgonda.filterDate('2021-07-01','2021-08-
01').map(addNDVI).max().clip(roi)

  var ndvi3 =ndvi_Nalgonda.filterDate('2021-08-01', '2021-09-
01').map(addNDVI).max().clip(roi)

  var ndvi4 =ndvi_Nalgonda.filterDate('2021-09-01', '2021-10-
01').map(addNDVI).max().clip(roi)

  var ndvi5 =ndvi_Nalgonda.filterDate('2021-10-01', '2021-11-
01').map(addNDVI).max().clip(roi)

var stack=ndvi1.addBands(ndvi2).addBands(ndvi3).addBands(ndvi4).addBands(ndvi5)
.addBands(VV1).addBands(VV2).addBands(VV3).addBands(VV4)

.addBands(VV5).addBands(VH1).addBands(VH2).addBands(VH3).addBands(VH4).ad
dBands(VH5)

Map.addLayer(stack)

var bandNames= stack.bandNames();

print(bandNames);

var training = stack.sampleRegions({
  collection: table,
  properties: ['value'],
  scale: 10
});

var trained = ee.Classifier.smileRandomForest(200).train(training,'value', bandNames);

var classified = stack.classify(trained);

Map.addLayer(classified);

Export.image.toDrive({
  image:classified.clip(roi),
  description: 'nalgonda_cropmap',
  scale: 10,
  region: roi,
  maxPixels: 1e12,
});
```

GEE code for downloading Remote Sensing products

```
var oct_1 = ee.ImageCollection("COPERNICUS/S2")
            .filterDate('2021-10-01','2021-10-10')
            .filterBounds(table)
            .select(['B8']).median()
var oct_2 = ee.ImageCollection("COPERNICUS/S2")
            .filterDate('2021-10-20','2021-10-30')
            .filterBounds(table)
               .select(['B8']).median();
var stack=oct_1.addBands(oct_2)
var points = stack.reduceRegions({
  collection: table2,
  reducer: ee.Reducer.max(),
  scale:10
})
print(points)
Export.table.toDrive(
            points,
             "table");
Map.centerObject(table);
```

GEE Code for downloading values of NDVI

```
function addNDVI(image) {
  var ndvi = image.normalizedDifference(['B8', 'B4']).rename('ndvi')
  return ndvi
}
var oct_1 = ee.ImageCollection('COPERNICUS/S2_SR')
            .filterDate('2021-10-01','2021-10-10')
          // .filter(ee.Filter.lt('CLOUDY_PIXEL_PERCENTAGE',20))
           //.map(maskS2clouds)
           .filterBounds(table).map(addNDVI).max().clip(table);
```

```
var oct_2 = ee.ImageCollection('COPERNICUS/S2_SR')
          .filterDate('2021-10-20','2021-10-30')
          .filter(ee.Filter.lt('CLOUDY_PIXEL_PERCENTAGE', 20))
          .filterBounds(table).map(addNDVI).max().clip(table);
var stack= oct_1.addBands(oct_2);
var points = stack.reduceRegions({
 collection: table2,
 reducer: ee.Reducer.max(),
 scale:10
})
Map.addLayer(stack);
print(points)
// Export tables
Export.table.toDrive(
          points,
           "table");
Map.centerObject(table);
```

GEE Code for downloading VV values

```
var collectionVV = ee.ImageCollection('COPERNICUS/S1_GRD')
  .filter(ee.Filter.eq('instrumentMode', 'IW'))
  .filter(ee.Filter.listContains('transmitterReceiverPolarisation', 'VV'))
  var oct_1 = collectionVV.filterDate('2021-10-01', '2021-10-20')
  .filterBounds(table)
  .select(['VV']).max();
  var oct_2 = collectionVV.filterDate('2021-10-21', '2021-10-30')
  .filterBounds(table)
  .select(['VV']).max();
var stack=oct_1.addBands(oct_2)
var points = stack.reduceRegions({
 collection: table2,
 reducer: ee.Reducer.max(),
 scale:10
})
```

```
print(points)
Export.table.toDrive(
            points,
             "table");
Map.centerObject(table);
```

GEE Code for downloading VH values

```
var collectionVH = ee.ImageCollection('COPERNICUS/S1_GRD')
   .filter(ee.Filter.eq('instrumentMode', 'IW'))
   .filter(ee.Filter.listContains('transmitterReceiverPolarisation', 'VH'))
   var oct_1 = collectionVH.filterDate('2021-10-01', '2021-10-20')
   .filterBounds(table)
   .select(['VH']).max();
   var oct_2 = collectionVV.filterDate('2021-10-21', '2021-10-30')
   .filterBounds(table)
   .select(['VH']).max();
var stack=oct_1.addBands(oct_2)
var points = stack.reduceRegions({
  collection: table2,
  reducer: ee.Reducer.max(),
  scale:10
})
print(points)
Export.table.toDrive(
            points,
             "table");
Map.centerObject(table);
```

Weather data used in the APSIM model to simulate rice yields for Mallaram village

!title = Mallaram					
[weather.met.weather]					
latitude = 16.961 (DECIMAL DEGREES)					
longitude = 79.2435 (DECIMAL DEGREES)					
tav = 26.2 (°C) ! annual average ambient temperature					
amp = 10.92(°C) ! annual amplitude in mean monthly temperature					
year	day	radn	maxt	mint	rain
()	()	(MJ/m^2)	(oC)	(oC)	(mm)
2021	1	14.6	26.1	17.1	0.0
2021	2	16.1	25.6	16	0.0
2021	3	16.9	25.8	14.8	0.0
2021	4	17.4	26.2	15.4	0.0
2021	5	14.3	28.3	16.6	0.0
2021	6	6.5	26.8	19.7	0.0
2021	7	11.5	28.4	20.1	0.0
2021	8	15.9	28.6	19.3	0.0
2021	9	16.1	28.3	17	0.0
2021	10	16.3	29	18.4	0.0
2021	11	15.5	29.4	18.5	0.0
2021	12	15.3	29.6	18.8	0.0
2021	13	14.8	29.6	19.6	0.0
2021	14	16.5	29.4	19.3	0.0
2021	15	16.3	29.5	17.6	0.0
2021	16	15.9	29.6	18.2	0.0
2021	17	17.7	29.3	18	0.0
2021	18	15.8	28.9	18	0.0
2021	19	17.2	29.6	18.3	0.0
2021	20	18.6	30.6	17.3	0.0
2021	21	18	31.6	17.1	0.0
2021	22	15.3	30.3	18.2	0.0
2021	23	16.5	30.4	18.5	0.0
2021	24	19	31.3	16.9	0.0
2021	25	19.5	31.4	17	0.0
2021	26	19.8	31.6	17.2	0.0
2021	27	16.6	30.8	17.3	0.0
2021	28	16.5	30.4	17.9	0.0
2021	29	15.6	30.6	18.5	0.0
2021	30	17.7	30.5	18.8	0.0
2021	31	16.9	30.6	18.3	0.0
2021	32	16.4	29.3	18.3	0.0
2021	33	17.7	30.1	16.5	0.0
2021	34	19.1	30.2	17.8	0.0
2021	35	20.4	30.5	16.5	0.0
2021	36	21	30.7	15.3	0.0

2021	37	20.7	31.2	15.4	0.0
2021	38	21	30.4	14.7	0.0
2021	39	20.2	30.1	13	0.0
2021	40	20.3	31.2	17	0.0
2021	41	21.4	32.2	15.9	0.0
2021	42	21	32.1	15.7	0.0
2021	43	21.2	32	16	0.0
2021	44	21.8	32.4	15.9	0.0
2021	45	21.6	32.6	16	0.0
2021	46	21.3	33.1	16.7	0.0
2021	47	21.3	33.9	16.9	0.0
2021	48	21.5	33.5	17.1	0.0
2021	49	21	32.3	17.2	0.0
2021	50	8.6	29.9	19.3	0.0
2021	51	17.6	30.3	18.7	0.0
2021	52	16.2	30.6	18.6	0.0
2021	53	20.2	31.4	20.2	0.0
2021	54	21.1	34.2	19.6	0.0
2021	55	22.1	35.3	17.8	0.0
2021	56	23	36.3	18.1	0.0
2021	57	22.7	36.9	20.1	0.0
2021	58	21.3	37	20.3	0.0
2021	59	22.5	36.9	20.3	0.0
2021	60	22.7	37.6	19.7	0.0
2021	61	22.4	37.1	20.4	0.0
2021	62	23.9	37.4	18.5	0.0
2021	63	23.9	37.3	19.3	0.0
2021	64	24.7	37.5	18.6	0.0
2021	65	24.7	38.3	18	0.0
2021	66	23.9	38	19.2	0.0
2021	67	23.6	37.4	19.2	0.0
2021	68	23.6	37	19.3	0.0
2021	69	24.6	37.9	19.8	0.0
2021	70	25	37.9	19.2	0.0
2021	71	25.2	36.8	18.7	0.0
2021	72	26	37.3	19	0.0
2021	73	24.7	38	18.9	0.0
2021	74	24.1	38.1	20.4	0.0
2021	75	21.4	38	20.7	0.0
2021	76	20.3	38.6	22.3	0.0
2021	77	18.6	38.4	21.6	0.0
2021	78	20.4	37.3	22.8	0.0
2021	79	21.6	37.5	22.3	0.0
2021	80	21.6	39.1	22.6	0.0
2021	81	19.7	38.9	23	0.0
2021	82	25.2	39.3	23.2	0.0

2021	83	24.6	39.7	22.9	0.0
2021	84	21.4	40.4	24	0.0
2021	85	21.7	40.1	25.6	0.0
2021	86	19.5	40.7	24.4	0.0
2021	87	22.1	41	23.6	0.0
2021	88	21.8	41.2	23.1	0.0
2021	89	22.7	42.4	22.9	0.0
2021	90	25.9	43.5	24.1	0.0
2021	91	26.5	42.9	23.7	0.0
2021	92	26.3	43	25.5	0.0
2021	93	23.9	41.9	24	0.0
2021	94	23.6	41.1	24.9	0.0
2021	95	19.9	40.6	24.5	0.0
2021	96	23.3	40.6	25	0.0
2021	97	21.7	40.7	23.7	0.0
2021	98	23	42	24.6	0.0
2021	99	22	40.3	24.3	0.0
2021	100	21.9	39.3	23.9	0.0
2021	101	23.4	39.4	24	0.0
2021	102	23.4	40	24.1	0.0
2021	103	24.4	40.1	25.2	0.0
2021	104	18.2	38.6	26.8	0.0
2021	105	25	38.6	26.1	0.0
2021	106	24.1	39.5	25.5	0.0
2021	107	24.3	40.5	25	0.0
2021	108	23.2	41.2	26.1	0.0
2021	109	21.2	41.7	26.8	0.0
2021	110	18.4	41.8	28.3	0.0
2021	111	17.7	40.4	27.4	0.0
2021	112	19.1	38	27.7	0.0
2021	113	15.1	35	26.1	0.0
2021	114	22.3	38.5	25.6	0.0
2021	115	24.2	40.4	24.7	0.0
2021	116	22.5	38.8	26.8	0.0
2021	117	23.4	40.5	26.1	0.0
2021	118	19.7	41.1	26.9	0.0
2021	119	22.7	41.7	27.1	0.0
2021	120	21.7	41.5	26.5	0.0
2021	121	23.7	40.9	25.3	0.0
2021	122	24.8	40.8	25.5	0.0
2021	123	24.3	39.9	25.5	0.0
2021	124	24.6	40.3	25.6	0.0
2021	125	25.3	41	26.6	0.0
2021	126	25	40.8	27	0.0
2021	127	25.5	40.5	26.6	0.0
2021	128	26.4	40.4	26.7	0.0

2021	129	26.1	40.8	26.9	0.0
2021	130	23	40.3	28.2	0.0
2021	131	19.1	38.8	28.9	0.0
2021	132	22.7	40.1	27.3	0.0
2021	133	16.6	37.9	28.5	0.0
2021	134	21.9	40.4	27	0.0
2021	135	22	35.5	26.7	0.0
2021	136	17	33.8	26.7	0.0
2021	137	22	34.2	25.9	0.0
2021	138	22.3	34.3	27.2	0.0
2021	139	21.9	36.3	27.9	0.0
2021	140	21.4	34.2	27.3	0.0
2021	141	15	34.9	26.6	0.0
2021	142	16.2	35.8	25.9	0.0
2021	143	20.2	40.6	25.1	0.0
2021	144	17.5	38.4	27.5	0.0
2021	145	20.1	40.7	28.2	0.0
2021	146	22.4	42.7	28	0.0
2021	147	24.5	41.9	31	0.0
2021	148	23.5	38.5	30.7	0.0
2021	149	22.4	39.3	29.2	0.0
2021	150	24.1	41.5	29.3	0.0
2021	151	22.5	40.5	29.3	0.0
2021	152	21.9	38.6	27	0.0
2021	153	22.3	35.9	28.3	0.0
2021	154	9.5	31.5	26.9	8.1
2021	155	19.2	33.6	25.8	4.3
2021	156	24.2	33.7	25.7	2.3
2021	157	24.2	35.6	25.5	0.1
2021	158	25.4	35.5	26.3	0.0
2021	159	26.3	35.1	26.4	0.0
2021	160	20.9	33.3	26.6	0.0
2021	161	17	33.5	25.3	1.0
2021	162	12.5	35.8	23.9	5.8
2021	163	18.7	35.2	24.3	0.8
2021	164	13.3	32	23.7	7.2
2021	165	13.8	31	24.3	9.5
2021	166	15.3	34.9	24.4	0.2
2021	167	17.4	35.1	24	23.1
2021	168	17.5	34	24.6	0.0
2021	169	14.3	34.9	25.4	6.4
2021	170	20.2	35.6	24.9	0.0
2021	171	20.1	36.2	24.9	0.0
2021	172	23	35.6	25.3	0.0
2021	173	17.7	31.8	25.4	0.0
2021	174	15.4	34.4	24.9	0.0

2021	175	18.6	33.3	25.3	0.1
2021	176	19.8	36.5	24.6	0.0
2021	177	16.5	31.8	25.1	0.0
2021	178	10.9	30.6	24.9	5.4
2021	179	20	32.9	24.9	15.7
2021	180	21.2	33.8	25.6	0.1
2021	181	22.9	34.9	25.8	0.0
2021	182	11.6	30.5	26.3	0.8
2021	183	9.3	31.7	24.7	5.2
2021	184	19.1	32.6	24.5	0.1
2021	185	20.9	34.5	25	0.0
2021	186	19.6	32.6	25.4	0.0
2021	187	21	32.7	25.8	0.0
2021	188	17.3	33.4	26.3	6.6
2021	189	13	29.5	25.3	3.7
2021	190	14	33.4	24.4	0.0
2021	191	15.9	30.4	25	21.7
2021	192	7.4	30.1	23.6	0.3
2021	193	12.6	32.1	24.1	40.6
2021	194	14.4	31.1	24.1	2.0
2021	195	12.6	29.3	23.3	25.4
2021	196	15	32.7	24.1	33.3
2021	197	17.9	31.9	23.6	0.5
2021	198	20.5	31.5	24.9	26.8
2021	199	13.8	31	25.5	32.4
2021	200	20.7	31.7	24.7	0.1
2021	201	19	31.6	24.6	0.0
2021	202	4.9	29.3	23.8	5.6
2021	203	4.9	27.7	23.8	49.1
2021	204	19.1	30.5	24.1	28.4
2021	205	21.3	33.7	23.7	0.0
2021	206	21.7	33.6	24.5	0.0
2021	207	19.5	32.5	24.6	4.7
2021	208	22.2	30.8	24	0.1
2021	209	19.5	33.1	23.5	0.0
2021	210	13.4	31.9	23.7	0.0
2021	211	17.3	30.5	23.8	0.0
2021	212	8.6	30.6	23.9	0.0
2021	213	19.7	32.3	23.9	0.0
2021	214	21.8	32.9	23.4	0.0
2021	215	21.5	32.1	23.3	0.0
2021	216	19.5	32.6	24.3	0.0
2021	217	20.1	31.3	24.4	0.0
2021	218	21.5	33.1	24.5	0.0
2021	219	23.1	32	25	0.0
2021	220	20.6	30.3	24.7	0.0

2021	221	19.4	31.9	25.2	0.8
2021	222	19	32.4	25.2	8.5
2021	223	20.7	31	25.2	4.0
2021	224	16.2	29.8	25	0.0
2021	225	13.7	30.5	24.2	15.9
2021	226	15.1	31.2	23.9	0.0
2021	227	17.9	29.2	24.1	0.0
2021	228	9	28.7	23.6	29.5
2021	229	10.7	31.7	22.9	11.3
2021	230	16.9	32.3	23.2	1.9
2021	231	16	31.9	23.5	0.4
2021	232	12.3	30.2	23.5	0.0
2021	233	7.3	29.5	23.5	0.5
2021	234	23.8	31.5	23	0.0
2021	235	24.7	31.6	23.5	5.1
2021	236	23.6	32.9	23.6	0.2
2021	237	22.4	31.5	24.9	2.3
2021	238	13.3	30.3	24.8	2.3
2021	239	13.1	30.2	23.7	52.6
2021	240	10.3	31.6	23.8	3.1
2021	241	13.5	31.2	23.6	46.4
2021	242	6.6	30.7	23.2	41.7
2021	243	12.6	28.7	22.2	7.3
2021	244	9.4	30.2	22.7	33.7
2021	245	19.9	31.3	23.6	0.3
2021	246	14.2	29.7	24.5	3.8
2021	247	16.3	30.6	23.6	1.0
2021	248	20.1	29.1	23.8	11.7
2021	249	5.6	26.8	23.5	1.0
2021	250	15.4	30.1	23	17.3
2021	251	19.1	32.1	22	4.7
2021	252	21.4	32.1	22.8	0.0
2021	253	17.7	31.7	23.8	0.0
2021	254	16.3	30.8	24.3	0.0
2021	255	16.5	30.3	24	0.0
2021	256	15.8	30.8	23.7	0.0
2021	257	17.8	32.5	23.9	5.2
2021	258	18.8	31.2	23.6	0.0
2021	259	21.7	31.6	23.7	0.0
2021	260	21.4	31.8	23.9	0.0
2021	261	19.8	31.2	23.8	0.0
2021	262	18.3	31.8	23.8	0.0
2021	263	17.4	30.8	24.8	0.3
2021	264	14.6	30	24.2	35.1
2021	265	15.8	29.8	23.6	3.5
2021	266	17.3	29.7	23.9	6.6

2021	267	18.9	30.8	23.2	22.7
2021	268	19	31	24.3	0.8
2021	269	18.3	31.4	23.9	7.7
2021	270	4.8	28.9	23	6.9
2021	271	15.4	30.7	22.2	21.4
2021	272	21.9	30.6	20.9	0.0
2021	273	18.4	31.4	23.1	0.0
2021	274	21.1	30	24.2	0.0
2021	275	21.7	29.8	23.1	0.0
2021	276	22.2	31	24.1	0.0
2021	277	20.4	31.2	24	0.0
2021	278	20.3	29.5	24.3	4.0
2021	279	13.7	29.3	23.7	0.0
2021	280	19	30.3	23.7	2.6
2021	281	21.5	30.3	24	0.0
2021	282	18.4	31	24.4	0.2
2021	283	18.1	28.8	24.3	35.7
2021	284	20.1	30.1	22.3	0.0
2021	285	19.1	31	21.9	0.0
2021	286	16.7	30.6	22.7	0.0
2021	287	17.6	30.1	22.8	0.0
2021	288	15.8	30.9	22	0.0
2021	289	12	30.4	24.3	6.7
2021	290	15.8	29.3	23.4	4.1
2021	291	20	31.3	23.7	0.0
2021	292	16.2	30.9	22.8	0.0
2021	293	16.7	29.9	21.1	0.0
2021	294	18	30.3	21	0.0
2021	295	19.4	29.9	20.2	0.0
2021	296	18.4	30	19.6	0.0
2021	297	16	29.2	20.3	0.0
2021	298	18.7	29.2	20	0.0
2021	299	19.1	28.9	19.3	0.0
2021	300	19.4	28.9	18.7	0.0
2021	301	16.1	29.3	20.2	0.0
2021	302	10.3	28.3	22.4	0.0
2021	303	14.3	28.9	22.9	3.1
2021	304	13.9	28.7	21.6	0.0
2021	305	9.1	26.5	19.1	5.2
2021	306	13.6	28.7	21.7	0.0
2021	307	12.1	28.3	22	0.0
2021	308	13.5	28.6	22.1	0.2
2021	309	15.5	29.3	21.7	0.0
2021	310	15.4	29	21.1	0.0
2021	311	12.5	28	19.8	0.0
2021	312	17.1	27.9	18.5	0.0

2021	313	14	27.9	17.1	0.0
2021	314	14.7	27	17.3	0.0
2021	315	8.1	26.6	18	0.0
2021	316	7.4	27.2	20.6	0.0
2021	317	8.7	29.1	22.3	0.8
2021	318	12.9	29.5	22.8	0.0
2021	319	12.5	29.8	22.7	15.3
2021	320	11.2	29.7	22.6	0.0
2021	321	12	28.9	23.2	7.8
2021	322	7.4	28.5	22.6	0.0
2021	323	5.5	27.3	22.7	2.8
2021	324	10.3	29.7	22.8	6.5
2021	325	11.1	29.4	22.8	4.2
2021	326	16.8	30.3	23.3	6.1
2021	327	17.2	30.4	22.6	0.0
2021	328	15	29.2	22.9	1.8
2021	329	15.7	30.1	21.8	7.1
2021	330	16	29.7	19.2	0.0
2021	331	13.1	27.8	17.1	0.0
2021	332	7.4	27	17.3	0.0
2021	333	7.1	27.1	20.1	0.0
2021	334	13.9	26.6	19.6	0.0
2021	335	15.2	28.1	18.5	0.0
2021	336	16.4	27.8	16.8	0.0
2021	337	15.8	27.2	17.6	0.0
2021	338	17.5	29.3	17.4	0.0
2021	339	17.8	29.7	17.5	0.0
2021	340	18	29.9	17.1	0.0
2021	341	17.7	29.2	17.4	0.0
2021	342	12	28.9	20.4	0.0
2021	343	12.3	28.8	20.7	0.0
2021	344	14.5	28.8	20.8	3.2
2021	345	16	29.2	19.7	3.9
2021	346	14.4	28.6	20.4	0.0
2021	347	12.4	27.8	19.3	0.0
2021	348	12	26.7	19.5	0.0
2021	349	12.3	25.1	19.3	0.0
2021	350	13.9	27.6	15.9	0.0
2021	351	16.7	27.4	14.9	0.0
2021	352	17.9	27.1	13.3	0.0
2021	353	16.8	26.8	13.2	0.0
2021	354	16	26.5	12.2	0.0
2021	355	17.1	27.3	9.8	0.0
2021	356	17.2	28.4	11.6	0.0
2021	357	17	29.3	13.5	0.0
2021	358	16.5	29.5	13.6	0.0

2021	359	16.6	30.6	15.3	0.0
2021	360	15.1	29.9	16.6	0.0
2021	361	13.5	29.1	17.4	0.0
2021	362	15.4	29.4	17.7	0.0
2021	363	16.1	29.7	16.8	0.0
2021	364	14.8	28.7	16.8	0.0
2021	365	16.1	28.9	17.1	0.0

Weather data used in the APSIM model to simulate rice yields for Telakantigudem village

!title = Telakantigudem					
[weather.met.weather]					
latitude = 16.961 (DECIMAL DEGREES)					
longitude = 79.2435 (DECIMAL DEGREES)					
tav = 26.2 (ºC) ! annual average ambient temperature					
amp = 10.92(ºC) ! annual amplitude in mean monthly temperature					
year	day	radn	maxt	mint	rain
()	()	(MJ/m^2)	(oC)	(oC)	(mm)
2021	1	14.6	26.1	17.1	0
2021	2	16.1	25.6	16	0
2021	3	16.9	25.8	14.8	0
2021	4	17.4	26.2	15.4	0
2021	5	14.3	28.3	16.6	0
2021	6	6.5	26.8	19.7	0
2021	7	11.5	28.4	20.1	0
2021	8	15.9	28.6	19.3	0
2021	9	16.1	28.3	17	0
2021	10	16.3	29	18.4	0
2021	11	15.5	29.4	18.5	0
2021	12	15.3	29.6	18.8	0
2021	13	14.8	29.6	19.6	0
2021	14	16.5	29.4	19.3	0
2021	15	16.3	29.5	17.6	0
2021	16	15.9	29.6	18.2	0
2021	17	17.7	29.3	18	0
2021	18	15.8	28.9	18	0
2021	19	17.2	29.6	18.3	0
2021	20	18.6	30.6	17.3	0
2021	21	18	31.6	17.1	0
2021	22	15.3	30.3	18.2	0
2021	23	16.5	30.4	18.5	0
2021	24	19	31.3	16.9	0
2021	25	19.5	31.4	17	0
2021	26	19.8	31.6	17.2	0
2021	27	16.6	30.8	17.3	0
2021	28	16.5	30.4	17.9	0
2021	29	15.6	30.6	18.5	0
2021	30	17.7	30.5	18.8	0
2021	31	16.9	30.6	18.3	0
2021	32	16.4	29.3	18.3	0
2021	33	17.7	30.1	16.5	0
2021	34	19.1	30.2	17.8	0
2021	35	20.4	30.5	16.5	0
2021	36	21	30.7	15.3	0
2021	37	20.7	31.2	15.4	0
2021	38	21	30.4	14.7	0

2021	39	20.2	30.1	13	0
2021	40	20.3	31.2	17	0
2021	41	21.4	32.2	15.9	0
2021	42	21	32.1	15.7	0
2021	43	21.2	32	16	0
2021	44	21.8	32.4	15.9	0
2021	45	21.6	32.6	16	0
2021	46	21.3	33.1	16.7	0
2021	47	21.3	33.9	16.9	0
2021	48	21.5	33.5	17.1	0
2021	49	21	32.3	17.2	0
2021	50	8.6	29.9	19.3	0
2021	51	17.6	30.3	18.7	0
2021	52	16.2	30.6	18.6	0
2021	53	20.2	31.4	20.2	0
2021	54	21.1	34.2	19.6	0
2021	55	22.1	35.3	17.8	0
2021	56	23	36.3	18.1	0
2021	57	22.7	36.9	20.1	0
2021	58	21.3	37	20.3	0
2021	59	22.5	36.9	20.3	0
2021	60	22.7	37.6	19.7	0
2021	61	22.4	37.1	20.4	0
2021	62	23.9	37.4	18.5	0
2021	63	23.9	37.3	19.3	0
2021	64	24.7	37.5	18.6	0
2021	65	24.7	38.3	18	0
2021	66	23.9	38	19.2	0
2021	67	23.6	37.4	19.2	0
2021	68	23.6	37	19.3	0
2021	69	24.6	37.9	19.8	0
2021	70	25	37.9	19.2	0
2021	71	25.2	36.8	18.7	0
2021	72	26	37.3	19	0
2021	73	24.7	38	18.9	0
2021	74	24.1	38.1	20.4	0
2021	75	21.4	38	20.7	0
2021	76	20.3	38.6	22.3	0
2021	77	18.6	38.4	21.6	0
2021	78	20.4	37.3	22.8	0
2021	79	21.6	37.5	22.3	0
2021	80	21.6	39.1	22.6	0
2021	81	19.7	38.9	23	0
2021	82	25.2	39.3	23.2	0
2021	83	24.6	39.7	22.9	0
2021	84	21.4	40.4	24	0
2021	85	21.7	40.1	25.6	0
2021	86	19.5	40.7	24.4	0

2021	87	22.1	41	23.6	0
2021	88	21.8	41.2	23.1	0
2021	89	22.7	42.4	22.9	0
2021	90	25.9	43.5	24.1	0
2021	91	26.5	42.9	23.7	0
2021	92	26.3	43	25.5	0
2021	93	23.9	41.9	24	0
2021	94	23.6	41.1	24.9	0
2021	95	19.9	40.6	24.5	0
2021	96	23.3	40.6	25	0
2021	97	21.7	40.7	23.7	0
2021	98	23	42	24.6	0
2021	99	22	40.3	24.3	0
2021	100	21.9	39.3	23.9	0
2021	101	23.4	39.4	24	0
2021	102	23.4	40	24.1	0
2021	103	24.4	40.1	25.2	0
2021	104	18.2	38.6	26.8	0
2021	105	25	38.6	26.1	13.4
2021	106	24.1	39.5	25.5	0
2021	107	24.3	40.5	25	0
2021	108	23.2	41.2	26.1	0
2021	109	21.2	41.7	26.8	0
2021	110	18.4	41.8	28.3	0
2021	111	17.7	40.4	27.4	0
2021	112	19.1	38	27.7	0
2021	113	15.1	35	26.1	15.7
2021	114	22.3	38.5	25.6	0
2021	115	24.2	40.4	24.7	0
2021	116	22.5	38.8	26.8	0
2021	117	23.4	40.5	26.1	0
2021	118	19.7	41.1	26.9	0
2021	119	22.7	41.7	27.1	0
2021	120	21.7	41.5	26.5	0
2021	121	23.7	40.9	25.3	0
2021	122	24.8	40.8	25.5	0
2021	123	24.3	39.9	25.5	0
2021	124	24.6	40.3	25.6	0
2021	125	25.3	41	26.6	0
2021	126	25	40.8	27	0
2021	127	25.5	40.5	26.6	0
2021	128	26.4	40.4	26.7	0
2021	129	26.1	40.8	26.9	0
2021	130	23	40.3	28.2	0
2021	131	19.1	38.8	28.9	0
2021	132	22.7	40.1	27.3	25.4
2021	133	16.6	37.9	28.5	0
2021	134	21.9	40.4	27	0

2021	135	22	35.5	26.7	0
2021	136	17	33.8	26.7	0
2021	137	22	34.2	25.9	0
2021	138	22.3	34.3	27.2	0
2021	139	21.9	36.3	27.9	4.1
2021	140	21.4	34.2	27.3	0
2021	141	15	34.9	26.6	0
2021	142	16.2	35.8	25.9	0
2021	143	20.2	40.6	25.1	0
2021	144	17.5	38.4	27.5	0.9
2021	145	20.1	40.7	28.2	0
2021	146	22.4	42.7	28	0
2021	147	24.5	41.9	31	0
2021	148	23.5	38.5	30.7	0
2021	149	22.4	39.3	29.2	0.5
2021	150	24.1	41.5	29.3	0
2021	151	22.5	40.5	29.3	0.3
2021	152	21.9	38.6	27	18.2
2021	153	22.3	35.9	28.3	0
2021	154	9.5	31.5	26.9	39.7
2021	155	19.2	33.6	25.8	7.4
2021	156	24.2	33.7	25.7	0
2021	157	24.2	35.6	25.5	2.4
2021	158	25.4	35.5	26.3	0
2021	159	26.3	35.1	26.4	0
2021	160	20.9	33.3	26.6	0
2021	161	17	33.5	25.3	0
2021	162	12.5	35.8	23.9	3.7
2021	163	18.7	35.2	24.3	0
2021	164	13.3	32	23.7	92.9
2021	165	13.8	31	24.3	16.3
2021	166	15.3	34.9	24.4	0
2021	167	17.4	35.1	24	0
2021	168	17.5	34	24.6	0
2021	169	14.3	34.9	25.4	0
2021	170	20.2	35.6	24.9	0
2021	171	20.1	36.2	24.9	0
2021	172	23	35.6	25.3	0
2021	173	17.7	31.8	25.4	0
2021	174	15.4	34.4	24.9	3.5
2021	175	18.6	33.3	25.3	7.2
2021	176	19.8	36.5	24.6	0
2021	177	16.5	31.8	25.1	0
2021	178	10.9	30.6	24.9	22.1
2021	179	20	32.9	24.9	66.9
2021	180	21.2	33.8	25.6	0
2021	181	22.9	34.9	25.8	0
2021	182	11.6	30.5	26.3	0.7

2021	183	9.3	31.7	24.7	34.9
2021	184	19.1	32.6	24.5	0.3
2021	185	20.9	34.5	25	0
2021	186	19.6	32.6	25.4	0
2021	187	21	32.7	25.8	0
2021	188	17.3	33.4	26.3	0
2021	189	13	29.5	25.3	5.8
2021	190	14	33.4	24.4	0
2021	191	15.9	30.4	25	9.6
2021	192	7.4	30.1	23.6	0.3
2021	193	12.6	32.1	24.1	24.5
2021	194	14.4	31.1	24.1	0
2021	195	12.6	29.3	23.3	35.7
2021	196	15	32.7	24.1	8
2021	197	17.9	31.9	23.6	4.3
2021	198	20.5	31.5	24.9	2.9
2021	199	13.8	31	25.5	18.6
2021	200	20.7	31.7	24.7	2.6
2021	201	19	31.6	24.6	0
2021	202	4.9	29.3	23.8	4.7
2021	203	4.9	27.7	23.8	35.9
2021	204	19.1	30.5	24.1	15.4
2021	205	21.3	33.7	23.7	0
2021	206	21.7	33.6	24.5	0
2021	207	19.5	32.5	24.6	0
2021	208	22.2	30.8	24	0
2021	209	19.5	33.1	23.5	0
2021	210	13.4	31.9	23.7	0
2021	211	17.3	30.5	23.8	0
2021	212	8.6	30.6	23.9	0
2021	213	19.7	32.3	23.9	0
2021	214	21.8	32.9	23.4	0
2021	215	21.5	32.1	23.3	0.3
2021	216	19.5	32.6	24.3	0
2021	217	20.1	31.3	24.4	0
2021	218	21.5	33.1	24.5	0
2021	219	23.1	32	25	0
2021	220	20.6	30.3	24.7	0
2021	221	19.4	31.9	25.2	4.6
2021	222	19	32.4	25.2	0
2021	223	20.7	31	25.2	0
2021	224	16.2	29.8	25	0
2021	225	13.7	30.5	24.2	51.6
2021	226	15.1	31.2	23.9	0
2021	227	17.9	29.2	24.1	0
2021	228	9	28.7	23.6	13.2
2021	229	10.7	31.7	22.9	33.5
2021	230	16.9	32.3	23.2	0.7

2021	231	16	31.9	23.5	0
2021	232	12.3	30.2	23.5	0
2021	233	7.3	29.5	23.5	0
2021	234	23.8	31.5	23	0
2021	235	24.7	31.6	23.5	0
2021	236	23.6	32.9	23.6	0
2021	237	22.4	31.5	24.9	21.2
2021	238	13.3	30.3	24.8	25.7
2021	239	13.1	30.2	23.7	12.1
2021	240	10.3	31.6	23.8	12.5
2021	241	13.5	31.2	23.6	3.9
2021	242	6.6	30.7	23.2	98.6
2021	243	12.6	28.7	22.2	13.4
2021	244	9.4	30.2	22.7	1.3
2021	245	19.9	31.3	23.6	0
2021	246	14.2	29.7	24.5	54.2
2021	247	16.3	30.6	23.6	0.3
2021	248	20.1	29.1	23.8	54.9
2021	249	5.6	26.8	23.5	7
2021	250	15.4	30.1	23	10.7
2021	251	19.1	32.1	22	0
2021	252	21.4	32.1	22.8	0
2021	253	17.7	31.7	23.8	0
2021	254	16.3	30.8	24.3	0
2021	255	16.5	30.3	24	0
2021	256	15.8	30.8	23.7	0
2021	257	17.8	32.5	23.9	0.7
2021	258	18.8	31.2	23.6	0
2021	259	21.7	31.6	23.7	0
2021	260	21.4	31.8	23.9	0
2021	261	19.8	31.2	23.8	0
2021	262	18.3	31.8	23.8	0
2021	263	17.4	30.8	24.8	1
2021	264	14.6	30	24.2	27.9
2021	265	15.8	29.8	23.6	11.7
2021	266	17.3	29.7	23.9	4.3
2021	267	18.9	30.8	23.2	0
2021	268	19	31	24.3	0
2021	269	18.3	31.4	23.9	30
2021	270	4.8	28.9	23	3.1
2021	271	15.4	30.7	22.2	29.8
2021	272	21.9	30.6	20.9	0
2021	273	18.4	31.4	23.1	0
2021	274	21.1	30	24.2	4.7
2021	275	21.7	29.8	23.1	0
2021	276	22.2	31	24.1	0
2021	277	20.4	31.2	24	0
2021	278	20.3	29.5	24.3	0

2021	279	13.7	29.3	23.7	0
2021	280	19	30.3	23.7	0
2021	281	21.5	30.3	24	0
2021	282	18.4	31	24.4	8.3
2021	283	18.1	28.8	24.3	9
2021	284	20.1	30.1	22.3	0
2021	285	19.1	31	21.9	0
2021	286	16.7	30.6	22.7	0
2021	287	17.6	30.1	22.8	0
2021	288	15.8	30.9	22	0
2021	289	12	30.4	24.3	0
2021	290	15.8	29.3	23.4	1.3
2021	291	20	31.3	23.7	0
2021	292	16.2	30.9	22.8	0
2021	293	16.7	29.9	21.1	0
2021	294	18	30.3	21	0
2021	295	19.4	29.9	20.2	0
2021	296	18.4	30	19.6	0
2021	297	16	29.2	20.3	0
2021	298	18.7	29.2	20	0
2021	299	19.1	28.9	19.3	0
2021	300	19.4	28.9	18.7	0
2021	301	16.1	29.3	20.2	0
2021	302	10.3	28.3	22.4	0
2021	303	14.3	28.9	22.9	0
2021	304	13.9	28.7	21.6	3.1
2021	305	9.1	26.5	19.1	9.2
2021	306	13.6	28.7	21.7	15.9
2021	307	12.1	28.3	22	1.2
2021	308	13.5	28.6	22.1	0
2021	309	15.5	29.3	21.7	0
2021	310	15.4	29	21.1	0
2021	311	12.5	28	19.8	0
2021	312	17.1	27.9	18.5	0
2021	313	14	27.9	17.1	0
2021	314	14.7	27	17.3	0
2021	315	8.1	26.6	18	0
2021	316	7.4	27.2	20.6	0
2021	317	8.7	29.1	22.3	3.5
2021	318	12.9	29.5	22.8	0
2021	319	12.5	29.8	22.7	0
2021	320	11.2	29.7	22.6	0
2021	321	12	28.9	23.2	15.5
2021	322	7.4	28.5	22.6	0
2021	323	5.5	27.3	22.7	2.7
2021	324	10.3	29.7	22.8	1.3
2021	325	11.1	29.4	22.8	6.6
2021	326	16.8	30.3	23.3	1.2

2021	327	17.2	30.4	22.6	0
2021	328	15	29.2	22.9	0
2021	329	15.7	30.1	21.8	16.4
2021	330	16	29.7	19.2	0
2021	331	13.1	27.8	17.1	0
2021	332	7.4	27	17.3	0
2021	333	7.1	27.1	20.1	0.9
2021	334	13.9	26.6	19.6	0
2021	335	15.2	28.1	18.5	0
2021	336	16.4	27.8	16.8	0
2021	337	15.8	27.2	17.6	0
2021	338	17.5	29.3	17.4	0
2021	339	17.8	29.7	17.5	0
2021	340	18	29.9	17.1	0
2021	341	17.7	29.2	17.4	0
2021	342	12	28.9	20.4	0
2021	343	12.3	28.8	20.7	0
2021	344	14.5	28.8	20.8	7.4
2021	345	16	29.2	19.7	0
2021	346	14.4	28.6	20.4	0
2021	347	12.4	27.8	19.3	0
2021	348	12	26.7	19.5	0
2021	349	12.3	25.1	19.3	0
2021	350	13.9	27.6	15.9	0
2021	351	16.7	27.4	14.9	0
2021	352	17.9	27.1	13.3	0
2021	353	16.8	26.8	13.2	0
2021	354	16	26.5	12.2	0
2021	355	17.1	27.3	9.8	0
2021	356	17.2	28.4	11.6	0
2021	357	17	29.3	13.5	0
2021	358	16.5	29.5	13.6	0
2021	359	16.6	30.6	15.3	0
2021	360	15.1	29.9	16.6	0
2021	361	13.5	29.1	17.4	0
2021	362	15.4	29.4	17.7	0
2021	363	16.1	29.7	16.8	0
2021	364	14.8	28.7	16.8	0
2021	365	16.1	28.9	17.1	0

APPENDIX-E

Derivation of VV, VH, VH/VV, Band8, Band4 and NDVI values for the field points

during visit-1

Field ID	B8	B4	NDVI	VV	VH	VH/VV
T1	3826.0	878.0	0.7	-6.4	-12.6	1.9
T2	3624.0	833.0	0.7	-6.4	-9.2	1.4
T3	4403.0	1114.0	0.7	-3.3	-8.7	2.6
T4	3834.0	884.0	0.7	-6.7	-13.5	2.0
T5	3075.0	794.0	0.7	-5.8	-9.2	1.6
T6	3116.0	822.0	0.7	-6.0	-13.5	2.2
T7	3213.0	848.0	0.7	-6.7	-11.4	1.7
T8	3423.0	834.0	0.7	-4.5	-11.5	2.6
T9	3815.0	819.0	0.8	-5.0	-10.9	2.2
T10	2950.0	844.0	0.7	-0.6	-12.0	18.6
M1	3805.0	1690.0	0.5	-5.4	-15.1	2.8
M2	2565.0	934.0	0.5	-4.7	-11.2	2.3
M3	2658.0	811.0	0.7	-6.2	-9.9	1.6
M4	1900.5	760.0	0.6	-6.9	-14.0	2.0
M5	2868.0	921.0	0.7	-5.1	-14.8	2.9
M6	2252.0	851.0	0.6	-5.7	-12.5	2.2
M7	2369.5	945.0	0.5	4.2	-10.0	2.4
M8	3322.0	853.0	0.7	-7.3	-10.7	1.5
M9	3095.5	1181.0	0.6	-6.0	-12.2	2.0
M10	3639.5	889.0	0.7	-4.0	-10.4	2.6

Derivation of VV, VH, VH/VV, Band8, Band4 and NDVI values for the field points during visit-2

Field ID	B8	B4	NDVI	VV	VH	VH/VV
T1	2864.0	1242.5	0.5	-6.2	-10.6	1.7
T2	2757.5	1132.5	0.6	-6.6	-14.2	2.1
T3	3012.0	1578.5	0.4	-4.2	-10.9	2.6
T4	2952.5	1269.0	0.6	-6.6	-10.8	1.6
T5	2751.5	1175.5	0.7	-8.6	-13.6	1.6
T6	2641.5	1234.5	0.5	-7.2	-13.7	1.9
T7	2783.0	1207.5	0.6	-6.0	-11.8	2.0
T8	2605.5	1222.0	0.4	-6.9	-13.6	2.0
T9	2894.0	1051.5	0.7	-7.8	-14.2	1.8
T10	2799.5	1148.5	0.7	-5.6	-12.0	2.2
M1	2135.5	1185.5	0.3	-5.1	-12.2	2.4
M2	2456.0	1125.0	0.4	-6.4	-11.2	1.7
M3	3126.0	1546.5	0.4	-6.5	-8.5	1.3
M4	2584.0	1048.5	0.6	-7.7	-13.3	1.7
M5	2669.0	1256.0	0.6	-6.6	-12.3	1.9
M6	2986.5	1316.5	0.7	-7.5	-13.7	1.8
M7	2703.5	1547.0	0.3	-6.6	-10.5	1.6
M8	2763.5	1183.0	0.6	-7.1	-12.0	1.7
M9	2722.0	1153.0	0.6	-5.8	-12.7	2.2
M10	3079.5	1448.5	0.4	-7.1	-11.3	1.6